Engineered Metallic Dendrites and Their Nano-composites for Electrochemical Biosensing Applications

A Thesis submitted in partial fulfillment of the requirements for the award of the degree of

DOCTOR OF PHILOSOPHY

by

BUDDHADEV PUROHIT

JANUARY 2020

Department of Biosciences and Bioengineering

Indian Institute of Technology Guwahati

Guwahati- 781039, INDIA

Buddhadev Purohit
Registration No. 166106110
Department of Biosciences and Bioengineering
Indian Institute of Technology Guwahati
Guwahati-781039, Assam, INDIA

Declaration

I hereby declare that the matter embodied in this thesis is the result of investigations carried out by me at the Department of Biosciences and Bioengineering, Indian Institute of Technology Guwahati, Guwahati, India, under the supervision of Dr. Pranjal Chandra**.** Due acknowledgements have been made wherever the work described in this thesis is based on the finding of other researchers. This thesis has not been submitted to any university, institute or elsewhere for the award of any degree or diploma to the best of my knowledge and belief.

Buddhadev Purohit

Date: 25 Jan 2020 **Buddhadev Purohit**

Department of Biosciences and Bioengineering
Indian Institute of Technology Guwahati
Guwahati-781039, Assam, INDIA

Certificate

It is to certify that the work described in this thesis entitled "Engineered Metallic Dendrites and Their Nano-composites for Electrochemical Biosensing Applications" done by Mr. Buddhadev Purohit (Roll No - 166106110) for the award of the degree of doctor of philosophy is an authentic record of the results obtained from the research work carried out under my supervision in the Department of Biosciences and Bioengineering, Indian Institute of Technology Guwahati, India.

The results embodied in this thesis have not been submitted to any other university or institute for the award of any degree.

January 2020

Dr. Pranjal Chandra

(Supervisor)

Dedicated to my family

ACKNOWLEDGEMENTS

First of all, my sincere gratitude to all my teachers who taught and inspired me in numerous ways which cannot be expressed in words; I am forever indebted to you.

I want to express foremost gratitude to my research supervisor, Dr. Pranjal Chandra, for his constant care, support, guidance, encouragement, and supervision throughout my research work. I am grateful for the ample freedom he allowed me in exploring different directions of my work, and for the endless hours, he dedicated to improve the quality of my work. I am fortunate enough that I had the opportunity to work under his dynamic and inspiring supervision.

I am also grateful to my doctoral committee members, Prof. Ranjan Tamuli, Dr. Lalit Mohan Pandey, and Dr. Shirisha Nagotu for their valuable suggestions, which helped me to improve the work immensely. I owe my thanks to the present and past Head of Department of Biosciences and Bioengineering, Prof. Latha Rangan and Prof. Kannan Pakshirajan for providing me the necessary facilities to carry out my research work. I am also grateful to Prof. Vikash Kumar Dubey and Dr. Shankar Prasad Kanaujia for their help at numerous instances to complete the work on time. I am also grateful to all the non-teaching staff at the Department of Biosciences and Bioengineering, and Central Instrumentation facilities, Indian Institute of Technology Guwahati for their invaluable help in administrative as well as research work. I owe my sincere gratitude to Dr. Ananya Srivastava, National Institute of Pharmaceutical Education and Research Guwahati for her valuable suggestions and motivation, which helped me a lot to improve the research work. I would like to thank Ministry of Human Resource Development, India, and Indian Institute of Technology Guwahati for providing financial assistance during my Ph.D. tenure.

My time in the Laboratory of Bio/Physio sensors and nanobioengineering has been an enjoyable one due to all my current and past lab mates. I would like to thank Dr. Kuldeep, Ashutosh, and Anupriya, for their suggestions and time throughout my Ph.D. tenure. I am

also deeply indebted to Dr. Ritesh, Dr. Kartikeya, Dr. Suresh, Dr. Jay, Dr. Sunita, Dr. Gundappa, Dr. Adarsh, Dr. Kamalesh, Jiban, Srijib, Prachi, and Chayanika for their affection, guidance, and help. A special thanks to Chitta Ranjan Barik, Sukumar Purohit, Nabakumar Bhoi, Md. Muzaffar Iqbal for helping me in my early days in IIT Guwahati. I would like to thank my friends Pratap, Subhankar, Deepak, Ratan, Adhiraj, Veenit, and Soheeni for some enjoyable time in campus. I would also like to thank Himansu Charan Sahu, Somanath Behera, Sunil Jal, and Shaswat Hota for being my constant companion for so many years. I would also like to thank Sarangadhara Hota for his encouragement and motivation. Words cannot express my gratitude to Shiwani Dash, for she is the constant source of love and courage during this journey.

I would also like to thank my three younger brothers Sukradev, Bruhaspatidev, and Rabindradev for standing there whenever I need. I take this opportunity to express my love and gratitude to my Bapa, Nilamani Purohit and Maa, Rebati Purohit. I owe everything to them for their unconditional love and support. I want to acknowledge my grandparents Late Kapileswar Purohit and Late Champafula Purohit, for their affection and loving memories.

At last, most of all, thanks to the one Almighty for his blessing to complete the research work successfully.

Date: ……

Buddhadev Purohit

Chandra's
Laboratory of Bio/physio Sensors
and Nanobioengineering

Abstract

Biosensors are bioanalytical tools capable of detecting an analyte of interest in a sample solution offer a quick and sensitive diagnostic. Biosensors in clinical diagnostics have certain advantages over the conventional based diagnostics which require dedicated laboratory space, advanced infrastructure, trained personnel, and time-consuming process. The heavy and bulky instruments also can't be carried to remote locations and operated under emergency conditions. Biosensors are continuously being improved to achieve higher sensitivity and selectivity, with the incorporation of novel signal amplification strategies, and nanomaterials. The surface of the sensing matrix is being fabricated with functionalized nanomaterials for immobilization of biorecognition elements as well as to achieve larger surface area, high catalytic activity, and anti-fouling property. In this work, we have developed different sensor systems detecting molecules of clinical importance, using metallic dendritic nanomaterials in the sensing matrix for enhanced electrochemical property. The developed sensors can detect the analytes in clinically significant concentrations, both in ideal as well as real biological samples. Biosensors offer the further development of miniaturized portable devices for onsite detections, which may enable the user ease in the diagnosis of diseases at the earliest phase for better healthcare.

In this work, four different biosensing works have been designed using the metallic dendrites and their composites, and their material property was thoroughly studied and applied to use in biosensor development. In the first work, we have developed a nonenzymatic nanosensor for the ultrafast and label-free detection of hydrogen peroxide (H_2O_2) based on a sputtered Indium tin oxide electrode comprising gold nano hierarchical 3D structure. The monometallic Au dendrite was able to show greater electronic as well as catalytic property. H_2O_2 is considered to be associated with various pathological

conditions (aging, diabetes, cardiovascular diseases, neurodegenerative disorders, cancer, *etc.*) and it's quick and ultrasensitive detection in biological matrices can help clinicians to suggest accurate therapeutic strategies for patients. The material and electronic properties of the developed nanosensor was thoroughly characterized by various physical and electrochemical techniques. The sensor was able to detect H_2O_2 in ≤ 1.0 sec, and with two linear dynamic ranges (LDR) of 10^{-12} M to 10^{-10} M and 10^{-10} M to10^{-5} M, and a limit of detection (LOD) of 9.8 (±0.02) x 10^{-13} M. The ability of H_2O_2 detection using the developed sensor falls well between clinical ranges and it is also applicable for trace analysis as well. The gold sputtered hierarchical dendrite sensor probe also shows negligible response ($p < 0.001$, $n = 3$) towards the coexisting which are commonly present in the biological matrices.

In the second work, we attempted to develop a biosensor with enhanced material property using bimetallic dendrites in the sensing matrix. The bimetallic dendrites possess properties of both of their monometallic metals. Given their enormous bioelectronics possibilities, we have developed a gold-copper (Au-Cu) bimetallic dendritic matrix over a glassy carbon electrode by tuning the electrodeposition parameters for the ultrafast and sensitive detection of analytes in real samples. The sensing property of the developed final sensor probe was evaluated by taking acetaminophen as a model molecule. Acetaminophen is a commonly used antipyretic and analgesic drug associated with nephrotoxicity and hepatotoxicity. The sensor shows excellent analytical performances with a linear dynamic range of 100 to1000 nM, with a low limit of detection of 8.5 (±0.03) nM. The Au-Cu bimetallic dendrite shows negligible response towards co-existing interfering molecules, which are commonly found in real samples ($p < 0.001$, $n=3$). Real sample analysis was performed in human urine by spike and recovery method, where the

recoveries were between 91 and 97%. The shelf life of the bimetallic sensor probe was evaluated and found to be stable for eight weeks.

In the next sections, a layered nanohybrid comprising of multi-walled carbon nanotubes (MWCNT) - gold nanoparticles (AuNPs) over glassy carbon electrode (GCE) has been designed as a matrix for the development of Au dendritic nanostructures (AuDN) with enhanced catalytic activity. The developed sensor probe was used for the label-free detection of acetaminophen. The sensor shows excellent analytical performances with a linear dynamic range (LDR) of 100 to 7500 nM, and a low limit of detection (LOD) of 2.12 (±0.03) nM, which is better than recently reported AP sensors. The practical application / clinical possibilities of the final sensor were evaluated by real sample analysis in human urine by spike and recovery method, where the AP recoveries were found in between 92% to 96%. The sensor probe shows a negligible response towards co-existing interfering molecules like glucose, urea, uric acid, and various amino acids, which are commonly found in real samples ($p < 0.001$, $n=3$). The fabricated sensor probe using MWCNT-AuNPs/AuDN is easy to fabricate, simple, robust, and able to detect AP in urine with high recoveries shows its possibilities to be used in clinical settings.

In the fifth chapter, we have discussed the development of a biosensor for the detection of a cancer biomarker, Carcinoembryonic antigen (CEA), using a composite of Au nanodendrite (AuND), reduced graphene oxide (rGO), and chitosan (CS). CEA is a well-known cancer biomarker found in serum expressed in various types of cancer viz. colon, breast, lung, pancreas, *etc*. CEA is not only used for the detection of cancer progression but also to detect cancer relapse. The developed sensor utilizes AuND as a highly conducting matrix with high active surface area, CS as a biocompatible matrix for the attachment of anti-CEA antibody for the selective binding of CEA, and rGO for signal amplification, respectively. The AuND is electrodeposited by optimizing the AuNP layer

on the electrode for the maximum current response. The AuNP/AuND/CS-rGO/Anti-CEA sensor is capable of detecting the biomarker in the range of 1 x 10^{-13} to 1 x 10^{-8} g/mL, which covers the clinical range of CEA in blood serum. The biosensor achieved a LOD of 2.3 (±0.03) x 10^{-14} g mL^{-1}. No significant interference effect of other co-existing molecules was found on the signal generation due to CEA Real sample analysis was done in the presence of blood serum and % recovery of CEA was found to be between 94-96%. The analytical performances of the biosensor show that the developed sensor can be further developed for commercial purposes.

This work aims toward the development of clinical electrochemical biosensors with better sensitivity exploring the electronic possibilities of metallic dendrites and its composites as a sensing material. The work can be further utilized for the development of miniaturized hand-held devices that can be portable to any location under any circumstances and be used with little technical training to be used for better health care to everybody.

Contents

List of figures

List of tables

Chapter # I

General Introduction

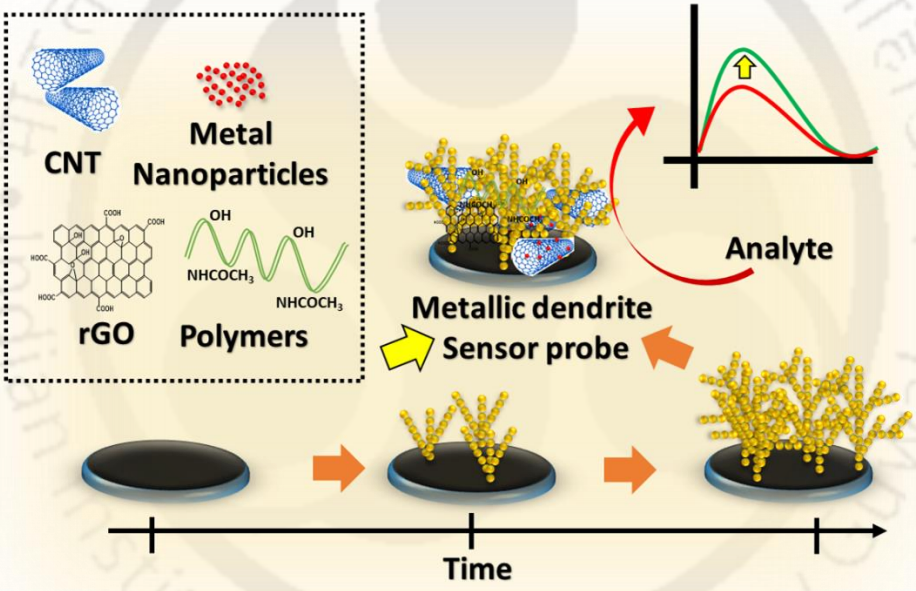

1. Need of newer diagnostic devices

Among all the challenges we face nowadays, health care for all is becoming a major problem despite all the medical inventions and advanced techniques. This lead to the United Nations general assembly's developmental agenda "Transforming our world: the 2030 agenda for sustainable development", healthy life for every individual, and at all ages is prioritized as an important factor for sustainable development (Organization 2016). However, we are living in a world, where disease outbreaks are becoming more common. An epidemic outbreak of infectious diseases are becoming more common (Cohen 2000; Colizza et al. 2006; Gautreau et al. 2008), a large number of new cases of metabolic disorders like obesity and diabetes are detected in younger people due to changed lifestyle (Barrès and Zierath 2016; Saklayen 2018). The number of new cases of cancer is rising each year even though the new technologies and new medications saving lives (Parry et al. 2011; Siegel et al. 2019). The cases of complications due to drug overdosage and drug resistance are also becoming a major problem (Barriere 2015; Ruhm 2017; Mobarki et al. 2019). The number of cases as well as fatality due to this can be reduced drastically, if we can detect these cases at the earliest (Etzioni et al. 2003). The diagnostics devices, which detect the disease can also be used to make a record of the health issues to monitor diseases like diabetes, which is essential for further medications (Mol 2000).

For these health issues, several instruments have been developed and routinely used for the analysis of clinical samples. Instruments like colorimetry, chromatography, and spectrophotometer are used to carry out these biochemical tests in hospitals.

Part of the introduction has been published as Purohit et al. (2020) Smartphone-assisted personalized diagnostic devices and wearable sensors. *Current Opinion in Biomedical Engineering* 13: 42-50.

All these instruments look for a molecule of biological/chemical origin associated with the particular disease known as biomarkers. In diseased conditions, the concentration of these biomarkers is altered than healthy individuals. So, these biomarkers are used for clinical analysis of diseases and can be used for the development of POC device development (Purohit et al. 2020). Although these instruments are very powerful, they have some limitations. These instruments follow a very time-consuming process, require advanced infrastructure, dedicated laboratory space, large sample volume, and well-trained personnel. These limitations hinder quick diagnostics, onsite detection, and portability of the devices.

To avoid such limitations in diagnosis, miniaturized devices have been developed to detect the biomarkers. Miniaturization of the devices would make them robust, reliable under emergency cases, and can be carried to remote locations easily.

2. Biosensors

According to the International Union of Pure and Applied Chemistry biosensors are defined as "A device that uses specific biochemical reactions mediated by isolated enzymes, immune-systems, tissues, organelles or whole cells to detect chemical compounds usually by electrical, thermal or optical signals" (Thévenot et al. 2001a).

Biosensor is a bio-analytical device that detects an analyte by the action of various biological or chemical molecules present in the sensing matrix with specific properties. A biosensor is primarily consisting of three important parts namely the biorecognition element, transducer, and processor. Biorecognition elements like enzymes, antibody, aptamer, whole-cell, *etc*. are chemical or biological moieties that can selectively interact with the analyte. This biorecognition event is converted to a form of a measurable signal by the transducer coupled with the biorecognition

element. The transducer can perceive the change in pH, temperature, charge, mass, *etc*., and converts that signal to other measurable forms. In the next part of biosensors, an amplifier minimizes the background noise of the signal and strengthens the weak signals for the measurements of the analyte. The processor analyzes the data and presents it in the digital display for further uses. A schematic representation of the different parts of a biosensor and its working is shown in figure 1.1. With the advancement of technology, new signal amplification strategies are incorporated in the biosensor to achieve superior analytical performances (Kumar et al. 2019).

Biosensors have seen tremendous growth and development since its inception in 1956. Clark developed the first biosensor *i.e.* oxygen electrode, which became the foundation for further research in this area. Based on this work, the first commercialized biosensor, a glucose biosensor was later developed by Yellow Spring Instruments in 1975, the YSI Model 23 Analyzer (Clark Jr and Lyons 1962). Based on the principle of this biosensors, a lot of new commercial sensors like self-testing blood glucose strips and subcutaneous implantable *in-vivo* glucose monitoring electrodes came to market in the next decades to detect glucose and other clinically important molecules (Frew and Hill 1987; Bindra et al. 1991; Hilditch and Green 1991; Wilson and Gifford 2005).

3. Classification of biosensors:

The biosensors can be classified based on the biorecognition molecules, the uses of labels, and transducers for sensing purposes. A detailed account of the classification of biosensors is explained in the next section.

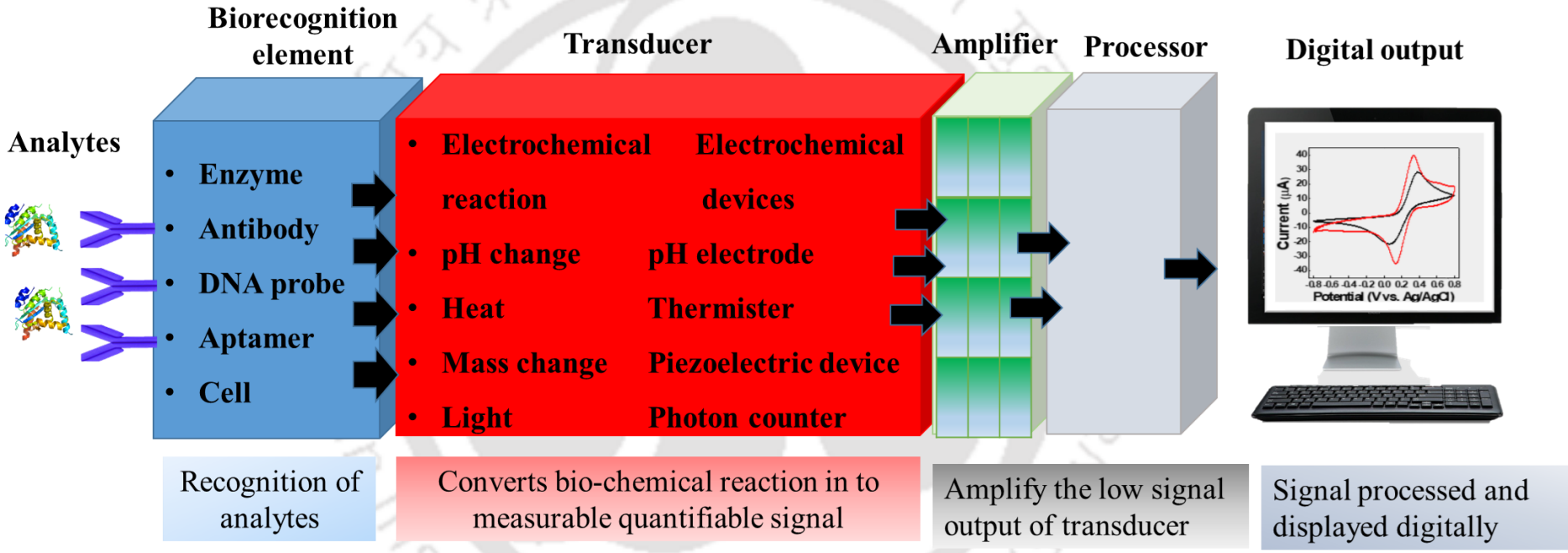

Figure 1.1. A pictorial representation of a biosensor, consisting of three major components: (i) Biorecognition elements, (ii) Transducer, (iii) Amplifier, and processor.

3.1. Classification based on biological recognition element

Based on the biorecognition elements, biosensors are grouped under biocatalytic (e.g. enzymes, nano-catalyst, direct electron transfer, *etc*.) and bio-affinity (e.g. antibody, protein receptor molecules, aptamer, *etc*.) subgroups.

3.1.1. Biocatalytic Recognition Element

Biocatalytic recognition based biosensors incorporate a previously isolated or manufactured biological entity capable of catalysis. The most commonly used bioreceptors in biocatalytic biosensors are:

(a) Enzymes: known as biocatalyst, capable of catalyzing specific reactions with specific substrates. Both mono- or multi-enzymes are used in the sensing matrix for the detection of analytes.

(b) Whole cells and their organelles: bacteria, fungi, cells, and cell organelles like mitochondria are also used for the detection of certain molecules.

Enzymes belonging to the oxidoreductase class are highly preferred for the biocatalytic biosensor development. Glucose oxidase (GOx) is the most widely used enzyme in biosensors development (Fortier et al. 1990; Liu et al. 2005). Enzymes possess high specificity towards the substrates, which enables the sensor to detect the analyte in complex materials without any pretreatment reactions. Biosensors using genetically engineered bacteria are developed for biosensing applications like heavy metal detection (Leth et al. 2002).

3.1.2. Bioaffinity Recognition Element

This type of biosensor is based on the selective interactions between the analyte and the biorecognition molecules like an antibody, aptamer, DNA probe, *etc*. Antibody-based biosensors *i.e.* immunosensors are constructed based on the concept of antibody-antigen complex formation, where antigen /antibody are immobilized on

the solid sensing matrix. Immunosensors offer highly sensitive detection of the analyte, where the recent advances in the development of monoclonal and recombinant antibodies have greatly contributed. Apart from the antibody, non-catalytic protein-based biosensors are also developed, mostly using cell membrane proteins such as metabotropic receptors or ionotropic receptors (Paddle 1996; Misawa et al. 2018). DNA biosensors are developed based on the complementary base pairing of the nucleic acid sequence of the analyte and the probe on the sensor surface (Du and Dong 2017). Aptamer, ssDNA or RNA molecule with < 100 bp with a distinct 3D structure, used in biosensors for sensing of a wide range of molecules. Unlike antibody, aptamers can be developed to bind multiple analytes like proteins, bacteria, viruses, or even ions (Song et al. 2008; Zou et al. 2019).

3.2. Classification based on the uses of label:

Biosensors can be classified based on the applications of external labels i.e. agents to facilitate the analytical performances of the biosensors.

3.2.1. Label-free biosensors

When the biosensor doesn't need any external label to detect the analyte, it is called as label-free biosensors. If the analyte is a redox-active molecule, or the biosensing matrix is designed specifically to interact/ catalyze the analyte, there is no need of any external label for sensing activity (Purohit et al. 2019b). Most of the label-free biosensors are based on impedimetric or potentiometry biosensors. Muramatshu et al., developed an unlabeled biosensor for the detection of immunoglobulin IgG based on the change in resonating frequency of the matrix components (Muramatsu et al. 1987). The sensor was able to detect the IgG from IgA. The advantage of using a label-free biosensor is the direct sensing of the analyte, eliminating a step of a secondary antibody or tagged molecule immobilization.

3.2.2. Labeled biosensors

When the biosensors incorporate external labels for the detection of the analyte, termed as labeled biosensors. The advantage of using a labeled tag is the dual-confirmation of the presence of an analyte. Also, a labeled tag can detect the presence of a single molecule in a sample (*e.g.* fluorescence tag), which is not easy to achieve by unlabeled biosensors. The most commonly used labels are various enzymes (e.g. alkaline phosphatase (ALP), horseradish peroxidase) and fluorescently tagged DNA probe. Pallela et al., developed a labeled biosensor for the detection of metastatic cancer cells, where they used AuNPs-polymer-antibody to capture the cell (Pallela et al. 2016). A secondary hydrazine-AuNP-Ab_2 tag was used for dual confirmation of the presence of cells, where the analytical signal was generated by the catalysis of H_2O_2 by hydrazine. The disadvantages of using a tagged molecules are their sensitivity towards various environmental conditions (e.g. fluorescent tags are sensitive to incident light and interference from commonly coexisting molecules).

3.3. Classification based on transducers

3.3.1. Optical Biosensors

A biosensor that measures the change in optical behavior of the target analyte is called as optical biosensors. Photometric behaviors that are most commonly used in optical biosensors are UV-visible absorption and reflectance, fluorescence, phosphorescence, luminescence, surface plasmon resonance, internal reflection, *etc.* Optical biosensors measure the change in altered phase, polarization, or frequency of input light in response to physical or chemical changes in the analyte sample (Damborský et al. 2016). The optical biosensors can be classified into two main categories: one that measures the changes in the intrinsic optical property of the biomolecules, often involving the interaction with a specific target molecule (Borisov and Wolfbeis 2008). This class doesn't involve the use of any label or

optical probe, so it is low cost and follows simple procedures. The majority of the non-labeled optical biosensors can be grouped into SPR based biosensors, interferometer based biosensors (like Mach-Zehnder interferometer, Young's interferometer, Hartman interferometer, backscattering interferometer), optical-waveguide based biosensors, optical-resonator based biosensors, optical-fiber based biosensors, photonic crystal biosensors, *etc*. (Fan et al. 2008). The second class is the fluorescence-based labeled biosensors, where a fluorescence tag is attached to the molecule of interest. However, the limitation of this class is the addition of one more step of labeling the molecules. Label based biosensors can be sensitive enough to detect a single molecule of analyte in the sample, as the sensing of circulating tumor cells (Krivacic et al. 2004). Recently, multiple work on optical biosensors follow innovative ways to quantify analytes. One such work was performed by Mahato and Chandra, where they incorporated smartphone in the sensing platform to capture and process the analytical signal produced by the enzymatic activity of ALP to monitor milk pasteurization (Mahato and Chandra 2019). ALP present in the matrix cleaves a reagent to produce a blue color, where the intensity of the color is proportional to the amount of ALP. Digital image colorimetry (DIC) based on RGB (red-green-blue) color co-ordinates was used to quantify the concentration of ALP. Recently, new cost-effective wearable devices are being developed for continuous health monitoring based on the optical measurements of analytes (Curto et al. 2012; Huang et al. 2014; Yang and Gao 2019).

3.3.2. Mechanical/ Piezoelectric biosensors

Another class of biosensors is the mechanical/ piezoelectric biosensors, which sense the analyte by measuring the change in its mechano-physical properties like pressure, acceleration, temperature, strain, or force applied (Tamayo et al. 2013).

Piezoelectric material like berlinite, quartz, Rochelle salt, *etc*. vibrates under the influence of an electric field depending on the thickness and nature of the material. Each piezoelectric material vibrates with a certain resonating frequency, which is measured by the biosensor. The change in resonating frequency is proportional to the mass added/ removed from the sensing surface, which can be calculated using the Sauerbrey equation (Sauerbrey 1959; Muramatsu et al. 1987). The piezoelectric biosensors can reach a resolution of 1 µg. Quartz crystal microbalance (QCM) is the most widely used mechanical biosensor capable of sensing an analyte in solid, liquid, and gas phases (Tsionsky and Gileadi 1994; Rodahl et al. 1995; O'Sullivan and Guilbault 1999; Liu et al. 2003). The most advantageous fact of using mechanical biosensors, the analyte can be sensed directly, without using any label. However environmental factors, like humidity can affect the sensing activity of mechanical biosensors.

The biggest advantage of using mechanical sensors is excellent mass resolutions (nanoelectromechanical system have achieved a zeptogram resolution), label-free detection, ease to study the interaction between a biological entity and small molecules, and capability to fabricate small microfluidics devices (Braun et al. 2009; Arlett et al. 2011).

3.3.3. Electrochemical biosensors:

The Physical Chemistry and Analytical Chemistry division of International Union of Pure and Applied Chemistry (IUPAC), defined the electrochemical biosensors as follows: "An electrochemical biosensor is a self-contained integrated device, which is capable of providing specific quantitative or semi-quantitative analytical information using a biological recognition element (biochemical receptor) which is

retained in direct spatial contact with an electrochemical transduction element" (Thévenot et al. 2001b).

In electrochemical biosensors, the biorecognition event got converted into a quantifiable signal in terms of a measurable current, potential, or change in conductivity. Electrochemical biosensors are the most commonly used biosensors than the above-mentioned types due to its low cost, ease of fabrication, and possibilities of miniaturization. Unlike optical and mechanical biosensors, electrochemical biosensors can be operated in a very small sample volume. However, the biggest advantage of using electrochemical biosensors is to achieve very low LOD *i.e.* atto- (10^{-18}) or zepto (10^{-21}) molar of analyte have been detected by electrochemical immunosensors (Jenkins et al. 1988; Bauer et al. 1996). Also, electrochemical immunosensors are immune to the interference from fluorophores, chromophores or other particles that usually interfere in optical biosensors. Hence, electrochemical biosensors are more useful in detecting the whole cell, cancer cells, bacteria, *etc.* (Yao et al. 1993; Brajter-Toth and Chambers 2002; Purohit et al. 2019a).

Electrochemical biosensors are classified into three major categories: (i) Amperometry that measures variations in current, (ii) Potentiometry that measures the change in charge accumulation or potentials, and (iii) conductometry or impedimetric that measures the change in conducting behaviors of sensing sample (Ronkainen et al. 2010). These three types of biosensors are most commonly using a three-electrode system.

Amperometry: This kind of electrochemical biosensors function by measuring the current when a voltage is applied between the electrodes. The electrodes are held at a constant potential, and the changes in current are measured as a function of the

analyte concentration present in it. When a constant potential is applied, the current in the three-electrode system can be explained using the Butler-Volmer equation.

$$i = i_{0.} [\exp (\frac{\alpha A n F}{RT} \eta) - \exp (- \frac{\alpha c n F}{RT} \eta)] \text{ ...equation 1.}$$

Where i is electrode current density, i_o is the exchange current density, α_A is anodic charge transfer co-efficient, α_C is cathodic charge transfer co-efficient, F is Faraday constant, n is the number of electrons transferred, η is activation overpotential, R is the universal gas constant, and T is the absolute temperature.

The first working biosensors, Clark oxygen electrode is also an amperometric biosensor consisting of a Pt cathode and an Ag/AgCl reference electrode. When a potential of -0.7 V was applied, oxygen reduced at the cathode, and a current response was generated corresponding to oxygen concentration.

Potentiometry: In such biosensors, the accumulated charge potential at the working electrode is measured in comparison to the reference electrode, when no current flows between them. The potentiometry biosensors give information about the charged molecules present in the solution, where the concentration of the analyte and the potential is governed by Nernst equations.

$$E_{cell} = E^0 - \frac{RT}{nF} \ln (Q) \text{ ...equation 2}$$

Where E_{cell} is cell potential (or electromotive force), E^0 = standard cell potential, R is the universal gas constant, T is absolute temperature, n is the number of electrons transferred in cell reaction or half-reaction, F is Faraday constant, and Q is reaction quotient. The potential of the working electrode changes with the increase/decrease in the concentration of analytes.

Conductometry/ Impedimetry: Unlike to above-mentioned techniques, the impedimetric biosensors do not measure the charged ion concentrations, but measure the impedance of the cell across the working and counter electrode. Impedimetric biosensor doesn't require any detection tag, hence it is generally used for label-free detection of an analyte. This is also used to study protein or other biomolecule immobilization over the electrode surface. This can also be used for miniaturization of detection devices and can be integrated for chip development (Mahato et al. 2018).

4. Role of nanomaterials in electrochemical biosensors:

Nanomaterials with their unique geometric and electronic properties enhance the analytical performances of a biosensor (Kumar et al. 2019). The nanoparticles behave differently in comparison to its constituting individual atoms, and again it changes the property when present in close conjugation with a different complimentary material when forming a composite. The altered geometric and electronic properties make nanoparticles an extremely exciting material to develop biosensor with enhanced efficiency (Luo et al. 2018). The higher surface to volume ratio results in a larger catalytic surface, which is utilized to miniaturize the detection instrumentations without compromising on its sensitivity. This change can lead to the development of point of care (POC) detection modules, eliminating the need for bulky instruments and its associated disadvantages. The modification of the sensing surface by utilizing nanomaterials results in (Sharma et al. 2018):

a) Larger active surface area results in better sensitivity.

b) An increase in the conductivity results in a fast transfer of electrons between the electrode and reaction center.

c) An increase in the catalytic activity results in the oxidation/reduction of analyte at a lower potential, which helps distinguish structurally similar molecules in sensing.

d) Surface modification results in limited interaction of interfering molecules with the electrode and increases the selectivity.

e) A larger surface area also leads to fast diffusion and pre-concentration of target molecule at the electrode surface.

Different classes of nanomaterials are used in biosensor development based on their surface, chemical, and electronic properties. In this section, we have mentioned the most commonly used nanomaterials in various biosensor development.

Carbon-based NM: Nanomaterials that are based on carbon provide a new possibility in the development of modern novel biosensors because of their excellent mechanical characteristics, outstanding biocompatibility, and improved electrical conductivity (Kamran et al. 2019). Graphene, a one-atom-thick sp^2 hybridized layer of the six-carbon ring is well known for its excellent electrical and mechanical properties, biocompatibility, readily availability sites to dock analyte or analyte recognition elements, the high surface area for detection, and most importantly very low cost of synthesis. Graphene oxide (GO) and reduced graphene oxide (rGO) are two important pillars in biosensing research, due to their ease of fabrication and conductivity, respectively (Kuila et al. 2011). Carbon nanotubes (CNT) are another set of carbon material widely used in biosensor construction due to its unique tubular structure, modifiable sidewall, and conductivity. Currently, MWCNT and SWCNT are widely used for non-enzymatic, enzymatic, and immunosensor development by using various wet chemistry (Yang et al. 2015).

***Polymer-based nanomaterials*:** Predominantly, the conducting polymers are utilized as active materials for the development of modern biosensors. Conducting polymers offers large surface areas, excellent conductivity, and flexibility in designing the biosensors for various biomolecule attachment. These polymeric structures act as a selective barrier and also increase the biocompatibility of the sensing matrix (Davis and Higson 2007). Conducting polymers like polyaniline (PANI), polypyrrole (PPy), and polythiophene (PT) are used to construct novel affinity-based biosensors due to the presence of various functional group. Nafion, a perfluorinated polymer is used to enhance the antifouling effect by discriminating against the anions, and also to increase biocompatibility. Chitin, a polymer isolated from crustacean shells, is also used for biosensing owing to a high number of functional groups. Chitosan, a polymer isolated by deacetylation of chitin holds greater promises due to its biocompatibility, presence of functional groups, capacity to form thin films and ease of chemical modifications (Ohkawa et al. 2004; Suginta et al. 2013; Baranwal et al. 2018).

Metal nanoparticles (MNP): Nanoparticles of noble metals with excellent optical, electrical, chemical, and size-dependent properties have been mostly used in the development of non-enzymatic biosensing approaches. Gold (AuNP), silver (AgNP), and platinum (PtNP) nanoparticles are another set of the material extensively used due to their relative biocompatibility, electrical conductivity and optical properties (Doria et al. 2012). AuNP is one of the most used NP due to its optoelectronic properties and biocompatibility. As compared to other MN, AuNP has considerably very low cytotoxic effects, so it is used in the development of a number of biosensors those work in the interface of biological samples (Mahato et al. 2019). Metal oxide nanoparticles (MoNP), especially the d and f block MoNP

like Zn, Zr, Ce, Hf, Gd, Sn, Mn, Fe can be tuned to achieve a variety of shapes, different degree of catalysis, and due to their low cytotoxicity are widely utilized in various biosensors development (Kumar et al. 2019).

However, the recent trends of biosensor development involve the modification of electrode by hybrid materials to enhance catalysis and sensitivity. Carbon-based NM and polymers are mixed with MNP, where the former is used to capture the biorecognition elements, and later contributes to catalysis and conductivity of the sensing matrix (Sapsford et al. 2013).

4.1. Introduction to metallic Dendrites

Among the metallic nanomaterials, dendrites are a group of three-dimensional structure known for its distinct morphology and catalytic activity. The word dendrite is derived from the Greek word “dendron” meaning “tree”. Metallic dendrites are self-assembled, hierarchically arranged, and repetitive structures with a central stem and secondary side branches mimicking a fern-like structure (as shown in figure 1.2). These networked structures possess a high surface area, excellent conductivity, and different degrees of surface roughness. The dendrites follow a hierarchical arrangement of nanoparticles i.e. the primary branch formed first, followed by secondary and tertiary branches. The length and width of the primary branch are significantly more than the secondary branches. The branches are covered with edges, ridges, and end in a pointed tip. These structures are the active surface responsible for the excellent catalytic activity of dendrites. Metallic dendritic structures have been incorporated in the development of inexpensive and effective electro-catalysis, microdevices, electrical and thermal conduction, super-hydrophobicity, drug delivery, bio-imaging, photo-thermal therapy, *etc.* (Bakthavatsalam et al. 2016; Yuan and Zhang 2018).

The benefits of using dendrites rather than other nanomaterials in biosensing are:

1. High density of electroactive sites at the edges, corners, and ridges to facilitate some unique chemical reactions.
2. The metallic and electronic property of the dendrite can be changed, by optimizing some factors like time, the concentration of salt, applied potential, *etc.* (Wang and Yamauchi 2013; Shu et al. 2014).
3. Metallic dendrites have a very large active site, so fouling due to biomolecules has relatively less effect on its catalysis (Cheng et al. 2010).
4. Compared to a nanoscale sensor surface, a micro dimensional dendritic sensing surface can accumulate more biomolecules for ultrafast and sensitive detection (Soleymani et al. 2011).

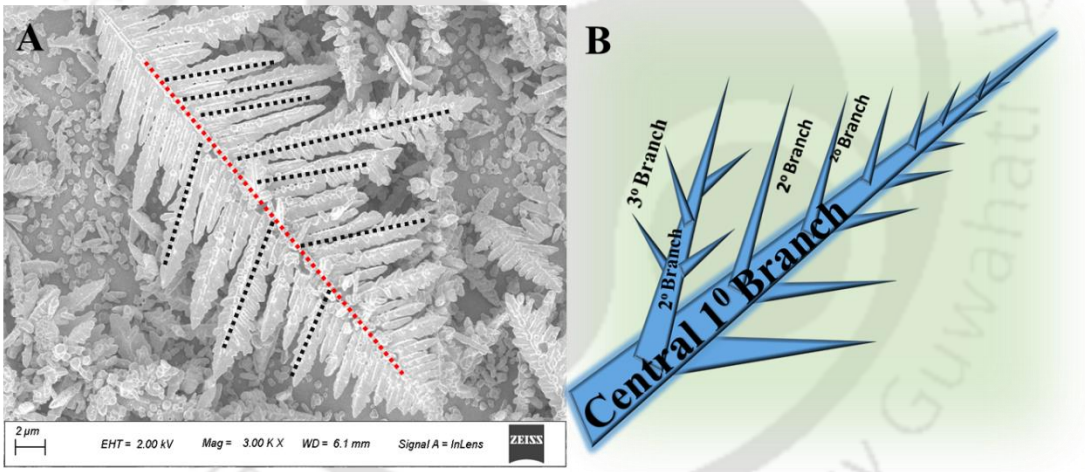

Figure 1. 2. (A) shows a growing Au dendrite with primary (red line), secondary (black line) with a morphology mimicking a fern. In the background, smaller immature dendritic structures are visible with a wide variety of shapes; **(B)** shows a pictorial representation of dendritic structure with hierarchically arranged branches.

4.2. Direct electrodeposition of metallic dendrites for electrochemical biosensing

Electrodeposition is favored over other synthesis methods, as it allows fast and direct growth of nanodendrites (ND) over the electrode. ND is electrodeposited by

applying constant potential, potential sweep or cycles, and electrostatic deposition. When a particular potential is applied, charged metal ions from the electrolyte solutions move towards the cathode, resulting in ND formed on the electrode. The electrodeposition process of metal can be explained by Faraday's law (Al-Bat'hi 2015), whereas the electrodeposition of ND can be explained by diffusion-limited aggregation and nanoparticle aggregated self-assembly crystallization mechanisms. By optimizing the parameters, ND can be synthesized for desired catalytic behavior (Kumar et al. 2015). The factors that play an important role in electrodeposition are the nature of the metal, pH, temperature, salt concentration, applied potential, electrodeposition time, *etc.*

The nature of the metal plays the most crucial role in the electrodeposition, leading to differential nucleation, growth kinetics, size, and number of ND per unit area. The pH of the electrolyte solution also influences the precipitation and decomposition of the salts, thus determines the uniformity of the ND deposition over the electrode surface. An increase in the electrolyte temperature leads to higher electrodeposition. The higher precursor salt concentration leads to a higher concentration of metal ions in the electrolyte solution, which leads to higher deposition as well as a fast rate of deposition. With the increase in the electrodeposition time, there is an increase in the amount of material deposited over the electrode surface. A general scheme of metallic dendrite growth is shown in figure 1.3.

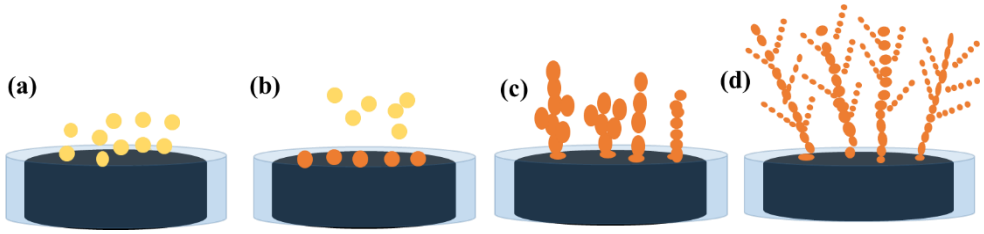

Figure 1.3. shows the different stages of dendrite growth by direct electrodeposition in a solution containing precursor salts: (a) Precursor molecule approach the

electrode surface, (b) Nucleation of the dendrite, (c) Further aggregation leads to primary branch formation, and (d) Formation of secondary and tertiary branches, leading to fern-like morphology.

4.3. Enzyme mimicking electrochemical biosensing using monometallic dendrites

The catalytic activity of monometallic dendrites is applied for the sensitive detection of analytes by direct electron transfer principle. Au monometallic dendrites (AuND) are well characterized for their ability to facilitate hydrogen and oxygen evolution reactions, also can be used for the biosensing of several analytes. Shu et al., developed the AuND structure directly over the GCE using -0.3 V in a 10 mM of $HAuCl_4$ in 0.1 M KCl solution for 3600 s (Shu et al. 2014). The fabricated surface was found to detect glucose in the range of 0.1 – 25 mM with a LOD of 0.05 mM, even in the presence of interfering molecules like ascorbic acid, uric acid, and acetaminophen. Heli and Amirizadeh also developed an AuND electrode, which they mentioned as a “pine-like structure”, by electrodepositing Au over a gold disk working electrode in presence of H_2SO_4 and 150 mmol L^{-1} of histidine (Heli and Amirizadeh 2016). The applied potential was 0 mV for a duration of 600s, and the sensor was able to detect glucose by amperometric method in the range of 20 to 240 µmol dm^{-3} and achieved a LOD of 3.39 µm dm^{-3}. Hau et al., developed another AuND structure over an FTO coated glass electrode for glucose sensing (Hau et al. 2017). They used 3-amino-propyl-tri-ethoxy-silane (APTS) (0.1 vol %) as a capping agent over the [1 1 0] and [1 0 0] facet for the anisotropic growth of [111] facet. This resulted in a [1 1 1] facet dominated AuND surface. The sensor was found to detect glucose in the range of 5 to 50 µM and LOD of 5µM. Ag, another novel metal is also a good candidate for dendrite development. Gutes et al., developed Ag dendrite

(AgND) by galvanic replacement reaction and noted its excellent SERS activity, which can be further used in biosensing (Gutés et al. 2010). Zhong et al., AgND on a GO film by using a double pulse electrochemical method for H_2O_2 sensing (Zhong et al. 2013). The sensor can detect H_2O_2 in the LDR of 2 x 10^{-5}–1 x 10^{-2} M, and with a LOD of 3 x 10^{-6} M. Zhang et al., developed another AgND electrode on a Cu rod for H_2O_2 and glucose detection, where they achieved an LDR of 0.2-19.2 mM and a LOD of 0.1 µM for H_2O_2 sensing (Zhang et al. 2013). The sensor can also detect glucose in the LDR of 0.02-7.4 Mm, and with a LOD of 0.1µM respectively. Wen et al., developed an innovative way to grow AgND over a waste DVD plate (Wen et al. 2013). They used a multi-potential step scan to electrodeposit AgND over the DVD, where a layer of previously present Ag layer catalyzes the growth of AgND formation. The sensor can detect H_2O_2 in the LDR of 5.88 x 10^{-7}–6.73 x 10^{-5} mol L^{-1}. The sensor also achieved a LOD of 2 x 10^{-7} mol L^{-1}. Pt, another excellent catalyst, was also used for monometallic dendrites development and found to be electrochemically active (El-Nagar et al. 2019).

Copper (Cu) is used as an electrocatalyst for multiple commercially important reactions. Zhang et al. developed a CuND structure, where DEA (diethanolamine) was used for uniform growth (Zhang et al. 2008). The sensor was able to detect L-tyrosine in the range of 0.2 - 500 µM, and a LOD of 0.1 µM. Kim et al. developed a non-enzymatic glucose sensor on a copper sulfate (CuS) dendrite (Kim et al. 2017). The dendrite was developed over Ni foam and treated with thiourea. The sensor shows an LDR of 0.001-4.9 mM, and a LOD of 0.05 µM, respectively. Like Cu, electrodeposited Zn dendrites are found to be electrically and catalytically more active (López and Choi 2006).

Monometallic dendrites offer a unique set of catalytic and conducting properties, based on the nature of the contributing metals. However, the incorporation of two or more metals in the dendritic structure may offer additional property due to their synergistic effect.

4.4. Enzyme mimicking electrochemical biosensing using Bi-metallic dendrites

Bimetallic/ multi-metallic dendrites are prepared by modifying the precursor elements during synthesis without altering its shape and size. The bi/ multi-metallic dendrites often exhibit materials properties other than their monometallic dendrites. Like Au based monometallic dendrites, Au based bimetallic dendrites are well characterized for their electrocatalytic and optical property (Zhang et al. 2009; Wang et al. 2016). Li et al. developed an ionic liquid assisted AuPd bimetallic dendrite for sensing of H_2O_2 (Li et al. 2013). Qui et al. developed CuNi dendritic material over a Cu foil by optimizing different applied potential to get a highly active sensing surface. The sensor was able to detect glucose with a LOD of 4.8×10^{-5} M (Qiu et al. 2007). Tong et al., also developed a CuNi electrode over a titanate thin film and used it to detect glucose in the range of a LOD of 3.5×10^{-7} M, respectively. Noh et al. developed a bimetallic Cu-Co dendritic electrode capable of detecting glucose and H_2O_2 in human serum samples (Noh et al. 2012a). They showed that the co-electrodeposited Cu-Co electrode was more catalytically active than the bimetallic electrodes where the control Cu//Co or Co//Cu electrode were formed by depositing Cu over Co layer or Co over Cu layer, respectively. The electrode was able to detect glucose in the range of 0.5-1400 µM, and LOD of 0.1 µM. The sensor exhibited a LDR of 1 µM-11 mM, and a LOD of 0.75 µM for H_2O_2 detection. Jung et al., developed a $Ni(OH)_2$@Cu dendritic electrode by depositing nickel hydroxide layer

over a layer of Cu electrode (Jung et al. 2014). The dendritic modified electrode was able to detect glucose in the range of 1-4500 µM, and a LOD of 0.24 µM with a response time of 2 s. Like bimetallic dendrite, multi-metallic dendrites are also being developed for their unique catalytic activity. However, the formation of multi-metallic dendrites and its application in biosensing applications is not well understood. In combination with other nanoparticles or carbon nanomaterials, the dendrites can be used for more biosensing activities.

4.5. Electrochemical biosensing using composites of metallic dendrites

Both mono- and bimetallic dendrite exhibit excellent electrochemical catalytic and sensing activity. However, the metallic dendrites lack functional groups for the immobilization of biorecognition elements. The addition of other nanomaterials and the use of the functionalization chemistry, allow the sensing surface not only to attach biorecognition elements but also to impart higher catalytic activity. However, the research in this domain of metallic dendrites in biosensing is very little explored. In the next section, we have mentioned the recent development of biosensors using metallic dendrites and their composites to develop sensitive biosensors.

Naveen et al. developed an AuNi electrode over an electrodeposited film of pTTBA the detection of H_2O_2 in the living cells (Naveen et al. 2016). The sensor achieved a very low LOD of 0.5 nM with three LDR of 5-40 nM, 80-30 µM, and 200-2.5 mM. Shen et al. developed a glycoprotein biosensor by modifying an AuND with a self-assembled monolayer (SAM) of 4-mercapto phenylboronic acid (MPBA) (Shen et al. 2015). The boronate group of the SAM can form a covalent bond with the cis-diol group of a glycoprotein forming a 5- or 6-membered cyclic esters in an alkaline aqueous solution. This chemistry can be further used to form a reusable biosensor as

the bond gets dissociated when introduced to acidic solutions. They used HRP as a model glycoprotein molecule, where the LDR of the sensor was found to be 2.5-2500 nM with a LOD of 0.5 nM. Torkashvand et al. used a composite of molecularly imprinted polymers and MWCNT to develop AgND and used for the sensing of ceftazidime, where the sensor achieved a LOD of 0.55 nM (Torkashvand et al. 2016). Seo et al. inserted a gold binding gene on the major coat protein of M13 (named further as M134E) and shown that electrodepositing Au in presence of the mutant M134E was yielding dendrite like structure, which the wild type M13 failed to do. The 4E peptides facilitate the electrochemical growth of AuND and used the system for the selective determination of nitrite (Seo et al. 2017). The electrode was able to sense nitrite in the LDR of 1-800 µM.

The above-mentioned sensing electrodes exhibit excellent catalytic property and are used as non-enzymatic sensing of both electroactive and electro-inactive molecules. However, the dendrites lack the presence of functional groups required for the immobilization of BREs for the sensing of various analytes. So, wet chemistry approaches and other functionalized NMs are used to immobilize BREs like an antibody, peptides, and DNA probes for sensitive detection of biological molecules like proteins, nucleic acid sequences, enzyme-substrate, *etc*. The specificity of BREs such as enzymes, aptamer, and antibody towards their analyte is unmatched by any other molecules, which is used for the construction of biosensors. Wu et al, developed an AuND electrode modified with an enzyme, superoxide dismutase to amperometric detection of superoxide anion ($O^{\cdot -}_2$) (Wu et al. 2014). After the formation of AuND, the electrode was dipped in 1.5 mM cysteine solution for 30 min, to get a SAM layer of cysteine. The GCE/AuND/Cys was further used to

immobilize superoxide dismutase, and used for superoxide detection. An LDR of 0.05-440 µM and LOD of 2.1 nM was achieved by the sensor.

Shi et al. optimized the development of AuND, to which a thiolated capture DNA probe (c-DNA) was immobilized (Shi et al. 2013). If the target DNA sequence (t-DNA) was present in the sensing solution, it would bind to c-DNA. Methylene blue (MB) would bind to the anionic phosphate of dsDNA enhancing the amperometric signal, where more c-DNA would lead to larger signals. The sensor achieved a wide LDR of 50 aM-1 pM. Nazari-Vanani et al. developed another DNA biosensors using AuND and a SAM of a thiolated DNA probe for the detection of *Enterococcus faecalis* gene (Nazari-Vanani et al. 2018). They used toluidine blue (TB) as a redox marker, that binds on the dsDNA, indirectly indicating the concentration of target DNA in the sample. The sensor was able to sense the gene in the range of 1×10^{-17}-1.0×10^{-10} mol L^{-1} and with a LOD of 4.7×10^{-20} mol L^{-1}. Tang et al., developed an aptasensors on an AuND microstructure modified electrode with a thionine functionalized silica nanosphere as a signal molecule (Tang et al. 2012). The aptamer was immobilized on the AuND surface by forming a weak covalent bond and/or electrostatic adsorption. The sensor achieved a LOD of 0.001-600 ng mL^{-1} and a LOD of 0.5 ng mL^{-1}. For nucleic-acid sensing, the 3D dendritic structure offers a large surface for the immobilization of a higher number of nucleic acid probe leading to high LDR and LOD, as well functioning as an electron tunnel for signal generation.

Though the potential of developing an immunosensors using the metallic ND has lots of potential due to its larger active surface area for BREs immobilization as well the electron tunneling property leading to higher signal generation, the work done in this arena is very less. Valera et al., have developed of a poly (2-cyanoethyl) pyrrole

(PCEPy) coated AuND sensor for the detection of cholera toxin (Valera et al. 2019). An OH- of primary antibody is attached to the –NH group of conducting polymer surface, and capture the Cholera toxin in the solution. A secondary antibody and a tertiary ALP conjugated antibody was used for dual-recognition of the antigen, where an ALP substrate p-amino phenyl phosphate (pAPP) was used for the signal generation. The sensor achieved a LOD of 1 ng mL^{-1}. However, the drawback of the system is the uses of multiple antibodies, and of the enzyme-substrate. Mahato et al. developed a label-free immunosensor for the detection of ALP in serum samples with accuracy comparable to clinical testing (Mahato et al. 2020a). They developed a nano-dendrite system over a disposable SPCE electrode and used GO for the immobilization of anti-ALP by using EDC-NHS chemistry. The sensor achieved an LDR of 100–1000 U/L, and a LOD of 9.10 (±0.12) U/L. The metallic dendrites possess very high conducting and catalytic property which can be used for the development of sensitive biosensors. Metallic dendrites as a support matrix for BREs immobilization in conjugation with different other NM, for the development of a wide range of analytes. Figure 1.4 highlights the use of metallic dendrite biosensor for the detection of different biological molecules.

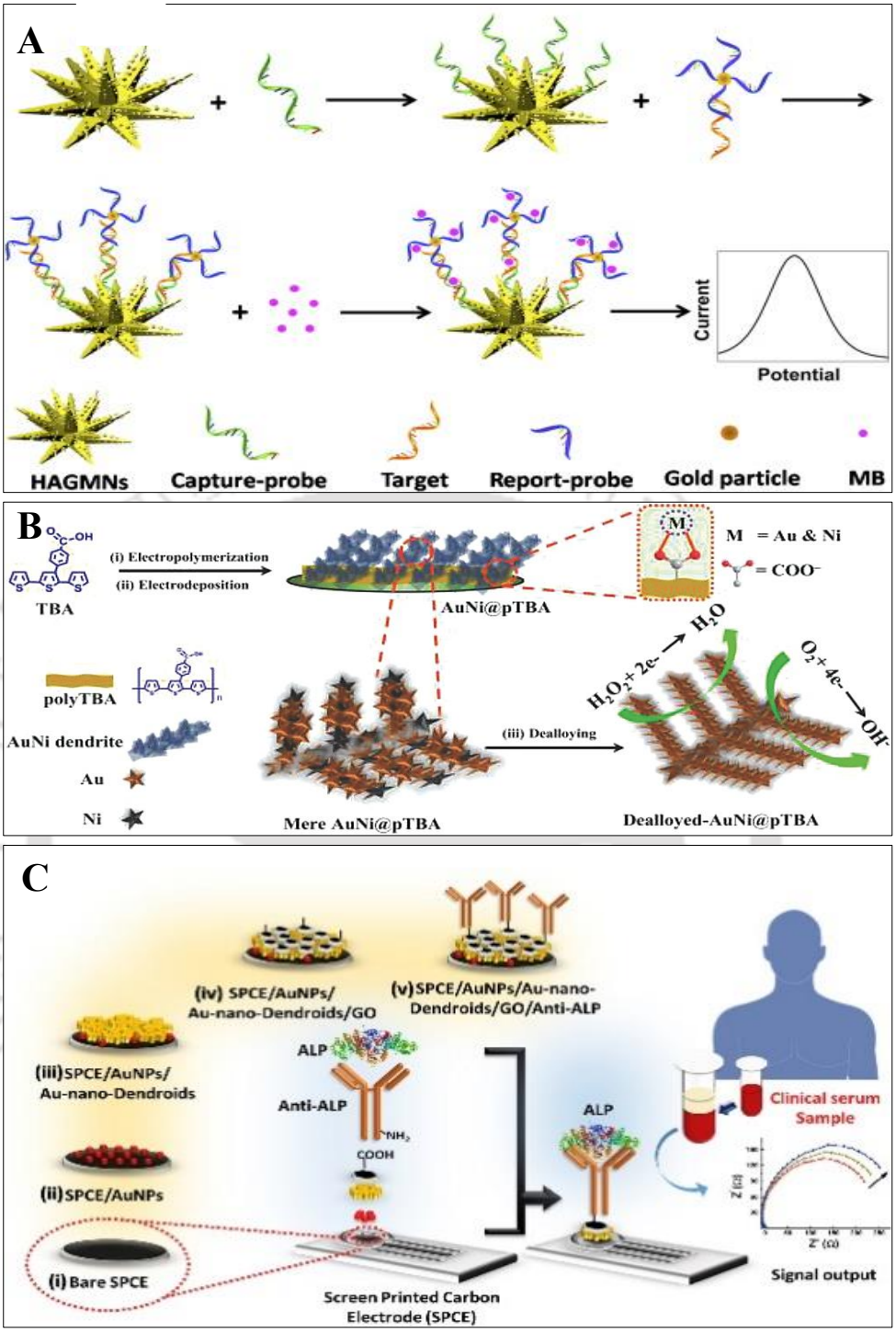

Figure 1. 4. shows the possibilities of using metallic dendrites in sensing surface for the sensitive detection of proteins, nucleic acid, free radicals, *etc.* (A) A DNA biosensor developed by direct functionalization of Au dendrite (Shie et al. 2013), reused with permission from *Elsevier*; (B) Development of dendrite -polymer nanocomposite for hydrogen peroxide detection in living cells (Naveen et al. 2016), reused with permission from *Wiley*; and (C) a GO-Au dendrite composite for the

label-free detection of a protein in human serum (Mahato et al. 2019), image reused with permission from *Elsevier*.

5. Electrochemical biosensing probe development

For the electrochemical biosensing, the probe is specifically developed based on the type of sensing strategies and nature of the analyte. The sensor probe is developed carefully using various surface modification strategies to give stable and sensitive sensing (Chandra 2016). The first task of developing a sensing probe is to choose the right support matrix. Over the support matrix, all the nano-fabrication and biomaterial immobilization for sensing activity is done. Paper, graphite, carbon paste, glassy carbon electrode, screen printed electrodes, *etc.* are normally used for biosensing applications based on their material and electrical properties (Dekanski et al. 2001; Lee et al. 2018). For electrochemical sensing, support matrices that can facilitate charge transfer like ITO and GCE are used, over which sensor is fabricated with nanomaterials to enhance their conductivity. Nanomaterials, owing to their optoelectronic property are used in the sensing probe development for enhancing the accuracy of the sensors. The developed probe is also functionalized with very specific bio-recognition element (BRE) based on the nature of the analyte of interest. For the detection of the protein biomarkers, antibodies are used due to their specific antigen-antibody interactions (Mahato et al. 2020b). Recently, aptamers are also being used to detect proteins, as the aptamers are more temperature resistant than proteins (Zhou et al. 2014). Nucleic acid probes are used on the transducer surface to detect a complementary nucleic acid sequence of clinical importance based on the Watson-Crick base pairing rule, and redox-active molecules are generally used to enhance the signal(Fan et al. 2003; Xiao et al. 2006). Another important BRE, enzymes are used to detect specific molecules where the catalysis process or the

product generates the signal (Mahato and Chandra 2019). These BREs are immobilized on to the transducer surface by physical adsorption, or by using chemical modifications. The covalent modifications are preferred over the physical methods due to its stability and specificity (Sapsford et al. 2013). Based on the nature of the nanoparticle used in the sensing surface a suitable method of BREs conjugation is followed like using a simple conjugation chemistry, or using polymers/ quantum dots/ carbon nanomaterials *etc.* (Sapsford et al. 2013). These nanomaterials are used not only for bio-conjugation but also for the signal amplification by bridging the reaction sites and the electrode. The redox mediators are used as shuttle molecules in chemical reactions for enhancing the signal, especially where the analyte concentration is very low (Kumar et al. 2019).

6. Characterization of electrochemical biosensing probe

The physical and chemical characterization of the developed nanomaterials and sensor probe is required to evaluate its optical, mechanical, electrical, and catalytic properties (Rao and Biswas 2009). UV-Vis spectrophotometer is a facile and low-cost instrument usually used as the first phase of material characterization for the optimization of the NM synthesis, based on the intensity and position of characteristics absorption maxima. Based on Beer-Lamberts law and its derivative forms, UV-Vis spectroscopy is used for the determination of concentration as well as the optical properties, size, agglomeration, shape of the NM(Kaufmann 2003). However, the exact size and morphology of the NM can be visualized by scanning electron microscopy (SEM), transmission electron microscopy (TEM), and atomic force microscopy (AFM) at higher magnification. SEM images are produced by the back-scattered electrons when a high energy electron beam is focused on a sample surface. The advantages of using SEM is to get a detailed image of sample

topography of NM, bulk materials, films, foils, *etc.* SEM can cover a large surface area under its focus with a resolution between <1 nm and 20 nm. However, SEM is not suitable to image individual atoms, whereas TEM with a resolution of 0.1 nm used for atomic-level visualization where the high energy electron beam is allowed to pass through a sample (Naito et al. 2018). The difference in contrast in comparison to the background is used to study the NM shape and size. In TEM, selected area electron transfer (SAED) analysis is performed to study the crystal lattice formation (Park et al. 2004). Although electron microscopes are very powerful in the visualization of NM, the high energy beam can damage some samples. AFM analysis is performed to study morphology and structural properties of such NM. Surface profiling by AFM involves a microcantilever scanning the surface topography with a very high resolution of 0.2 nm and used to study surface charge distribution, surface magnetization, and hardness of the surface (Samorì 2004).

Another technique comparable to AFM, scanning tunneling microscopy (STM) is used to measure the electronic state and morphology of the NM. Energy-dispersive X-ray spectroscopy (EDX), one technique usually associated with SEM and TEM, used for elemental analysis and chemical characterization of the NM (Goldstein et al. 2017). Another technique, X-ray photoelectron spectroscopy (XPS) is also used to study the electronic structure, elemental composition, oxidation states, ligand binding to NM(Naito et al. 2018). The working principle behind XPS is the photoelectric effect, mostly used to study the interaction of NM with biological samples. Another X-ray based characterization technique, X-ray diffraction (XRD) is used to determine the crystalline property of NM i.e. nature of phase, lattice parameters, crystal grain size, *etc.* (Naito et al. 2018). It is one of the most extensively used techniques, where the peak size and intensity is correlated with

ICDD (International Center for Diffraction Data) or JCPDS (Joint Committee on Powder Diffraction Standards) database to decipher the crystal structure. However, XRD is not suitable to study amorphous NM, and the NM with size <3 nm (Rao and Biswas 2009). Fourier transform infrared spectroscopy (FTIR) is another technique used to study the surface composition and ligand binding of NM. A 4000-500 cm^{-1} wavelength spectrum is generated corresponding to the strength and nature of the specific functional groups (Smith 2011; Tsai et al. 2011). Another highly sophisticated instrument, complementary to FTIR is Raman spectroscopy, which operates based on the inelastic scattering of the light, used for a lot of purposes, especially to study carbon NM (Dresselhaus and Eklund 2000; Ferraro 2003). Raman spectroscopy is used to study mechanical strain, degree of crystallinity, the effect of physical parameters like temperature and pressure on the NM (Tian et al. 2002). Magnetic properties such as diamagnetism, para-magnetism, ferromagnetism, ferri-magnetism, *etc*., can be studied by vibrating sample magnetometer (VSM).

After studying the physical properties of the nanomaterial and sensor probe, the electrochemical characterization is performed using the following techniques.

Cyclic voltammetry (CV), is a voltammetric technique where a range of potential is applied, and the resulting current is measured to sense the analyte (Kissinger and Heineman 1983; Elgrishi et al. 2018). In CV, the voltage is swept between two fixed potentials (V_1 to V_2) and then rescanned back from V_2 to V_1. The resultant measurements are plotted as current vs. potential, where the plot is known as a voltammogram. CV is useful to know the redox potential of an analyte and the chemical rate constant of analytes. In the forward scan, when the applied voltage approaches the redox potential of the analyte, the current will increase and as the

applied potential went pass the redox potential, the current will decrease forming a distinct peak. From the peak value of current, the concentration of the analyte can be measured. Important factors that affect CV analysis are the scan rate (V_2-V_2 / t_2-t_1), the electrode surface, pH, temperature, *etc*.

Another voltammetric technique, differential pulse voltammetry (DPV) is a more sensitive technique than the CV due to the application of differential pulse and hence used for trace analysis. In DPV, a series of pulses are applied at regular intervals with a staircase pattern, and the current is measured just before the change in potential. The current differences between the successive pulses are measured and plotted as a function of potential (Bard et al. 1980).

Chronoamperometry, another voltammetric technique, a square wave potential is applied and the analyte is measured after attaining a steady-state current. The principles of chronoamperometry are based on the expansion/reduction of the diffusion layer at the electrode surface which can be explained by the Cottrell equation (Bard et al. 1980):

$$I = n F A c_0 \sqrt{\frac{D}{\pi t}} \qquad \text{...equation 3}$$

Where I stand for current, n is the number of electrons transferred per molecules, F is faraday's constant, A is electrode area, c_0 is analyte concentrations, D is diffusion coefficient, and t stands for time. The current response depends on the rate of diffusion of the analyte to the electrode surface. Chronoamperometry is one of the most trusted electrochemical method used for the real-time monitoring of biological samples.

The electrochemical impedance spectroscopy (EIS) is used to study the intrinsic material property, conductivity, capacitance, and resistance of an electrochemical system (Bard et al. 1980). The impedance is measured as a function of angular frequency (ω) combines both the real (Z_r) and imaginary (Z_i) components of impedance i.e. electrical resistance and reactance. EIS is measured by varying the excitation frequency (*f*) of the applied potential in a range of frequency, and measuring the sum of Z_r and Z_i, as shown:

$$Z(j\omega) = \frac{U(j\omega)}{I(j\omega)} = Zr(\omega) + j\,Zi(\omega) \quad \text{...equation 4}$$

There are some other complementary biosensing techniques used along electrochemical biosensors are surface plasmon resonance (SPR), waveguided based techniques, ellipsometry, scanning probe microscopy, *etc*. for various purposes.

7. Stepwise evaluation of analytical performance for electrochemical biosensors

The clinical possibilities of biosensors are evaluated by some analytical parameters such as linear dynamic range, the limit of detection, sensitivity, selectivity, response time, recovery time, reproducibility, stability, *etc*., which tells us whether the developed biosensor can be applied for real sensing or not.

7.1. Linear dynamic range (LDR)

LDR is a range where the difference in signal response corresponding to two different concentrations of an analyte is proportional to the difference in concentration of samples. Usually, these responses appear to be in a straight line in a calibration plot. Most biosensors eventually follow a nonlinear pattern as they attain an increased concentration of analyte concentration. So it is important to know the upper limit of a sensor to avoid errors in calculation. The LDR can be

optimized/altered by using recognition elements with different degrees of affinity towards its analyte (Marvin et al. 1997; Yamazaki et al. 2000; Drabovich et al. 2007; Andersson et al. 2009). A wider LDR of a biosensor can be used to measure a more number of concentrations, and often designed to cover the clinically important concentrations.

7.2. Limit of quantification (LOQ)

LOQ refers to the minimum amount of analyte that can be detected by a biosensor. LOQ can be explained in equation 5.

$$LOQ = 10\ SD\ Blank/\ Slope \quad \text{…equation 5}$$

Where SD Blank is the standard deviation of blank response, and the slope refers to the sensitivity of the sensor.

7.3. Limit of detection (LOD)

The minimum amount of analyte that can generate a signal response in a biosensor is called as LOD. LOD is the minimum concentration of analyte that can be theoretically detected by a biosensor as

$$LOD = 3\ SD\ Blank/\ Slope \quad \text{…equation 6}$$

Where SD Blank is the standard deviation of blank response, and the slope refers to the sensitivity of the sensor.

LOD of a biosensor also depends on various factors other than sensitivity like mass transport and orientation of the biorecognition element over the transducing surface, *etc*.(Lifson et al. 2014; Guider et al. 2015; Montes et al. 2015). Biosensors are thus designed to attend lower LOD and a wider LDR for better biosensing activity, by surface modifications and use of nanomaterials.

7.4. Selectivity

The ability of a biosensor to recognize an analyte with precision, and at the same time discriminate against other non-specific molecules is an important criterion for the success of a biosensor. Enzymes, DNA probes, aptamers are used to enhance the selectivity of a biosensor due to high affinity towards the substrate or complementary strands of DNA. To enhance the selectivity of a biosensor based on direct electron transfer, a particular set of parameters are applied such as selected potential range, pH of the solution, inhibitor molecules, current density to catalyze the redox reaction of a particular molecule.

7.5. Sensitivity

The ability of a biosensor to detect the smallest fluctuation of an analyte of interest with precision is termed as its sensitivity. Mathematically it is represented as a ratio of the change in analyte concentration to the change in the corresponding signal.

Sensitivity = Slope of the regression line = $\frac{YP-YQ}{XP-XQ}$ …equation 7

X_P and X_Q are two points of the analyte concentration, and Y_P and Y_Q are the signal value at the corresponding points.

The higher the value of the regression slope, the higher is the sensitivity of the biosensors. A higher value of sensitivity reflects a larger change in the signal value in response to a smaller variation in analyte concentration. This helps to resolute two close concentrations of analytes from one another. Nanomaterials are chosen for (i) fast electron transfer of an electron between electrode and target, (ii) enhance electro-catalysis, (iii) fast diffusion of the analyte to the electrode surface, (iv) reduce fouling effects, and (v) signal amplification(Sharma et al. 2018). All these factors contribute to enhancing the sensitivity of a biosensor.

7.6. Response time

The time a biosensor requires to generate a quantifiable signal corresponding to an analyte concentration is known as response time. The response time of direct electron transfer based biosensors comes in some seconds (Purohit et al. 2019b), whereas the biosensors based on enzymes or other biorecognition molecules varies from some seconds to some minutes (Mahato and Chandra 2019).

7.7. Recovery time

The time a biosensor takes to initiate the next biosensing after completing one cycle of analyte detection. Most of the time, the recovery time reflects the fast oxidation-reduction catalysis by the nanomaterials used in the biosensor.

7.8. Real sample analysis

After evaluating all the above mentioned analytical parameters, the real sample analysis was performed in various samples containing analytes of interest. When the biosensing of analyte is not possible due to the complexity or some other factors of the biological matrix, it is filtered or processed to perform the biosensing. In some special cases, where the analyte is unavailable or gives rise to inconsistent in the signal, spike –recovery method or standard addition method is followed to determine the concentration of the analyte in the real sample matrix.

7.8.1. Standard addition method

The intrinsic behaviors of the real samples sometimes interfere with the signal generation by biosensors called matrix effects. In such cases, a calibration plot is developed using the standard concentration of the analyte in the real samples. Then this calibration plot is extrapolated by tracing the points of a standard addition to

find the unknown concentration of an analyte in the real samples (Bader 1980; Noh et al. 2012b).

7.8.2. Spike and recovery method

The presence of interfering molecules can hinder the signal generation in the real samples. A significant variation in signal response in the real sample can be interpreted as the presence of interfering molecules in the real samples(Sun and Liu 2018). A known concentration of analyte is spiked into the sensing matrix and a signal of that concentration is measured. Mathematically % recovery in real samples is calculated as follows:

$$\% \text{ Recovery} = \text{Observed} - \text{Neat} / \text{Expected} \times 100 \quad \text{...equation 8}$$

Where the observed refers to the value of analyte concentration obtained after spiking in the samples; Neat refers to the value of analyte concentration present in the sample prior to spiking; Expected signifies the concentration of the analyte sample spiked into the real samples.

A very high % recovery signifies a false positive result, where a signal is generated by the biosensor even in the absence of analyte molecules. Whereas, if the % recovery is very less, it refers to the possible interfering effect of the real sample matrix. The analyte molecule is not being present in its form due to reaction with other molecules present in the real sample.

8. Objectives and goals of the study:

The goal of the whole work is to develop electrochemical biosensors to sensitively detect various clinically important analytes. We tried to achieve the widest dynamic range and the lowest possible detection limit of the analyte covering the entire range found in healthy as well as diseased conditions for clinical significance. We tried to

incorporate metallic dendrites for its electro-catalysis activity to monitor electroactive molecules, and as a highly conducting material with the high surface area for immunosensing application. Other nanomaterials are also used in this work for their material and electrical property. The developed sensors were attempted to detect the analytes in real samples (e.g. whole blood, urine, serum) mimicking clinical diagnostics. The entire work mentioned in this thesis aimed towards the development of electrochemical biosensors utilizing the nanomaterials and for ultrasensitive detection of clinical biomarkers keeping in mind the probability to develop a miniaturized version of these devices further use in clinical settings.

The objectives are as follows:

Objective 1:

Sputtering assisted enhanced peroxidase like activity of a dendritic nanochip for label-free hydrogen peroxide detection in blood sample

Objective 2:

Direct co-electrodeposition of hierarchical novel bimetallic Au-Cu dendritic nanostructures for biomolecular sensing in human urine

Objective 3:

Engineered Gold Dendrites and a Multi-Walled Carbon Nanotube Nanohybrid for Detection of Acetaminophen in Human Urine Samples

Objective 4:

Electrochemical immunosensor based on gold nanodendrites/ chitosan-reduced graphene oxide for label free detection of cancer biomarker in human serum sample.

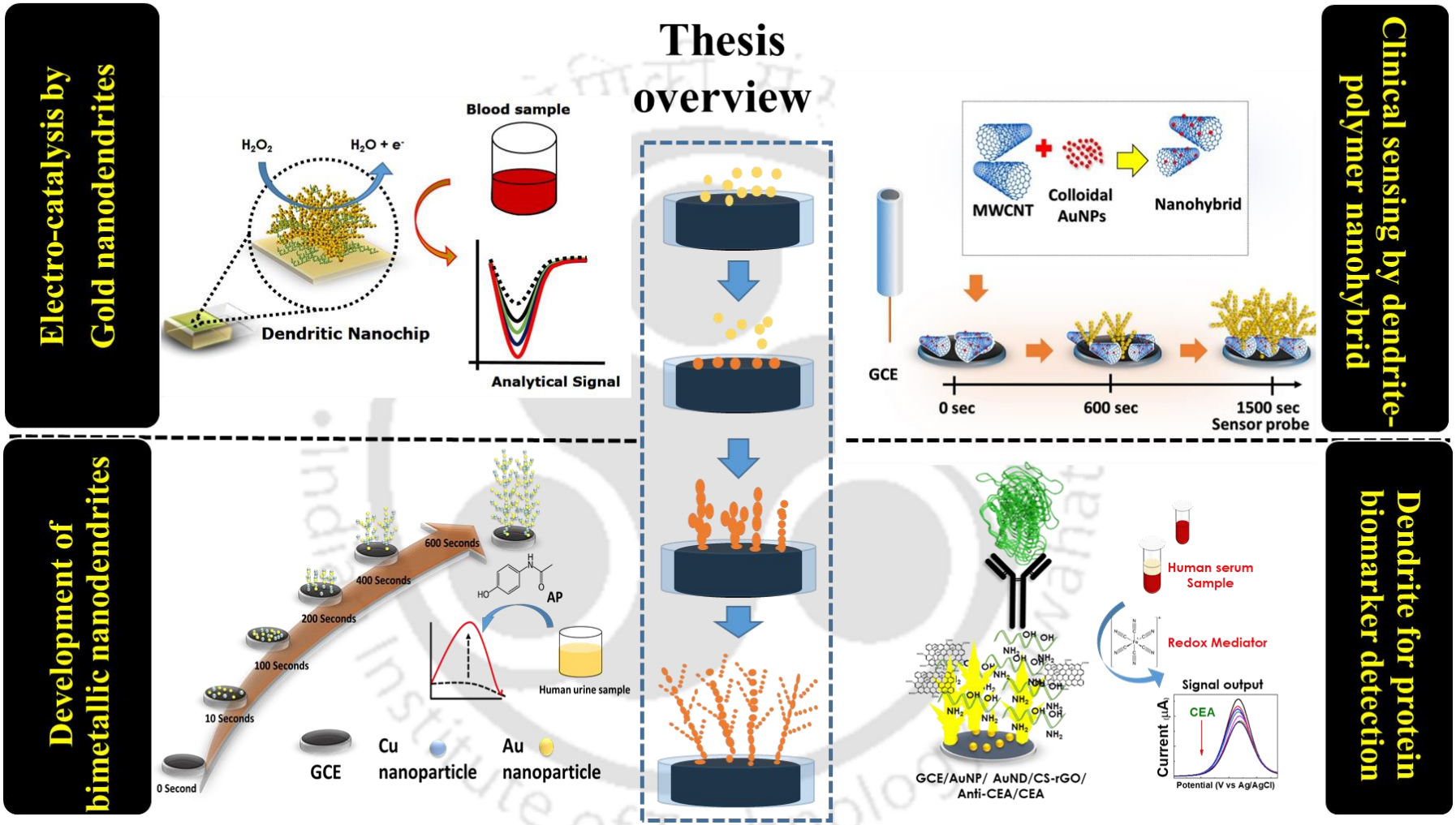

Fig 1.5. Pictorial representation of the work done in the thesis.

References:

Al-Bat'hi SAM (2015) Electrodeposition of Nanostructure Materials. Electroplat Nanostructures 3–26.

Andersson O, Nikkinen H, Kanmert D, Enander K (2009) A multiple-ligand approach to extending the dynamic range of analyte quantification in protein microarrays. Biosens Bioelectron 24:2458–2464

Arlett JL, Myers EB, Roukes ML (2011) Comparative advantages of mechanical biosensors. Nat Nanotechnol 6:203–215.

Bader M (1980) A systematic approach to standard addition methods in instrumental analysis. J Chem Educ 57:703.

Bakthavatsalam R, Ghosh S, Biswas RK, et al (2016) Solution chemistry-based nano-structuring of copper dendrites for efficient use in catalysis and superhydrophobic surfaces. RSC Adv 6:8416–8430.

Baranwal A, Kumar A, Priyadharshini A, et al (2018) Chitosan: An undisputed bio-fabrication material for tissue engineering and bio-sensing applications. Int J Biol Macromol 110:110–123.

Bard AJ, Faulkner LR, Leddy J, Zoski CG (1980) Electrochemical methods: fundamentals and applications. wiley New York

Barrès R, Zierath JR (2016) The role of diet and exercise in the transgenerational epigenetic landscape of T2DM. Nat Rev Endocrinol 12:441

Barriere SL (2015) Clinical, economic and societal impact of antibiotic resistance. Expert Opin Pharmacother 16:151–153.

Bauer CG, Eremenko A V, Ehrentreich-Förster E, et al (1996) Zeptomole-detecting biosensor for alkaline phosphatase in an electrochemical immunoassay for 2, 4-dichlorophenoxyacetic acid. Anal Chem 68:2453–2458.

Bindra DS, Zhang Y, Wilson GS, et al (1991) Design and in vitro studies of a needle-type glucose sensor for subcutaneous monitoring. Anal Chem 63:1692–1696

Borisov SM, Wolfbeis OS (2008) Optical Biosensors. Chem Rev 108:423–461.

Brajter-Toth A, Chambers J (2002) Electroanalytical Methods of Biological Materials. CRC Press

Braun T, Ghatkesar MK, Backmann N, et al (2009) Quantitative time-resolved measurement of membrane protein--ligand interactions using microcantilever array sensors. Nat Nanotechnol 4:179

Chandra P (2016) Nanobiosensors for Personalized and Onsite Biomedical Diagnosis, the Institution of Engineering and Technology, Michael Faraday House

Cheng TM, Huang TK, Lin HK, et al (2010) (110)-Exposed gold nanocoral electrode as low onset potential selective glucose sensor. ACS Appl Mater Interfaces 2:2773–2780.

Clark Jr LC, Lyons C (1962) Electrode systems for continuous monitoring in cardiovascular surgery. Ann N Y Acad Sci 102:29–45

Cohen ML (2000) Changing patterns of infectious disease. Nature 406:762

Colizza V, Barrat A, Barthélemy M, Vespignani A (2006) The role of the airline transportation network in the prediction and predictability of global epidemics. Proc Natl Acad Sci 103:2015–2020

Curto VF, Fay C, Coyle S, et al (2012) Real-time sweat pH monitoring based on a wearable chemical barcode micro-fluidic platform incorporating ionic liquids. Sensors Actuators B Chem 171:1327–1334

Damborský P, Švitel J, Katrlík J (2016) Optical biosensors. Essays Biochem 60:91–100.

Davis F, Higson SPJ (2007) Polymers in biosensors. In: Biomedical Polymers. Elsevier, pp 174–196

Dekanski A, Stevanović J, Stevanović R, et al (2001) Glassy carbon electrodes. Carbon N Y 39:1195–1205.

Doria G, Conde J, Veigas B, et al (2012) Noble Metal Nanoparticles for Biosensing Applications. Sensors 12:1657–1687.

Drabovich AP, Okhonin V, Berezovski M, Krylov SN (2007) Smart aptamers facilitate multi-probe affinity analysis of proteins with ultra-wide dynamic range of measured concentrations. J Am Chem Soc 129:7260–7261

Dresselhaus MS, Eklund PC (2000) Phonons in carbon nanotubes. Adv Phys 49:705–814.

Du Y, Dong S (2017) Nucleic Acid Biosensors: Recent Advances and Perspectives. Anal Chem 89:189–215.

El-Nagar GA, Muench F, Roth C (2019) Tailored dendritic platinum nanostructures as a robust and efficient direct formic acid fuel cell anode. New J Chem 43:4100–4105.

Elgrishi N, Rountree KJ, McCarthy BD, et al (2018) A Practical Beginner's Guide to Cyclic Voltammetry. J Chem Educ 95:197–206.

Etzioni R, Urban N, Ramsey S, et al (2003) Early detection: The case for early detection. Nat Rev cancer 3:243

Fan C, Plaxco KW, Heeger AJ (2003) Electrochemical interrogation of conformational changes as a reagentless method for the sequence-specific detection of DNA. Proc Natl Acad Sci U S A 100:9134–9137.

Fan X, White IM, Shopova SI, et al (2008) Sensitive optical biosensors for unlabeled targets: A review. Anal Chim Acta 620:8–26.

Ferraro JR (2003) Introductory raman spectroscopy. Elsevier

Fortier G, Brassard E, Belanger D (1990) Optimization of a polypyrrole glucose oxidase biosensor. Biosens Bioelectron 5:473–490

Frew JE, Hill HAO (1987) Electrochemical biosensors. Anal Chem 59:933A--944A

Gautreau A, Barrat A, Barthélemy M (2008) Global disease spread: Statistics and estimation of arrival times. J Theor Biol 251:509–522.

Goldstein JI, Newbury DE, Michael JR, et al (2017) Scanning electron microscopy and X-ray microanalysis. Springer

Guider R, Gandolfi D, Chalyan T, et al (2015) Sensitivity and Limit of Detection of biosensors based on ring resonators. Sens Bio-Sensing Res 6:99–102.

Gutés A, Carraro C, Maboudian R (2010) Silver dendrites from galvanic displacement on commercial aluminum foil as an effective SERS substrate. J Am Chem Soc 132:1476–1477.

Hau NY, Yang P, Liu C, et al (2017) Aminosilane-Assisted Electrodeposition of Gold

Nanodendrites and Their Catalytic Properties. Sci Rep 7:1–10.

Heli H, Amirizadeh O (2016) Non-enzymatic glucose biosensor based on hyperbranched pine-like gold nanostructure. Mater Sci Eng C 63:150–154.

Hilditch PI, Green MJ (1991) Disposable electrochemical biosensors. Analyst 116:1217–1220

Huang X, Liu Y, Chen K, et al (2014) Stretchable, wireless sensors and functional substrates for epidermal characterization of sweat. Small 10:3083–3090

Jenkins SH, Heineman WR, Halsall HB (1988) Extending the detection limit of solid-phase electrochemical enzyme immunoassay to the attomole level. Anal Biochem 168:292–299.

Jung H, Lee SH, Yang J, et al (2014) Ni (OH) 2@ Cu dendrite structure for highly sensitive glucose determination. RSC Adv 4:47714–47720

Kamran U, Heo Y-J, Lee JW, Park S-J (2019) Functionalized Carbon Materials for Electronic Devices: A Review. Micromachines 10:234.

Kaufmann EN (2003) Characterization of Materials, 2 Volume Set. Charact Mater 2 Vol Set, by Elt N Kaufmann (Editor), pp 1392 ISBN 0-471-26882-8 Wiley-VCH, January 2003 1392

Kim W Bin, Lee SH, Cho M, Lee Y (2017) Facile and cost-effective CuS dendrite electrode for non-enzymatic glucose sensor. Sensors Actuators, B Chem 249:161–167.

Kissinger PT, Heineman WR (1983) Cyclic voltammetry. J Chem Educ 60:702–706.

Krivacic RT, Ladanyi A, Curry DN, et al (2004) A rare-cell detector for cancer. Proc Natl Acad Sci 101:10501–10504.

Kuila T, Bose S, Khanra P, et al (2011) Recent advances in graphene-based biosensors. Biosens Bioelectron 26:4637–4648.

Kumar A, Purohit B, Maurya PK, et al (2019) Engineered Nanomaterial Assisted Signal-amplification Strategies for Enhancing Analytical Performance of Electrochemical Biosensors. Electroanalysis 31:1615–1629.

Kumar S, Pande S, Verma P (2015) Factor Effecting Electro-Deposition Process. Int J

Curr Eng Technol 5:

Lee VBC, Mohd-Naim NF, Tamiya E, Ahmed MU (2018) Trends in paper-based electrochemical biosensors: From design to application. Anal Sci 34:7–18.

Leth S, Maltoni S, Simkus R, et al (2002) Engineered Bacteria Based Biosensors for Monitoring Bioavailable Heavy Metals. Electroanalysis 14:35–42.

Li Z, Li R, Mu T, Luan Y (2013) Ionic liquid assisted synthesis of Au-Pd bimetallic particles with enhanced electrocatalytic activity. Chem - A Eur J 19:6005–6013.

Lifson MA, Basu Roy D, Miller BL (2014) Enhancing the Detection Limit of Nanoscale Biosensors via Topographically Selective Functionalization. Anal Chem 86:1016–1022.

Liu Y, Wang M, Zhao F, et al (2005) The direct electron transfer of glucose oxidase and glucose biosensor based on carbon nanotubes/chitosan matrix. Biosens Bioelectron 21:984–988

Liu Y, Yu X, Zhao R, et al (2003) Quartz crystal biosensor for real-time monitoring of molecular recognition between protein and small molecular medicinal agents. Biosens Bioelectron 19:9–19.

López CM, Choi K-S (2006) Electrochemical Synthesis of Dendritic Zinc Films Composed of Systematically Varying Motif Crystals †. Langmuir 22:10625–10629.

Luo M, Sun Y, Qin Y, et al (2018) Surface and Near-Surface Engineering of PtCo Nanowires at Atomic Scale for Enhanced Electrochemical Sensing and Catalysis. Chem Mater 30:6660–6667.

Mahato K, Chandra P (2019) Paper-based miniaturized immunosensor for naked eye ALP detection based on digital image colorimetry integrated with smartphone. Biosens Bioelectron 128:9–16.

Mahato K, Maurya PK, Chandra P (2018) Fundamentals and commercial aspects of nanobiosensors in point-of-care clinical diagnostics. 3 Biotech 8:1–14.

Mahato K, Nagpal S, Shah MA, et al (2019) Gold nanoparticle surface engineering strategies and their applications in biomedicine and diagnostics. 3 Biotech 9:57

Mahato K, Purohit B, Kumar A, Chandra P (2020a) Clinically comparable impedimetric

immunosensor for serum alkaline phosphatase detection based on electrochemically engineered Au-nano-Dendroids and graphene oxide nanocomposite. Biosens Bioelectron 148:111815.

Mahato K, Purohit B, Kumar A, Chandra P (2020b) Clinically comparable impedimetric immunosensor for serum alkaline phosphatase detection based on electrochemically engineered Au-nano-Dendroids and graphene oxide nanocomposite. Biosens Bioelectron 148:111815.

Marvin JS, Corcoran EE, Hattangadi NA, et al (1997) The rational design of allosteric interactions in a monomeric protein and its applications to the construction of biosensors. Proc Natl Acad Sci 94:4366–4371

Misawa N, Osaki T, Takeuchi S (2018) Membrane protein-based biosensors. J. R. Soc. Interface 15:20170952

Mobarki N, Almerabi B, Hattan A (2019) Antibiotic Resistance Crisis. Int J Med Dev Ctries 40:561–564.

Mol A (2000) What diagnostic devices do: The case of blood sugar measurement. Theor Med Bioeth 21:9–22.

Montes R, Bartrolí J, Baeza M, Céspedes F (2015) Improvement of the detection limit for biosensors: Advances on the optimization of biocomposite composition. Microchem J 119:66–74.

Muramatsu H, Dicks JM, Tamiya E, Karube I (1987) Piezoelectric Crystal Biosensor Modified with Protein A for Determination of Immunoglobulins. Anal Chem 59:2760–2763.

Naito M, Yokoyama T, Hosokawa K, Nogi K (2018) Nanoparticle technology handbook. Elsevier

Naveen MH, Gurudatt NG, Noh H-B, Shim Y-B (2016) Dealloyed AuNi Dendrite Anchored on a Functionalized Conducting Polymer for Improved Catalytic Oxygen Reduction and Hydrogen Peroxide Sensing in Living Cells. Adv Funct Mater 26:1590–1601.

Nazari-Vanani R, Sattarahmady N, Yadegari H, Heli H (2018) A novel and ultrasensitive electrochemical DNA biosensor based on an ice crystals-like gold nanostructure for

the detection of Enterococcus faecalis gene sequence. Colloids Surfaces B Biointerfaces 166:245–253.

Noh H, Lee K, Chandra P, et al (2012a) Application of a Cu–Co alloy dendrite on glucose and hydrogen peroxide sensors. Electrochim Acta 61:36–43.

Noh HB, Lee KS, Chandra P, et al (2012b) Application of a Cu-Co alloy dendrite on glucose and hydrogen peroxide sensors. Electrochim Acta 61:36–43.

O'Sullivan CK, Guilbault GG (1999) Commercial quartz crystal microbalances - Theory and applications. Biosens Bioelectron 14:663–670.

Ohkawa K, Cha D, Kim H, et al (2004) Electrospinning of chitosan. Macromol Rapid Commun 25:1600–1605

Organization WH (2016) World health statistics 2016: monitoring health for the SDGs sustainable development goals. World Health Organization

Paddle BM (1996) Biosensors for chemical and biological agents of defence interest. Biosens Bioelectron 11:1079–1113.

Pallela R, Chandra P, Noh HB, Shim YB (2016) An amperometric nanobiosensor using a biocompatible conjugate for early detection of metastatic cancer cells in biological fluid. Biosens Bioelectron 85:883–890.

Park J, An K, Hwang Y, et al (2004) Ultra-large-scale syntheses of monodisperse nanocrystals. Nat Mater 3:891–895

Parry C, Kent EE, Mariotto AB, et al (2011) Cancer Survivors: A Booming Population. Cancer Epidemiol Biomarkers Prev 20:1996–2005.

Purohit B, Kumar A, Mahato K, et al (2019a) Cancer Cytosensing Approaches in Miniaturized Settings Based on Advanced Nanomaterials and Biosensors. In: Nanotechnology in Modern Animal Biotechnology. Elsevier, pp 133–147

Purohit B, Kumar A, Mahato K, Chandra P (2020) Smartphone-assisted personalized diagnostic devices and wearable sensors. Curr Opin Biomed Eng 13:42–50.

Purohit B, Mahato K, Kumar A, Chandra P (2019b) Sputtering enhanced peroxidase like activity of a dendritic nanochip for amperometric determination of hydrogen peroxide in blood samples. Microchim Acta 186:658.

Qiu R, Zhang XL, Qiao R, et al (2007) CuNi dendritic material: Synthesis, mechanism discussion, and application as glucose sensor. Chem Mater 19:4174–4180.

Rao CNR, Biswas K (2009) Characterization of Nanomaterials by Physical Methods. Annu Rev Anal Chem 2:435–462. 6

Rodahl M, Höök F, Krozer A, et al (1995) Quartz crystal microbalance setup for frequency and Q-factor measurements in gaseous and liquid environments. Rev Sci Instrum 66:3924–3930.

Ronkainen NJ, Halsall HB, Heineman WR (2010) Electrochemical biosensors. Chem Soc Rev 39:1747.

Ruhm CJ (2017) Drug involvement in fatal overdoses. SSM - Popul Heal 3:219–226.

Saklayen MG (2018) The Global Epidemic of the Metabolic Syndrome. Curr Hypertens Rep 20:12.

Samorì P (2004) Scanning probe microscopies beyond imaging. J Mater Chem 14:1353–1366.

Sapsford KE, Algar WR, Berti L, et al (2013) Functionalizing Nanoparticles with Biological Molecules: Developing Chemistries that Facilitate Nanotechnology. Chem Rev 113:1904–2074.

Sauerbrey G (1959) Verwendung von Schwingquarzen zur Wägung dünner Schichten und zur Mikrowägung. Zeitschrift für Phys 155:206–222

Seo Y, Manivannan S, Kang I, et al (2017) Gold dendrites Co-deposited with M13 virus as a biosensor platform for nitrite ions. Biosens Bioelectron 94:87–93.

Sharma S, Singh N, Tomar V, Chandra R (2018) A review on electrochemical detection of serotonin based on surface modified electrodes. Biosens Bioelectron 107:76–93.

Shen D, Liu Y, Fang Y, et al (2015) A sensor for glycoproteins based on dendritic gold nanoparticles electrodeposited on a gold electrode and modified with a phenylboronic acid. J Solid State Electrochem 19:563–568.

Shi L, Chu Z, Liu Y, et al (2013) Facile synthesis of hierarchically aloe-like gold micro/nanostructures for ultrasensitive DNA recognition. Biosens Bioelectron 49:184–191.

Shu H, Cao L, Chang G, et al (2014) Direct electrodeposition of gold nanostructures onto glassy carbon electrodes for non-enzymatic detection of glucose. Electrochim Acta 132:524–532.

Siegel RL, Miller KD, Jemal A (2019) Cancer statistics, 2019. CA Cancer J Clin 69:7–34.

Smith BC (2011) Fundamentals of Fourier transform infrared spectroscopy. CRC press

Soleymani L, Fang Z, Lam B, et al (2011) Hierarchical nanotextured microelectrodes overcome the molecular transport barrier to achieve rapid, direct bacterial detection. ACS Nano 5:3360–6.

Song S, Wang L, Li J, et al (2008) Aptamer-based biosensors. TrAC Trends Anal Chem 27:108–117.

Suginta W, Khunkaewla P, Schulte A (2013) Electrochemical biosensor applications of polysaccharides chitin and chitosan. Chem Rev 113:5458–5479.

Sun J, Liu Y (2018) Matrix Effect Study and Immunoassay Detection Using Electrolyte-Gated Graphene Biosensor. Micromachines 9:142.

Tamayo J, Kosaka PM, Ruz JJ, et al (2013) Biosensors based on nanomechanical systems. Chem Soc Rev 42:1287–1311.

Tang J, Tang D, Niessner R, et al (2012) Hierarchical dendritic gold microstructure-based aptasensor for ultrasensitive electrochemical detection of thrombin using functionalized mesoporous silica nanospheres as signal tags. Anal Chim Acta 720:1–8.

Thévenot DR, Toth K, Durst RA, Wilson GS (2001a) Electrochemical biosensors: recommended definitions and classification1International Union of Pure and Applied Chemistry: Physical Chemistry Division, Commission I.7 (Biophysical Chemistry); Analytical Chemistry Division, Commission V.5 (Electroanalytical. Biosens Bioelectron 16:121–131.

Thévenot DR, Toth K, Durst RA, Wilson GS (2001b) ELECTROCHEMICAL BIOSENSORS: RECOMMENDED DEFINITIONS AND CLASSIFICATION *. Anal Lett 34:635–659.

Tian Z-Q, Ren B, Wu D-Y (2002) Surface-Enhanced Raman Scattering: From Noble to

Transition Metals and from Rough Surfaces to Ordered Nanostructures. J Phys Chem B 106:9463–9483.

Torkashvand M, Gholivand MB, Malekzadeh G (2016) Construction of a new electrochemical sensor based on molecular imprinting recognition sites on multiwall carbon nanotube surface for analysis of ceftazidime in real samples. Sensors Actuators, B Chem 231:759–767.

Tsai D-H, Davila-Morris M, DelRio FW, et al (2011) Quantitative Determination of Competitive Molecular Adsorption on Gold Nanoparticles Using Attenuated Total Reflectance–Fourier Transform Infrared Spectroscopy. Langmuir 27:9302–9313.

Tsionsky V, Gileadi E (1994) Use of the Quartz Crystal Microbalance for the Study of Adsorption from the Gas Phase. Langmuir 10:2830–2835.

Valera AE, Nesbitt NT, Archibald MM, et al (2019) On-Chip Electrochemical Detection of Cholera Using a Polypyrrole-Functionalized Dendritic Gold Sensor. ACS Sensors 4:654–659.

Wang L, Yamauchi Y (2013) Metallic nanocages: Synthesis of bimetallic Pt-Pd hollow nanoparticles with dendritic shells by selective chemical etching. J Am Chem Soc 135:16762–16765.

Wang Z, Zhang H, Xu L, et al (2016) Laser-induced fabrication of highly branched Au@TiO2nano-dendrites with excellent near-infrared absorption properties. RSC Adv 6:83337–83342.

Wen Y, Lin AJ, Chen HF, et al (2013) From DVD to dendritic nanostructure silver electrode for hydrogen peroxide detection. Biosens Bioelectron 41:857–861.

Wilson GS, Gifford R (2005) Biosensors for real-time in vivo measurements. Biosens Bioelectron 20:2388–2403

Wu L, Zhang X, Chen J (2014) A new third-generation biosensor for superoxide anion based on dendritic gold nanostructure. J Electroanal Chem 726:112–118.

Xiao Y, Lubin AA, Baker BR, et al (2006) Single-step electronic detection of femtomolar DNA by target-induced strand displacement in an electrode-bound duplex. Proc Natl Acad Sci 103:16677–16680.

Yamazaki T, Kojima K, Sode K (2000) Extended-range glucose sensor employing engineered glucose dehydrogenases. Anal Chem 72:4689–4693

Yang N, Chen X, Ren T, et al (2015) Carbon nanotube based biosensors. Sensors Actuators B Chem 207:690–715.

Yang Y, Gao W (2019) Wearable and flexible electronics for continuous molecular monitoring. Chem Soc Rev

Yao H, Jenkins SH, Pesce AJ, et al (1993) Electrochemical homogeneous enzyme immunoassay of theophylline in hemolyzed, icteric, and lipemic samples. Clin Chem 39:1432–1434

Yuan K, Zhang Y-W (2018) Bimetallic Dendritic Nanostructures. Bimetallic Nanostructures 247–270.

Zhang X, Ji R, Wang L, et al (2013) Controllable synthesis of silver nanodendrites on copper rod and its application to hydrogen peroxide and glucose detection. CrystEngComm 15:1173–1178.

Zhang X, Li D, Bourgeois L, et al (2009) Direct Electrodeposition of Porous Gold Nanowire Arrays for Biosensing Applications. 3800:436–441.

Zhang X, Wang G, Liu X, et al (2008) Copper dendrites: Synthesis, mechanism discussion, and application in determination of L-tyrosine. Cryst Growth Des 8:1430–1434.

Zhong L, Gan S, Fu X, et al (2013) Electrochemically controlled growth of silver nanocrystals on graphene thin film and applications for efficient nonenzymatic H2O2 biosensor. Electrochim Acta 89:222–228.

Zhou W, Jimmy Huang P-J, Ding J, Liu J (2014) Aptamer-based biosensors for biomedical diagnostics. Analyst 139:2627.

Zou X, Wu J, Gu J, et al (2019) Application of Aptamers in Virus Detection and Antiviral Therapy. Front Microbiol 10:1462.

Chapter # II

Sputtering assisted enhanced peroxidase like activity of a dendritic nanochip for label-free hydrogen peroxide detection in blood sample

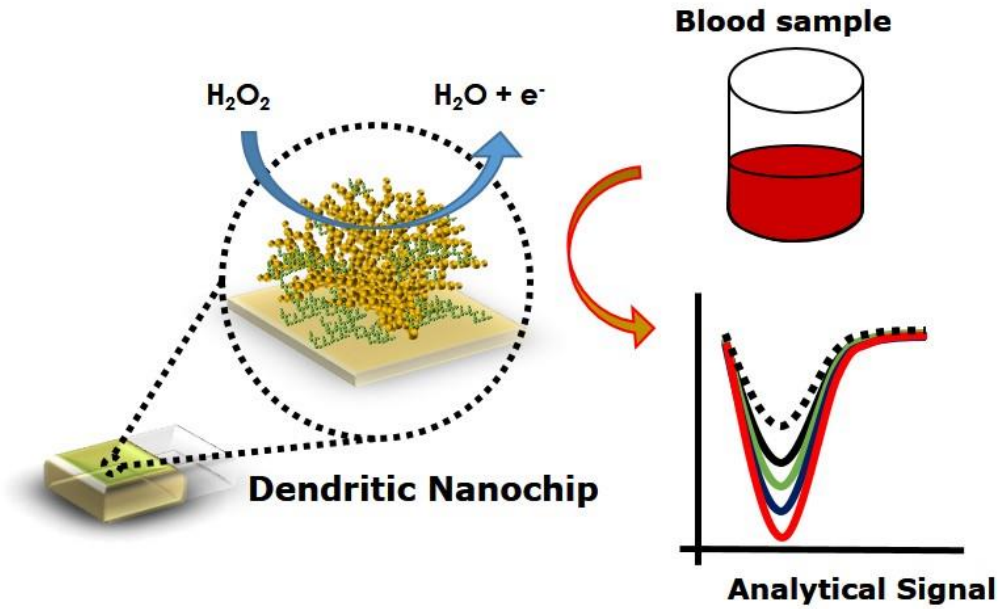

Status:

Published in Microchimica Acta (2019)

1. Introduction:

In the second chapter, we have attempted to develop an enzyme mimicking electrochemical peroxidase biosensor using monometallic nanodendrites. Hydrogen peroxide (H_2O_2) plays an important role in the cellular metabolism and it has tremendous importance in clinical research. It is produced as a byproduct of several oxidases including; glucose oxidase, cholesterol oxidase, glutamate oxidase, urate oxidase, lactate oxidase, *etc.* in various subcellular compartments and organelles (like endoplasmic reticulum, Golgi body etc.). H_2O_2 possess a very high reduction potential and binds with the proteins in the local microenvironment in the cysteine residue forming a reversible sulfenic group. H_2O_2 helps in maintaining the steady state of protein phosphorylation and acts as a secondary messenger the signaling process of various cellular functions involved in cell proliferation, differentiation, motility, *etc* (Tanner et al. 2011). However, when present in higher concentrations, H_2O_2 forms an irreversible sulfinic and sulfonic linkage and permanently damages proteins. Thus, the altered concentrations of H_2O_2 is reported to be associated with various pathological conditions *i.e.* inflammation, aging, diabetes, cardiovascular diseases, neurodegenerative disorders, cancer, *etc* (Brand 2016). The concentration of H_2O_2 also varies in human blood and other biological fluids in various diseased conditions. However, the exact concentration of H_2O_2 in the extracellular and intracellular matrix

---

Part of the work has been published as: Purohit et al., (2019) Sputtering enhanced peroxidase like activity of a dendritic nanochip for amperometric determination of hydrogen peroxide in blood samples. *Microchimica Acta* 186:658.

is a matter of debate, and several authors have reported different sets of data (Jay et al. 2016). In view of such clinical importance of H_2O_2 in diverse biological matrices, many methods have been developed to detect/quantify the concentration of H_2O_2 based on fluorescence (Liu et al. 2017a), colorimetry (Liu et al. 2017b), chemiluminescence (Luo et al. 2017), and spectroscopy (Hoshino et al. 2014).

These methods are though reliable to detect H_2O_2, they suffer due to the involvement of bulky instruments, low sensitivity, time-consuming protocols, color reagents, and interference from molecules commonly found in the complex biological matrices. Peroxidase enzyme based methods (such as Horseradish peroxidase, HRP) based biochemical methods uses the catalytic activity of H_2O_2 to oxidize some reagent, commonly known as electron donating detector compounds (AH) (i.e. scopoletin), where UV/ Visible spectroscopy is used to measure the H_2O_2 level in a time-dependent manner. However, this method also intereferd by thiols, ascorbate, and tissue-specific quenchers. Among all types of analytical systems, electrochemical sensing methods are considered to be robust, selective, and have the ability of miniaturization for point-of-care analysis (Zhu et al. 2012; Mahato et al. 2018; Kumar et al. 2019). For the development of electrochemical H_2O_2 sensor, HRP is commonly used due to its high specificity toward H_2O_2 (Krainer and Glieder 2015). Based on the activity of heme unit, HRP based biosensors are developed to detect H_2O_2 in the sample by using either a mediator molecule or by direct electron transfer between the redox center of protein and electrode. However, the limitation of using an enzyme for sensing purposes lies in the complicated immobilization process, temperature dependent denaturation, effect of micro-environment, less operational stability, low shelf-life, and high-cost [15]. In order

to overcome such limitations, nowadays nonenzymatic H_2O_2 sensors have gained major attention, where various nanomaterials based approaches have been employed. Metallic nanoparticles based on Pt (Liu et al. 2018), Ag (Ma et al. 2018), Cu (Liu et al. 2013) have been utilized for the development of nonenzymatic H_2O_2 sensor. The peroxidase like activity of gold nanoparticles have long been proven, and used for the development of H_2O_2 sensor (Liu et al. 2012). However, these metal nanoparticles based nonenzymatic sensors suffer due to the poisoning of the sensing surface with the analytes or the intermediates generated during the sensing process, which can be avoided by using a sensing matrix with higher surface area (Cheng et al. 2010). Metallic dendrites (MDs) can be used as a possible solution. MDs are nanostructure with hierarchical, repetitive, and defined in nature having a central stem with primary and secondary side branches resembling like fern**.** These MDs offers high surface area, high conductivity, and different degrees of surface roughness possessing a greater catalytic potential (Noh et al. 2012). Most of the MDs structures reported so far have been directly studied for its physical properties, leaving the biological possibilities unaddressed (Xu et al. 2010; Ye et al. 2010). Therefore, a new approach of exploring the dendritic nanostructures toward sensitive and selective detection of biologically important molecules is interesting to attempt. During our preliminary observation of the synthesis of gold MDs, we surprisingly found a sharp increase in the electron transfer of dendritic chip after gold sputtering compared to the unsputtered surface. Utilization of such MDs electrodes toward biomolecular sensing can establish the concept of repurposing of electrodes in the future.

In the present work, we have designed a nanoprobe utilizing the discarded gold dendritic nanostructure formed on indium tin oxide (ITO) electrode after gold sputtering, for H_2O_2 detection. The nanoprobe was thoroughly characterized by scanning electron microscope (SEM), transmission electron microscope (TEM), energy dispersive X-ray spectroscopy (EDX), selected area electron diffractogram (SAED), cyclic voltammetry (CV), electrochemical impedance spectroscopy (EIS), and chronoamperometry. Thereafter, the dose-dependent detection of H_2O_2 was performed using the fabricated nanoprobe to assess its analytical performance, *i.e.* linear dynamic range (LDR) and limit of detection (LOD) using differential pulse voltammetry (DPV). The practical applicability of the fabricated nanoprobe was examined by testing H_2O_2 in human blood samples using spike and recovery method. Interference due to various components was studied and the long-term stability of the designed nanoprobe was also evaluated.

2. Experimental:

2.1. Chemicals and Instruments:

All the chemicals used in the synthesis as well as analysis work are of analytical grade. Potassium chloride (KCl), chloroauric acid ($HAuCl_4$), potassium ferricyanide [$K_3Fe(CN)_6$], potassium ferrocyanide [$K_4Fe(CN)_6$], hydrogen peroxide (H_2O_2), and ITO (30 Ω/sq. slide) were obtained from Sigma-Aldrich Chemical Co. (India). Sodium chloride (NaCl), citric acid, ascorbic acid (C6H8O6), uric acid (C5H4N4O3), d-glucose, urea, l-glycine, l-alanine (C3H7NO2), l-glutamic acid, l-cysteine were purchased from SRL, India. Sulphuric acid (H2SO4), ammonium hydroxide (NH_4OH) were procured from Merck Millipore, India. All aqueous solutions were prepared in doubly distilled water obtained from a Milli-Q water purifying system (18 MΩ cm).

All the synthesis and electrochemical characterization was done by electrochemical workstation (Metrohm Autolab) using three electrode based electrochemical cell, where ITO, platinum (Pt) wire, and Ag/AgCl (saturated with KCl) were used as the working, counter, and reference electrodes, respectively. Surface morphological Imaging and EDX were performed using field emission scanning electron microscope (FESEM) (Make: Zeiss, Model: Gemini). TEM images and SAED were recorded from field emission transmission electron microscope (FETEM) (Make: JEOL, Model: 2100F). Gold sputtering was performed in a Quorum gold cathodic sputter coater (Model: Q150R S) applying a current of 20 mA under a pressure of 1 x 10^{-3} mBar.

2.2. Synthesis of AuND surface:

The ITO electrode was washed in a number of solutions to remove the impurities from the working surface. For that ITO was subjected to ultrasonication in acetone, ethanol, and double distilled MilliQ water for 15 minutes sequentially. Then it was heated at 70˚C for 1 hour in a solution containing NH_4OH: H_2O_2: H_2O in the ratio 1:1:5. Thereafter, the ITO was thoroughly rinsed with distilled water and dried. The ultra-cleaned ITO was used as the surface for synthesizing gold nanodendrite structures (AuND) using an electrochemical method. The AuND was electrodeposited over the ITO surface using chronoamperometry by applying -0.30 V vs. Ag/AgCl for an optimized 1500 secs in a three electrode system containing 0.01 M $HAuCl_4$ solution (in 0.1 M KCl). Before the electrodeposition step, nitrogen was purged into the solution to remove the oxygen content. After electrodeposition, the AuND deposited ITO was rinsed with ethanol and MilliQ water

2.3. Fabrication of ITO/AuND/AuSP nanoprobe surface:

In the next step, the electrodeposited ITO substrate (ITO/AuND) was subjected to gold sputtering (AuSP) for 60 secs in vacuum. Thereafter the electrode was washed with MilliQ water followed by rinsing with ethanol for 5 secs and air dried. The final electrode was termed as ITO/AuND/AuSP. It is worth mentioning that the ITO/AuND/AuSP nanoprobe fabrication requires less than 30 minutes offering a robust electrode fabrication strategy. The detailed process of sensor probe fabrication and its sensing application is diagrammatically shown in the scheme figure 2.1.

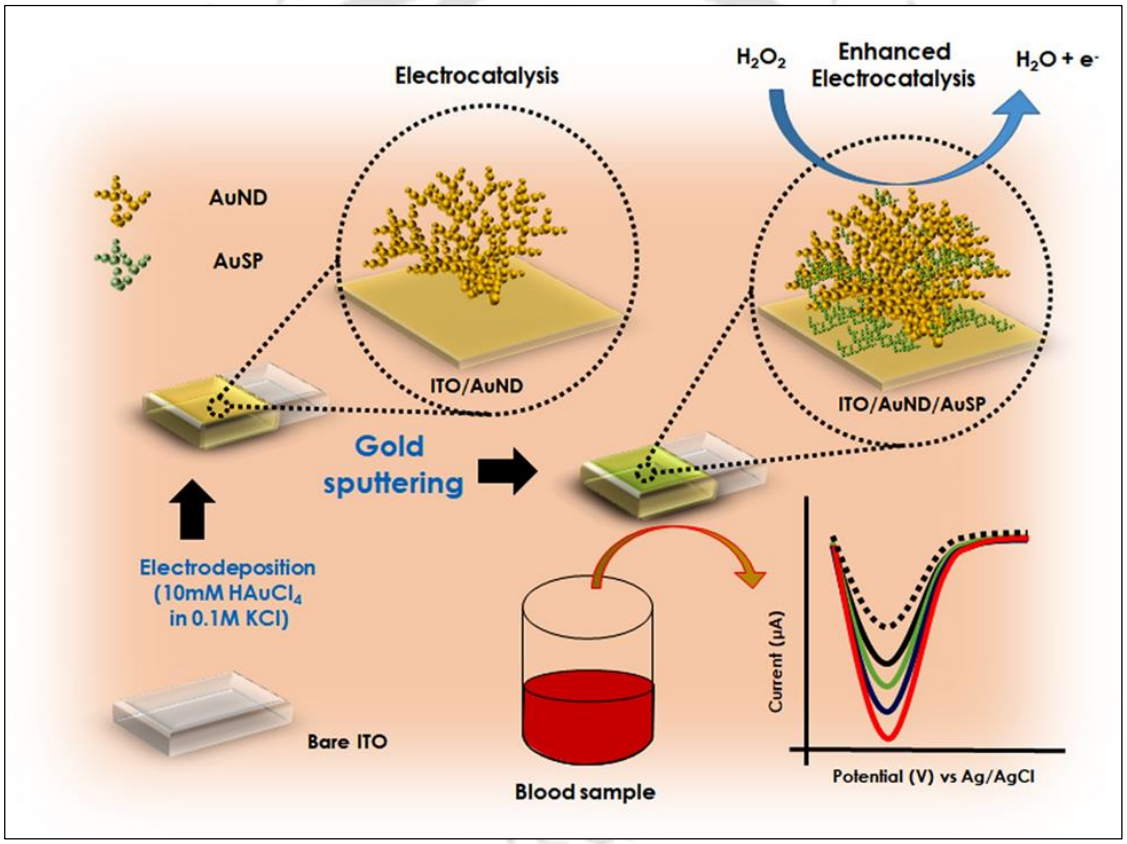

Figure 2.1. Schematic representation of the work depicting of the step wise development of the nonenzymatic probe.

2.4. Preparation for real sample matrix:

To test the clinical applicability of the developed ITO/AuND/AuSP nanoprobe, it was analyzed in complex biological matrices. Since H_2O_2 had been reported to be found in

a range of 10^{-9} M to 10^{-6} M in human blood in different pathological conditions, the analytical performance of fabricated ITO/AuND/AuSP probe was tested for H_2O_2 detection in blood (Jay et al. 2016). Blood samples of laboratory volunteers were collected using BD Vacutainer (USA) (www.bd.com) blood collection tube (REF 367863) in Government Hospital, Indian Institute of Technology Guwahati campus, Assam, India for sensing applications. The tests were performed immediately after the blood collection in order to avoid the clot formation.

3. Results and discussion:

3.1. Physical characterization of ITO/AuND/AuSP nanoprobe:

The fabricated ITO/AuND/AuSP probe was characterized step by step following the physical characterization methods. In the first step, the formation of AuND was confirmed on the ITO surface by chronoamperometry, where the increase in the current responses from 1 to 1500 secs was observed. In our experiment, we optimized a stable and sensitive AuND surface by tuning the electrodeposition time between 500 – 1800 secs **(figure 2.3 A-H)**. Further, CV responses were recorded in a 5.0 mM Zobell's solution after the electrodeposition of AuND at 500 (black curve), 1000 (blue curve), 1500 (green curve), and 1800 s (red curve). **Figure 2.3 A-B** show the formation of a dendrite at 500 s, which is much smaller than the dendrites with electrolysis time of 1000 s (**figure 2.3 C-D**). The number of dendrites formed over the electrode surface also increased with increase in electrolysis time. Electrolysis time of 1500 s resulted in the development of well grown Au dendrites with characteristic primary, secondary and tertiary branches growing evenly all over the electrode surface (**figure 2.3 E-F**), no much change was seen at electrolysis time of 1800 s. Interestingly, the current responses

increased from 500 to 1500 secs, however, at 1800 secs the current response drastically reduced, which was most likely due to the formation of high-density films forming an insulating layer on the electrode surface. Hence 1500 secs deposition time was applied in successive experiments due to the maximum current response. The increment in chronoamperometry reflects the increase in conducting behavior of electrode surface, which is due to the deposition of Au^0 from Au^{3+} on to the electrode surface, eventually forming AuND. A negative control experiment was performed under similar experimental conditions where the chronoamperometry was performed except the presence of gold salt in the measuring solution. In this case, no signal was observed, indicating the chronoamperometric signals observed in the previous case was merely due to the presence of gold salt in the solution forming dendritic structures on to the electrode surface. In addition, the visually distinguishable appearances of the control bare ITO (blank) and ITO/AuND electrode also confirms the electrodeposition. The transparent bare ITO (**figure 2.2. (i)**) turned into a golden brown color surface **(figure 2.2 (ii))**, which was not observed in bare ITO.

Figure 2.2 Shows the image of (i) ITO, (ii) ITO/AuND, (iii) ITO/AuND/AuSP. The rectangular dotted boxes in figure (ii) and (iii) show the deposited dendrites.

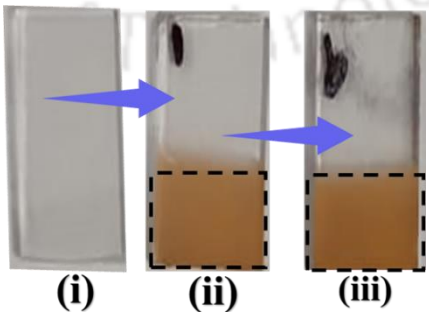

In order to further confirm that the golden brown film is composed of AuND over the ITO surface, we characterized bare ITO and a modified ITO/AuND electrode using

SEM. No pattern or structure was observed on the bare ITO surface (**figure 2.4 A**). A vertical SEM image of the gold sputtered dendritic electrode was captured after tilting the electrode at 90˚, where a clear 3D growth of the dendritic structure was observed (**figure 2.4 B-C**). The red dotted line in the image shows the surface of ITO, over which the vertical, as well as horizontal growth of the AuND was clearly visible (as shown in the X, Y, and Z axes). A well-defined tip of a branch with smaller processes over the primary branch shows the dendrite pattern. We simultaneously performed multipoint EDX over these patterned structures, where the Au concentration was found to be 88% **(figure 2.4 D)** indicating Au as the chief component of the structure. The ITO/AuND electrode was further characterized by TEM, where the electrode surface was sonicated in ethanol for 10 min and the sample was collected and air dried over the TEM grid. The image also showed a typical treelike pattern in the TEM analysis **(figure 2.4 E)**, and was comparable with the SEM results. In order to assess the material properties of ITO/AuND surface, SAED was performed. **Figure 2.4 F** shows ingle crystal having crystal planes (111) and (200), which refers to the crystalline structure of Au (Naveen et al. 2016).

After the gold sputtering over ITO/AuND electrode surface, an interesting change in dendritic topology occurred, where bright depositions on the entire dendritic structures were observed in SEM image (**figure 2.5 A**). Further in EDX analysis, interestingly the gold percentage increased to 97% (**figure 2.5 B**), showing a 9% increment in the overall gold content after sputtering.

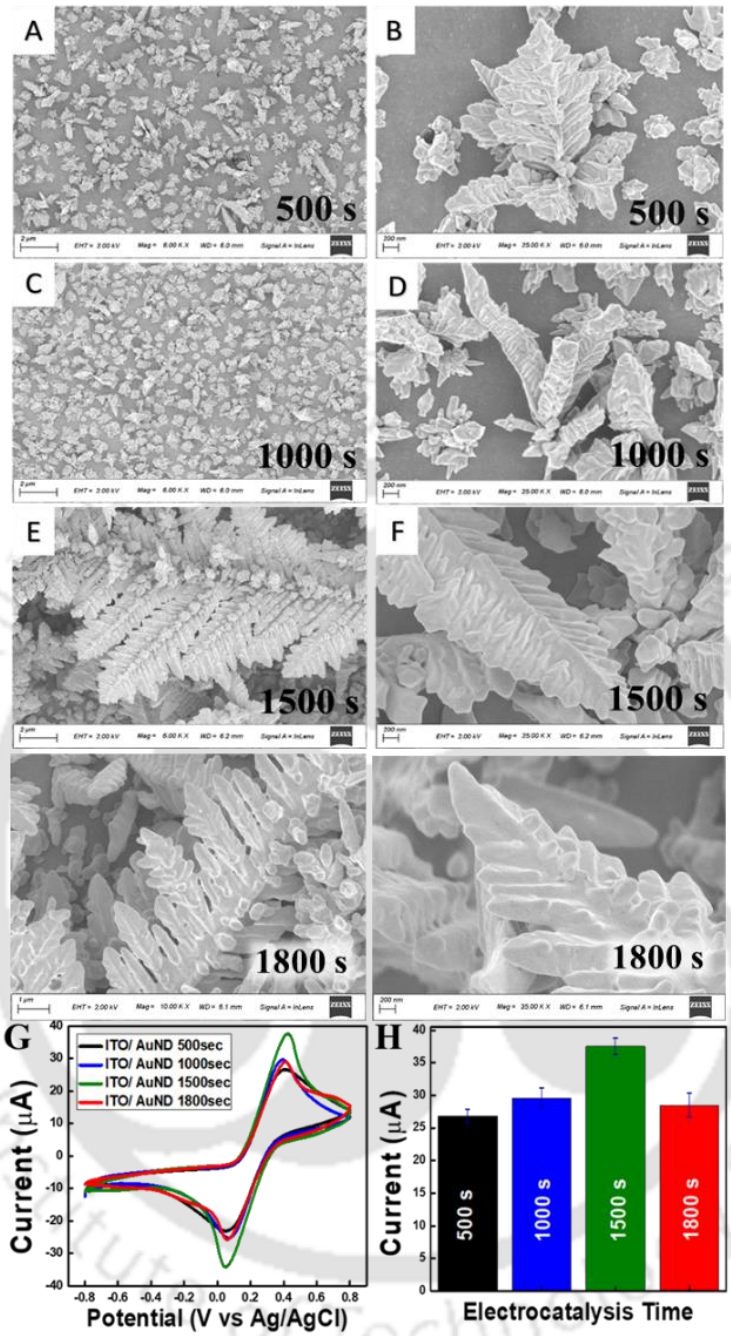

Figure 2.3 (A-F) SEM micrograph shows the size and distribution of Au nano-dendrites at different electrodeposition time. With increased electrolysis time, the dendrites became larger in size and, so the number of dendrites over the electrode surface; (G) shows the CV current responses of the ITO/AuND probe in ZS, with the maximum value at 1500 s, and the histograms in (H) shows the corresponding data.

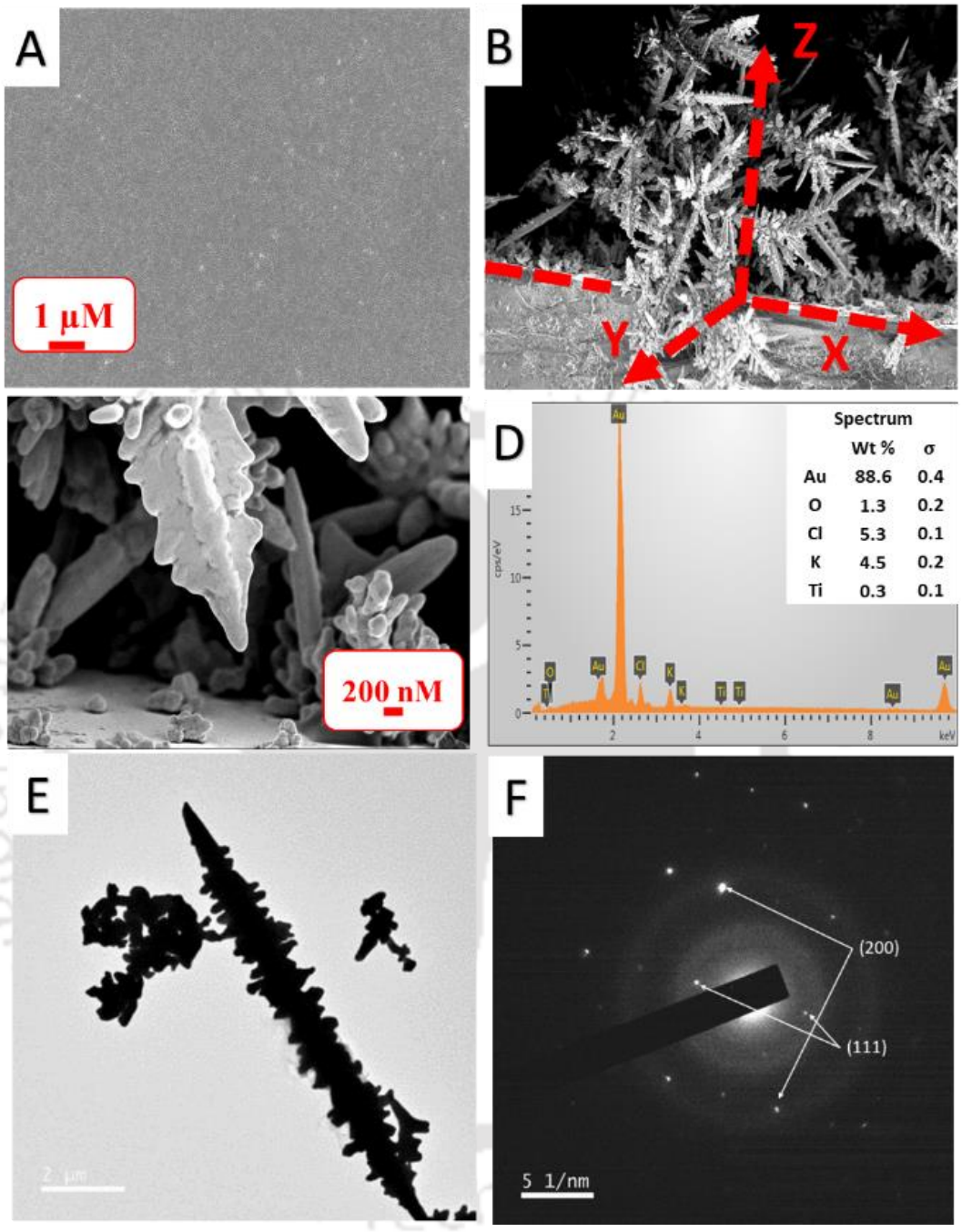

Figure 2.4. (A) SEM micrograph of bare ITO showing a plane surface without any particles; (B-C) SEM image of ITO/AuND taken by placing the ITO at 90 angle, (D) EDX analysis, (E) TEM image, and (E) SAED analysis of ITO/AuND depicting the formation of a monocrystalline hierarchical patterned Au dendrite.

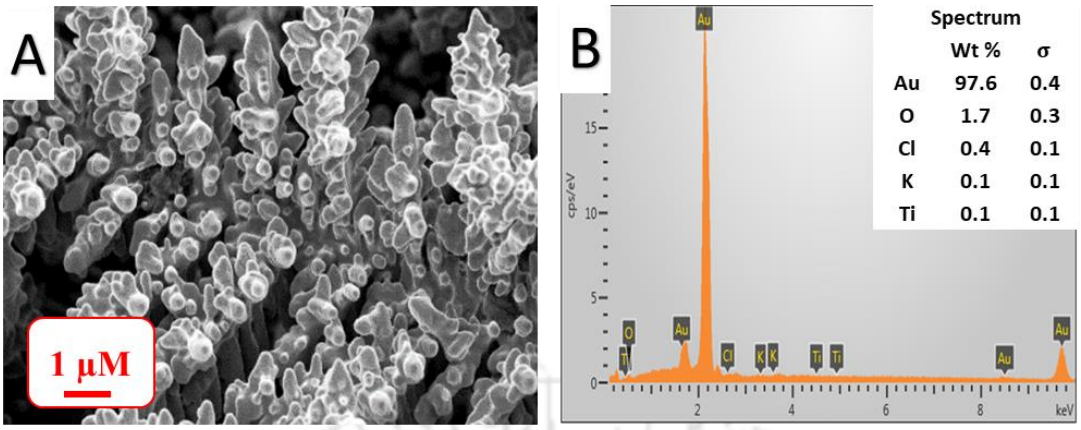

Figure 2.5 (A) SEM micrograph of ITO/AuND/AuSP showing bright deposition over the gold dendritic structures, and (G) EDX analysis of the ITO/AuND/AuSP surface shows an increase in the Au content.

3.2. Electrochemical characterization of the ITO/AuND/AuSP nanoprobe

The fabricated ITO/AuND/AuSP probe was also characterized electrochemically at every step of probe development. The initial electrochemical characterization involves CV responses of the electrode surfaces in 5.0 mM Zobell's solution (ZS) as shown in **figure 2.5 A**. The CV responses were measured in the potential range of -0.8 V to +0.8 V at a scan rate of 100 mV/s. A representative voltammogram due to the redox process of $[Fe(CN)_6]^{3-/4-}$ was observed at bare ITO (black curve), where anodic (I_{pa}) and cathodic (I_{pc}) peak currents were found to be increased for ITO/AuND (red curve) (**figure 2.5 B**). The signal response further increased at ITO/AuND/AuSP (blue curve) surface, which could be due to the presence of AuSP in the sensing matrix offering high conductivity and active surface area.

In order to further validate the results of CV, a complementary experiment was performed based on electrochemical impedance spectroscopy (EIS), and charge transfer

resistance (Rct) were recorded for ITO, ITO/AuND, and ITO/AuND/AuSP surfaces in PBS. Rct values have been evaluated using the Nyquist plot (**figure 2.5 C)**, where the Rct values were found to be 129 ± 3.2, 24.2 ± 0.7, and 8.4 ± 0.2 KΩ for bare ITO (black curve), ITO/ AuND (red curve), ITO/AuND/AuSP (blue curve) surfaces, respectively. The comparative Rct values of the modified electrode surfaces have been shown in the histogram (inset of **figure 2.5 D**). Further, in order to investigate the stability and charge transfer behavior of the sensing probes, CV responses were recorded at ITO/AuND and ITO/AuND/AuSP probe at different scan rates between 10 – 100 mV/s in 5.0 mM ZS as shown in **figure 2.7 (A-B)** and **figure 2.7 (C-D)**, respectively. The peak currents were found to be directly proportional to the square root of scan rate (inset of with the correlation co-efficient of 0.99, which clearly indicates higher stability and diffusion controlled charge transfer process at the electrode surface.

In order to evaluate the increased charge transfer as a result of gold sputtering over the ITO/AuND surface toward electrochemical sensing have been evaluated quantitatively by comparing the diffusion coefficients of the bare ITO, ITO/AuND, and ITO/AuND/AuSP surfaces using the Randles-Sevcik's model (equation 1) (Verma et al. 2017).

$$I_p = \left(2.69\times10^5\right) n^{3/2} ACD^{1/2} v^{1/2} \quad \ldots\ldots\ldots \text{equation 1}$$

Where, Ip is the peak current (in ampere), n is the number of electrons transferred in redox process (here n=1), A is the electrode surface area (in cm^2), C is the concentration of electroactive species (in mole cm^{-3}), D is the diffusion coefficient (in $cm^2\ s^{-1}$), and v is the scan rate (in Vs^{-1}).

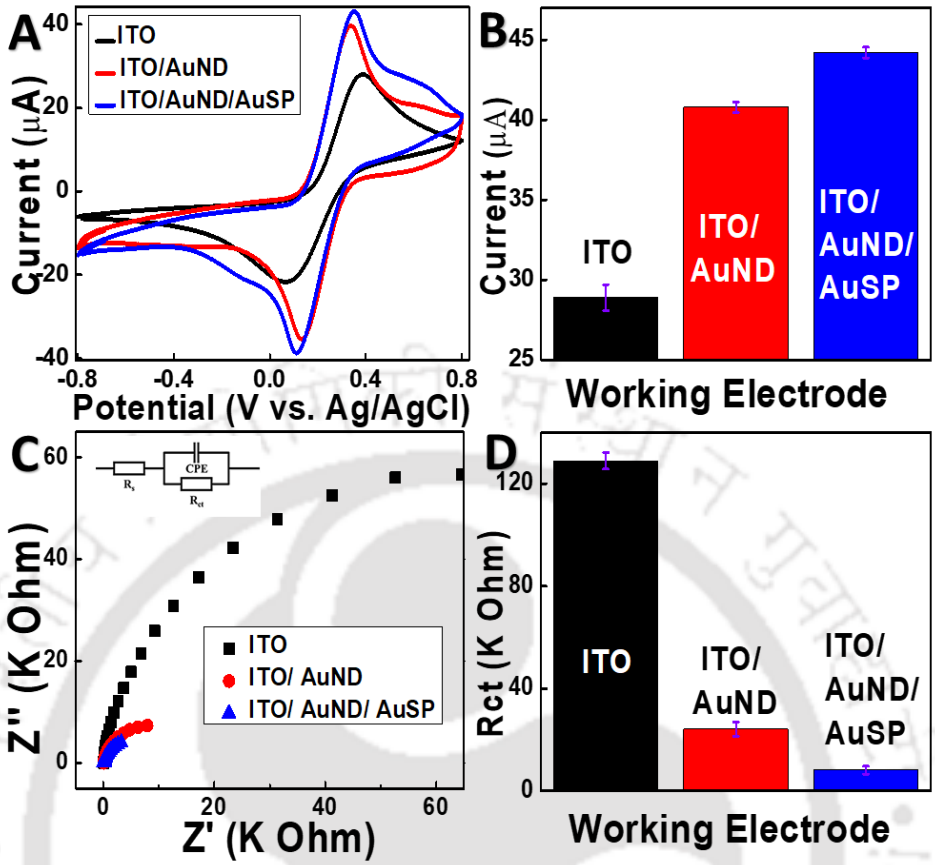

Figure 2.6 (A) CV responses at bare ITO(black), ITO/AuND(red), ITO/AuND/AuSP(blue) in Zobell's solution (5mM; pH- 7.0; Scan rate: 100mV/S), Corresponding peak current value shown in histogram (B);(C) Nyquist plot of bare ITO(black), ITO/AuND(red), and ITO/AuND/AuSP (blue) in 5.0 mM PBS buffer, histogram showing comparative Rct values in the different surfaces (D).

The diffusion coefficient (*D*) values for bare ITO, ITO/AuND, and ITO/AuND/AuSP electrode surfaces were found to be 2.0 x 10^{-6} cm^2s^{-1}, 3.9 x 10^{-6} cm^2s^{-1}, and 4.6 x 10^{-6} cm^2s^{-1}, respectively. The D value of ITO/AuND/AuSP was found to be the highest, indicating that ITO/AuND/AuSP modified electrode surface was more conducting and capable of transferring the electrons more efficiently than ITO, ITO/AuND surface.

Based on the CV responses and Rct values, it was evident that the ITO/AuND/AuSP surface showed the least resistance and maximum current responses, validating the potential applicability of the fabricated ITO/AuND/AuSP nanoprobe for electrochemical analysis. The higher conductivity of the surface may be due to the higher active surface area of the dendritic nanostructure constituting a more concentrated distribution of edges, ridges, and apex all over the surface. Further development of the nanoprobe with gold sputtering in the closed vacuum chamber leads to even higher anodic and cathodic peak current development. The defects formed as a result of sputtering on the nanodendrite structure, although preserving its branching patterns may lead to even more conducting capacity.

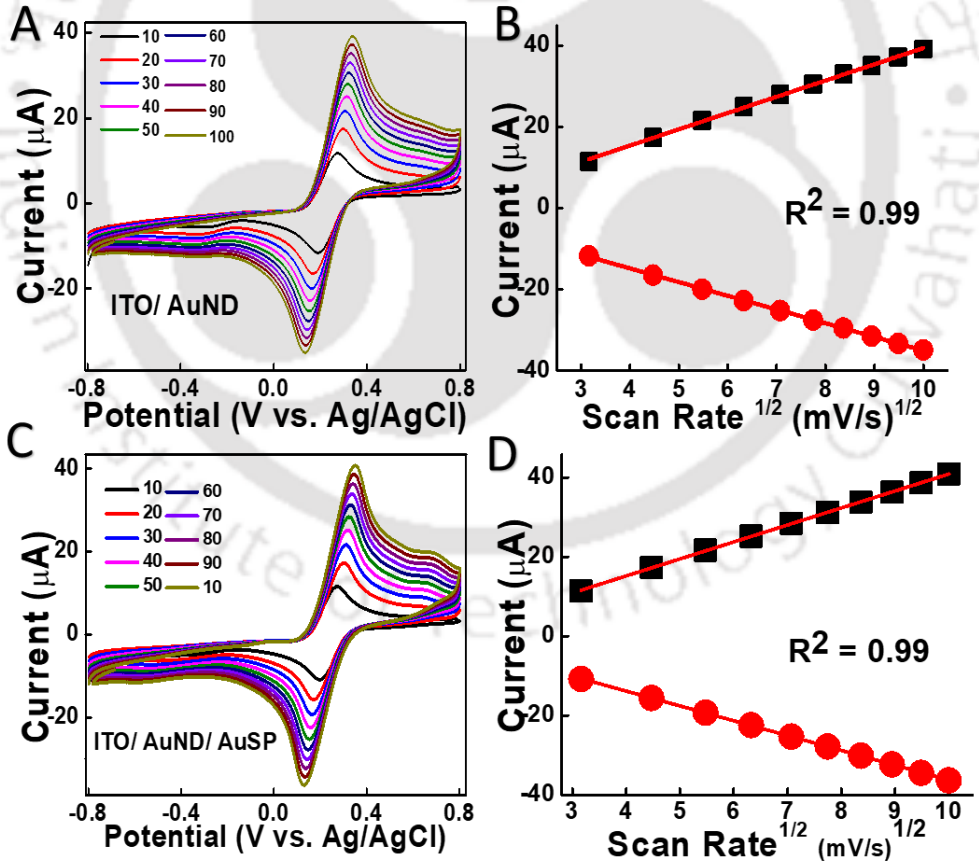

Figure 2.7 CV responses at scan rate 10-100 mV/s of (A-B) ITO/AuND and (C-D) ITO/AuND/AuSP in ZS, respectively.

3.3. Analytical performance of ITO/AuND/AuSP sensing probe

The ITO/AuND/AuSP nanoprobe was further applied for the detection of H_2O_2. All electrochemical studies were performed in nitrogen purged deoxygenated PBS to avoid oxygen interference. The nanoprobe was dipped in 5.0 mM PBS (no H_2O_2) and LSV was recorded by sweeping the potentials between -0.65 V and 0.20 V vs. Ag/AgCl. In this case, no peak (pink curve) was observed due to the absence of any redox species as shown in **figure 2.8 A**. Thereafter, the ITO/AuND/AuSP nanoprobe was placed in a 5.0 mM PBS solution containing 0.40 M H_2O_2 and LSV was recorded in a similar potential window. Interestingly, a sharp increase in the current response was observed at -0.40 V (indigo curve). Similar nonenzymatic catalytic reduction peak of H_2O_2 at comparable potential was observed elsewhere (Chandra et al. 2011; Pallela et al. 2016). This shows the catalytic potential of the ITO/AuND/AuSP probe to reduce H_2O_2. In order to check whether this is a property of dendritic structure, LSV responses of both ITO and ITO/AuND electrodes in 5.0 mM PBS (without H_2O_2) and 5.0 mM PBS (with 0.40 M H_2O_2) were recorded in similar experimental setting. No signal was observed at bare ITO in PBS (black curve) as well as in presence of 0.40 M H_2O_2 (red curve). In case of ITO/AuND, a clear reduction peak (green curve) at -0.40 V was observed which was approximately three times lower in magnitude than the response found at ITO/AuND/AuSP modified electrode, indicating the importance of AuSP in the sensing matrix.

In order to validate that the peak at -0.40 V at ITO/AuND/AuSP is merely due to H_2O_2 sensing, we performed two control experiments. In the first control experiment, H_2O_2 was tested in a dose dependent manner between 0.20 M and 0.50 M in 5.0 mM PBS

using ITO/AuND/AuSP electrode. **Figure 2.8 B** shows the representative LSV curves, where the current responses increased linearly with increasing H_2O_2 concentrations. The linear regression equation for concentration dependent plot is expressed as follows: ΔI (mA) = 0.17 (±0.003) + 0.0015 (± 0.0004) Conc [H_2O_2 (M)] with the correlation coefficient of 0.975, indicating the ability of ITO/AuND/AuSP nanoprobe for H_2O_2 detection effectively.

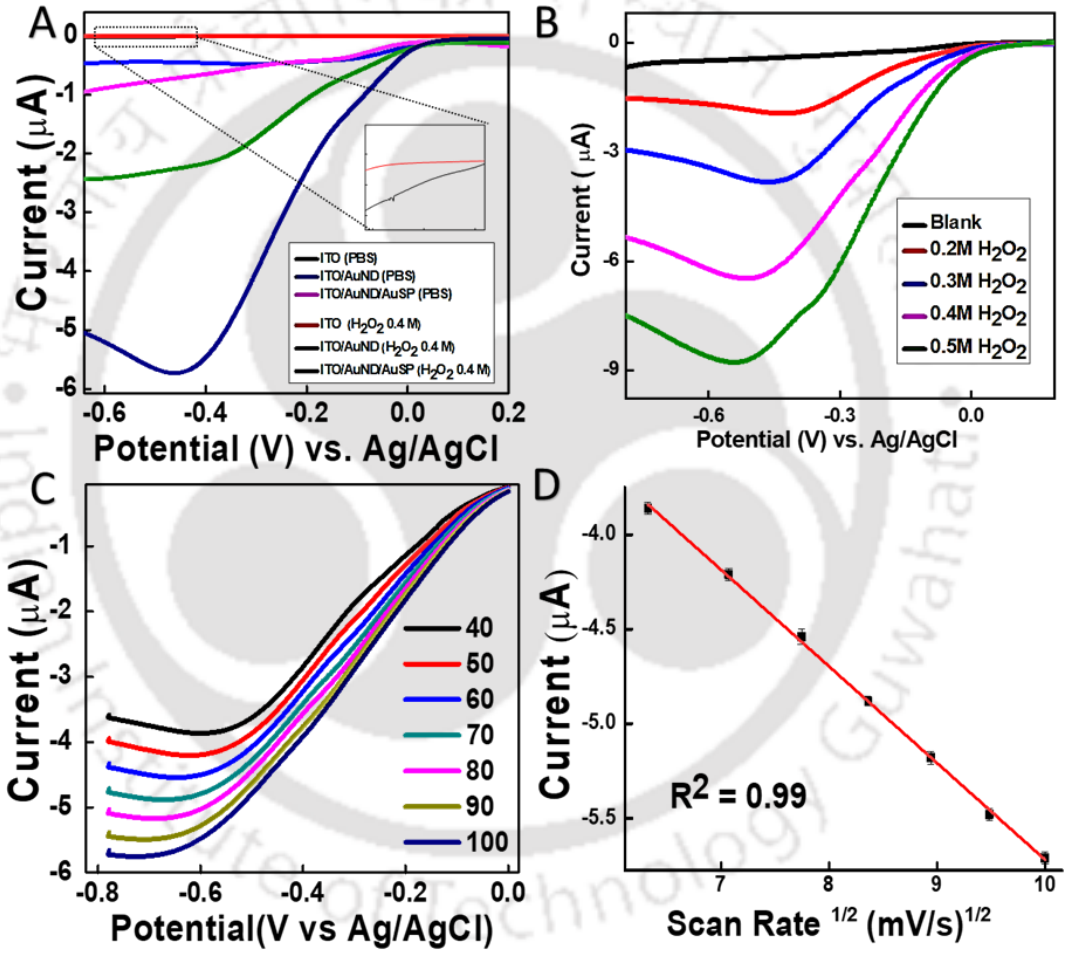

Figure 2. 8 (A) Comparative LSV responses of Bare ITO, ITO/AuND, and ITO/AuND/AuSP electrode surfaces in blank and 0.4 M H_2O_2 in PBS; (B) LSV response of ITO/AuND/AuSP modified electrode surface at different concentrations of H_2O_2; (C) LSV responses at scan rate 40-100 mV/s, and (D) shows the corresponding peak current following linearity.

In the second control experiment, a scan rate dependent study was performed at 0.2 M of H_2O_2 between 40 and 100 mV s^{-1} (**figure 2.8 C**). In this case, the reduction peak current was found to be directly proportional to the square root of scan rates which referred to the diffusion control electrochemical process of H_2O_2 reduction only (**figure 2.8 D)**. The results found from both the control experiments validate that the designed ITO/AuND/AuSP nanoprobe is stable and is able to detect H_2O_2 accurately.

We further investigated the analytical performance of designed ITO/AuND/AuSP probe by using DPV to detect various concentrations of H_2O_2 in 5.0 mM PBS. DPV is considered to be a very sensitive technique compared to LSV (Bard et al. 1980). Therefore, we have selected DPV for further analytical demonstration of the nanoprobe. The experimental condition for DPV measurements was as follows: pulse potential 0.025 V, pulse time 0.05 s and the scan rate 0.005 V sec^{-1}. **Figure 2.9 A** shows the representative DPV curves where the current responses increase with the increase in H_2O_2 concentrations. Based on the DPV responses, a calibration plot was plotted which shows the detection range between 1 x 10^{-12} and 1 x 10^{-5} M of H_2O_2 (**figure 2.9 B**). It is interesting to note that the DPV responses in the calibration plot shows two regions of linearity (LDRs) of 1 x 10^{-5} to 1 x 10^{-10} M and 1 x 10^{-10} to 1 x 10^{-12} M for H_2O_2 sensing with two different slopes. The linear regression equations of H_2O_2 detection are expressed for low and high concentrations ranges as follows:

$\Delta I\ (A) = 4.64\ (\pm\ 0.34) \times 10^{-6} + 0.36\ (\pm\ 0.03) \times 10^{-6}$ log Conc. [H_2O_2 (M)], and

$\Delta I\ (A) = 2.12\ (\pm\ 0.09) \times 10^{-6} + 0.11\ (\pm\ 0.01) \times 10^{-6}$ log Conc. [H_2O_2(M)] …. equation 2

with correlation coefficient of 0.979 and 0.997, respectively.

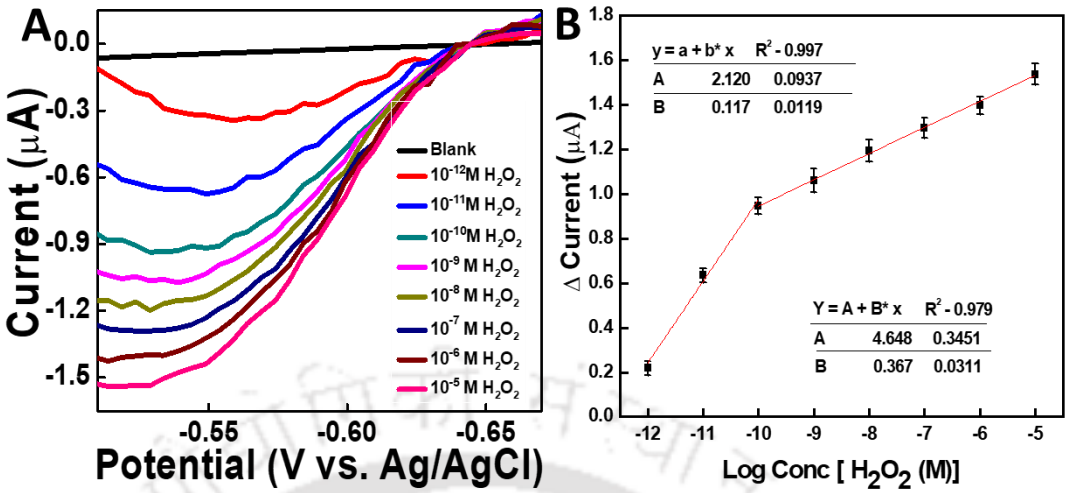

Figure 2. 9 (A) Dose-dependent DPV responses obtained from the ITO/AuND/AuSP sensor probe at various concentrations (10^{-12} M - 10^{-5} M); (B) calibration plot obtained from the DPV responses at ITO/AuND/AuSP sensor surface.

The detection limit of H_2O_2 was determined to be 9.8 (± 0.02) x 10^{-13} M (RSD < 4.2%) based on the standard deviation of three repeated measurements (95% confidence level, n=3) using equation 2.

$$LOD = \frac{3SD_B}{Slope} = \frac{3SD_B}{\frac{dy}{dx}} = \frac{3SD_B}{\frac{dy}{d\ln x} \times \frac{d\ln x}{dx}} = \frac{3SD_B}{\frac{dy}{2.303(d\log x)} \times \frac{1}{x}}$$

…… equation 3

$$= \frac{3(2.303)SD_B x}{\frac{dy}{(d\log x)}} = \frac{3(2.303)SD_B x}{\text{slope of the semilog plot}}$$

Where, SD_B is standard deviation of blank; x is the limit of quantification or lowest concentration measured.

This is worth mentioning that the nanoprobe possesses a very wide dynamic range, hence it can be directly used in diverse types of matrices where H_2O_2 concentration is

in traces or in high concentration in various pathological conditions. It is also important to note that our nanoprobe possesses simple fabrication steps and is devoid of any biomolecule even though it offers an unprecedented LOD and a wide LDR. This indicates the promise of the developed nanoprobe for robust and sensitive H_2O_2 detection in clinically relevant ranges in diverse real sample matrices. Importantly, the LDR and LOD in this work are significantly wider and lower, respectively compared to the most of previously reported H_2O_2 sensors. A detailed account of the comparative analytical performances of some previously reported sensors is shown in **Table 1**.

Robustness is an important criterion for the commercial success of any sensor (Chandra 2016). Hence, we have investigated the response time of ITO/AuND/AuSP nanoprobe, by performing chronoamperometry at -0.42 V vs. Ag/AgCl in dynamic mode. **Figure 2. 10 A** shows the amperometric response recorded after addition of H_2O_2 on a stabilized current(**a**). After the H_2O_2 injection at point (**b**), a sharp jump in the current (**c**) was observed between 222 and 223 secs (**inset**), indicating that the nanoprobe was able to detect H_2O_2 in ≤1.0 sec. It is important to note that a stable and considerably higher current value (**d**) was observed after the saturation of the signal. The response time found in our case is significantly lower compared to the most of previously reported H_2O_2 sensors.

3.4. Selectivity assay

In order to test the effect of interfering molecules on H_2O_2 signal generation, some common co-existing molecules in the complex biological fluids *viz.* glucose, citric acid, ascorbic acid, uric acid, urea, glycine, cysteine, alanine, and glutamic acid were selected. Selectivity assay was performed using these molecules at a relatively higher

concentration than normally found in body fluids. **Figure 2.10 B** shows a comparative histogram of the responses in presence of interfering molecules, where negligible or no deviation in reduction current was observed as compared to the response of H_2O_2. No response was observed possibly due to the electrochemical inactive behavior of the interfering species (e.g. glucose) and /or the negative potential window where the common metabolites do not give any signal in merely few seconds. The selectivity of the final probe is estimated mathematically by equation 3.

$$K_{sel} = (Signal)\ Interfering\ molecules\ /\ (Signal)_{H_2O_2} \ldots\ldots\ldots\ldots \quad \text{equation 4}$$

Where K_{sel} *is the coefficient of selectivity,* $Signal_{interfering\ molecules}$ *is the signal strength shown by the probe when treated with the interfering molecules, and* $Signal_{H_2O_2}$ *is the signal strength corresponds to* H_2O_2.

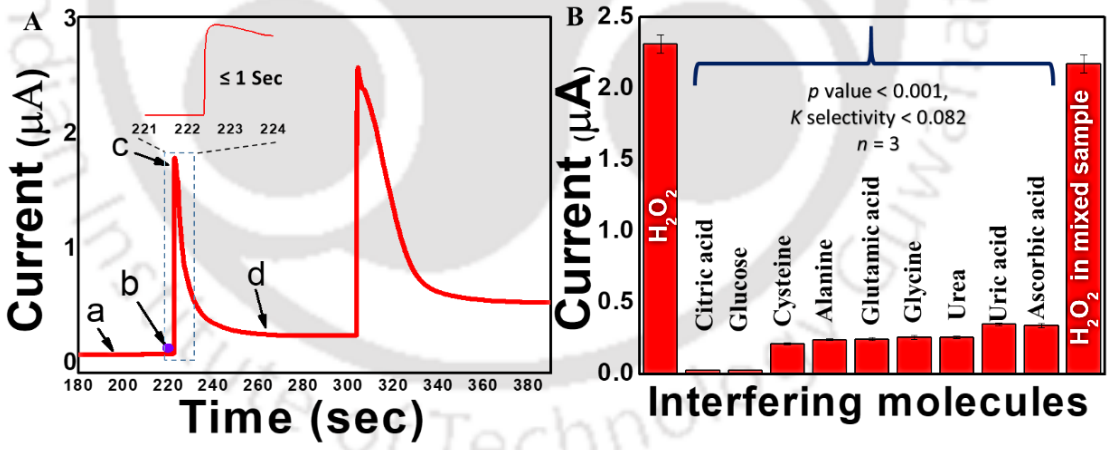

Figure 2.10 (A) Chronoamperometric response of ITO/AuND/AuSP probe in PBS buffer in addition of H_2O_2, showing the quick response time of ≤ 1 sec. (B) Interference study showing high selectivity of the sensor towards H_2O_2.

The calculated k_{sel} values for interfering molecules were found to be very low (k_{sel} <<1), indicating that the sensing surface was very selective toward H_2O_2. Also for the statistical significance of the result, we performed T-test for H_2O_2 and calculated p-values against all interfering molecules found to be << 0.001 (n = 3).

3.5. Real sample analysis

Blood is considered as a clinically relevant sample where the H_2O_2 concentration is associated with many pathological conditions and it has been routinely applied to diagnose various diseases. So, we selected blood as the real sample matrix for the detection of H_2O_2 using ITO/AuND/AuSP nanoprobe.

Immediately after collecting the blood, H_2O_2 was measured by the spike and recovery method. The H_2O_2 concentrations were measured by comparing the signals with the previously developed calibration plot as a standard reference and the results were expressed in terms of % recovery using equation 4.

$$\% \text{ Recovery} = [S]_{H2O2} - [B]_{H2O2} / [SS]_{H2O2} \quad \text{----equation 5}$$

Where, $[S]_{H2O2}$ and $[B]_{H2O2}$ are the analytical responses of H_2O_2 in the spiked and blank blood samples, respectively; and $[SS]_{H2O2}$ is the analytical response of H_2O_2 in the standard buffer solutions.

The DPV responses were measured in the PBS equilibrated blood sample (1:10) as a concentration-dependent function of H_2O_2. **Figure 2.11** shows the comparative histograms of analytical responses obtained in the blood (red) sample as a function of different concentrations of H_2O_2 and corresponding responses in standard calibration plot in buffer (black). Thereafter, the recoveries at each concentration of H_2O_2 (1 x 10^{-}

^{10} M – 1 x 10^{-5} M) had been calculated, and the minimum and maximum current recoveries were found in between 90% and 96% of the standard, respectively (RSD < 3.2, n=3).

Based on the response, a linear regression equation was obtained as follows: ΔI (A) = 1.91 (± 0.050) x 10^{-6} + 0.11 (± 0.006) x 10^{-6} log Conc. [H_2O_2 (M)] with correlation coefficient of 0.91 and the detection limit of 6.5 (+0.021) x 10^{-12} M for H_2O_2. The concentration measured in our study was selected based on the clinical ranges of H_2O_2 found in pathological conditions in blood, hence it can be used an analytical tool for fast detection of H_2O_2 in hospitals.

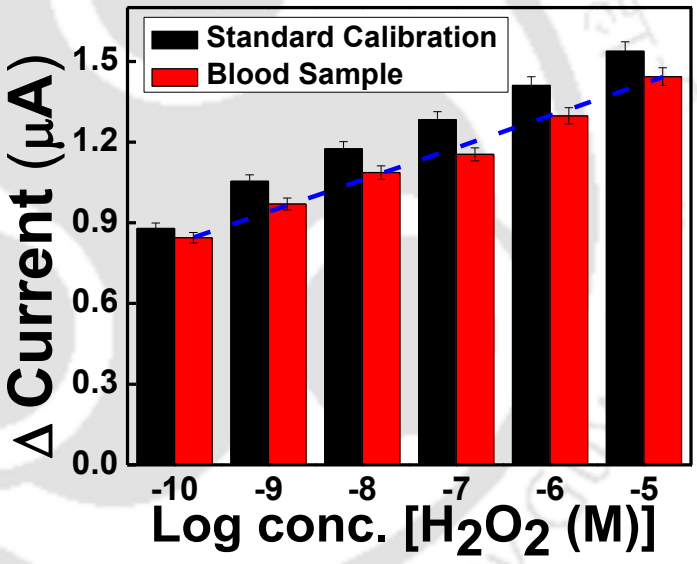

Figure 2. 11 Dose-dependent DPV responses obtained from the ITO/AuND/AuSP sensor probe at various concentrations (10-^{10}M - 10^{-5} M) in blood (red) and PBS (black).

SI No.	Electrode Fabrication	LDR	LOD	Response Time	Real Sample	References / Year
1	Ag@Cu_2O / N-RGO	54 – 700 x 10^{-9} M	10 x 10^{-9} M	10 secs	Blood plasma	(Li et al. 2018) /
2	GCE / Naf-rGO-APTES	0.05 - 15.25 x 10^{-3} M	17 x 10^{-6} M	5 secs	NR	(Bai et al. 2017)
3	GCE / SnO_2-PEI-Gr	1.64 x 10^{-3} - 9 x 10^{-6} M	1 x 10^{-6} M	3 secs	NR	(Liu et al. 2017c)
4	GCE / MoS_2-PBNCs	0.01 – 300 x 10^{-6} M	4.1 x 10^{-9} M	NR	NR	(Su et al. 2017)
5	GCE / Naf / $CoSn(OH)_6$ NC	4 – 400 x 10^{-6} M	1 x 10^{-6} M	5 secs	Serum	(Shu et al. 2017)
6	Ag / Sn_3O_4	5.25 x 10^{-3} - 0.8 x 10^{-6} M	0.8 x 10^{-6} M	NR	NR	(Tian et al. 2017)
7	GCE/ rGO NR / MnO_2	0.25 – 2245 x 10^{-6} M	0.071 x 10^{-6} M	NR	Fetal bovine serum	(Wu et al. 2017)
8	GCE / Naf / CuNi-NGr	0.01 – 1 x 10^{-6} M	10 x 10^{-6} M	5 secs	Urine	(Shabnam et al. 2017)
9	GCE/ GDC/ NiO	0.01 - 3.9 x 10^{-6} M	1.5 x 10^{-9} M	NR	Milk and tap water	(Sivakumar et al. 2019)
10	**ITO / AuND /AuSP**	**1 x 10^{-5} – 1 x 10^{-12} M**	**9.8 x 10^{-13} M**	**≤ 1 sec**	**Blood**	**This work**

Table 1. A comparative account of the developed nanoprobe with previously reported H_2O_2 sensors and their analytical performance.

NR = not reported.

3.6. Reproducibility and stability assay

To check the reproducibility of the nanoprobe as an efficient electrode for the detection of the H_2O_2, we separately tested five ITO/AuND/AuSP probes in PBS solution containing 0.40 M H_2O_2. We found variation in the peak current to be negligible ($p < 0.001$), however the subtle changes in the peak currents might be due to handling error and fluctuation in environmental conditions. We also tested the ability of a single nanoprobe for five consecutive analyses of H_2O_2 which shows 97% sensitivity without any pretreatment (RSD 3.7%, n =3). The long term stability had also been evaluated for the fabricated ITO/AuND/AuSP sensing probe. For that, the DPV responses were recorded periodically for 12 weeks, with an interval of one week for each measurement, and the retention of the signal was found to be 93-96%. This result shows that the nanoprobe is an efficient sensing surface with stability up to 12 weeks. High stability of the fabricated ITO/AuND/AuSP nanoprobe may be due to the fact that there are no biomolecules incorporated in the sensing matrix.

4. Conclusions

A simple, selective, and stable nonenzymatic nanoprobe for the detection of H_2O_2 has been designed based on the gold sputtering on hierarchical gold nano dendritic structures. The nanoprobe surface was thoroughly characterized using SEM, EDX, TEM, SAED, CV, EIS, DPV, and chronoamperometry. The LOD was found to be 9.8 (±0.024) x 10^{-13} M with two LDRs of 1 x 10^{-12} – 1 x 10^{-10} M and 1 x 10^{-10} –1 x 10^{-5} M, which was significantly improved than the previously reported H_2O_2 sensors. The nanoprobe was capable of effectively detecting H_2O_2 in blood, with 90-96% of recovery by spike and recovery method. The nanoprobe was found to be highly selective toward H_2O_2 with no interference by commonly present molecules found in blood, and was stable up to 12 weeks. To the best of our knowledge, for the first

time we have reported a nonenzymatic H_2O_2 nanoprobe based on the peroxidase activity of gold sputtered hierarchical gold dendritic nanoprobe. The inspiration behind the work to utilize and repurpose a metallic nanochip generally of no use after gold sputtering for SEM imaging (from waste to value). The nanoprobe follows a low cost, rapid synthesis, and fabrication steps which can be further utilized for the real-time monitoring of H_2O_2 in different pathological conditions. In the future, the ITO/AuND/AuSP nanoprobe can be miniaturized as a genuine point of care personalized biomedical device for H_2O_2 sensing.

5. References:

Bai H, Zhang L, Shen H, Liu L (2017) Facile synthesis of cuprous oxide/gold nanocomposites for nonenzymatic amperometric sensing of hydrogen peroxide. Electroanalysis 29:2773–2779

Bard AJ, Faulkner LR, Leddy J, Zoski CG (1980) Electrochemical methods: fundamentals and applications. wiley New York

Brand MD (2016) Mitochondrial generation of superoxide and hydrogen peroxide as the source of mitochondrial redox signaling. Free Radic Biol Med 100:14–31. https://doi.org/10.1016/j.freeradbiomed.2016.04.001

Chandra P (2016) Nanobiosensors for Personalized and Onsite Biomedical Diagnosis, the Institution of Engineering and Technology, Michael Faraday House

Chandra P, Noh H, Won M, Shim Y (2011) Biosensors and Bioelectronics Detection of daunomycin using phosphatidylserine and aptamer co-immobilized on Au nanoparticles deposited conducting polymer. Biosens Bioelectron 26:4442–4449.

Cheng TM, Huang TK, Lin HK, et al (2010) (110)-Exposed gold nanocoral electrode as low onset potential selective glucose sensor. ACS Appl Mater Interfaces 2:2773–2780.

Hoshino M, Kamino S, Doi M, et al (2014) Spectrophotometric determination of hydrogen peroxide with osmium (VIII) and m-carboxyphenylfluorone. Spectrochim Acta Part A Mol Biomol Spectrosc 117:814–816

Jay H, Bernardo A, Davies KJA (2016) What is the concentration of hydrogen peroxide in blood and plasma ? 603:48–53

Krainer FW, Glieder A (2015) An updated view on horseradish peroxidases: recombinant production and biotechnological applications. Appl Microbiol Biotechnol 99:1611–1625.

Kumar A, Purohit B, Maurya PK, et al (2019) Engineered Nanomaterial Assisted Signal-amplification Strategies for Enhancing Analytical Performance of Electrochemical Biosensors. Electroanalysis 31:1615–1629.

Li J, Jiang J, Xu Z, et al (2018) Facile synthesis of Ag@ Cu2O heterogeneous nanocrystals decorated N-doped reduced graphene oxide with enhanced electrocatalytic activity for ultrasensitive detection of H_2O_2. Sensors Actuators B Chem 260:529–540

Li L, Du Z, Liu S, et al (2010) A novel nonenzymatic hydrogen peroxide sensor based on MnO2/graphene oxide nanocomposite. Talanta 82:1637–1641.

Liu A-L, Hong L, Deng H-H, et al (2012) Comparison of the Peroxidase-Like Activity of Unmodified, Amino-Modified, and Citrate-Capped Gold Nanoparticles. ChemPhysChem 13:1199–1204.

Liu C, Ding Y, Li Q, Lin Y (2017a) Photochemical synthesis of glutathione-stabilized silver nanoclusters for fluorometric determination of hydrogen peroxide. Microchim Acta 184:2497–2503

Liu M, Liu R, Chen W (2013) Biosensors and Bioelectronics Graphene wrapped Cu 2 O nanocubes : Non-enzymatic electrochemical sensors for the detection of glucose and hydrogen peroxide with enhanced stability. Biosens Bioelectron 45:206–212.

Liu Q, Chen P, Xu Z, et al (2017b) A facile strategy to prepare porphyrin functionalized ZnS nanoparticles and their peroxidase-like catalytic activity for colorimetric sensor of hydrogen peroxide and glucose. Sensors Actuators B Chem 251:339–348

Liu X, Huang D, Lai C, et al (2019) Peroxidase-Like Activity of Smart Nanomaterials and Their Advanced Application in Colorimetric Glucose Biosensors. Small 1900133:1900133.

Liu Y, Shang T, Liu Y, et al (2018) Highly sensitive platinum nanoparticles-embedded porous graphene sensor for monitoring ROS from living cells upon oxidative stress. Sensors Actuators B Chem 263:543–549

Liu Y, Wang L, Yang L, et al (2017c) Nonenzymatic H2O2 Electrochemical Sensor Based on SnO2-NPs Coated Polyethylenimine Functionalized Graphene. Electroanalysis 29:2044–2052

Luo M, Wang W, Zhao Q, et al (2017) Chemiluminescence biosensor for hydrogen peroxide determination by immobilizing horseradish peroxidase onto PVA-co-PE nanofiber membrane. Eur Polym J 91:307–314

Ma B, Kong C, Hu X, et al (2018) A sensitive electrochemical nonenzymatic biosensor for the detection of H2O2 released from living cells based on ultrathin concave Ag nanosheets. Biosens Bioelectron 106:29–36

Mahato K, Maurya PK, Chandra P (2018) Fundamentals and commercial aspects of nanobiosensors in point-of-care clinical diagnostics. 3 Biotech 8:1–14.

Naveen MH, Gurudatt NG, Noh HB, Shim YB (2016) Dealloyed AuNi Dendrite Anchored on a Functionalized Conducting Polymer for Improved Catalytic Oxygen Reduction and Hydrogen Peroxide Sensing in Living Cells. Adv Funct Mater 26:1590–1601.

Noh HB, Lee KS, Chandra P, et al (2012) Application of a Cu-Co alloy dendrite on glucose and hydrogen peroxide sensors. Electrochim Acta 61:36–43.

Pallela R, Chandra P, Noh HB, Shim YB (2016) An amperometric nanobiosensor using a biocompatible conjugate for early detection of metastatic cancer cells in biological fluid. Biosens Bioelectron 85:883–890.

Shabnam L, Faisal SN, Roy AK, et al (2017) Nonenzymatic multispecies sensor based on Cu-Ni nanoparticle dispersion on doped graphene. Electrochim Acta 224:295–305

Shu Y, Li B, Xu Q, et al (2017) Cube-like CoSn (OH) 6 nanostructure for sensitive electrochemical detection of H2O2 in human serum sample. Sensors Actuators B Chem 241:528–533

Sivakumar M, Veeramani V, Chen SM, et al (2019) Porous carbon-NiO nanocomposites for amperometric detection of hydrazine and hydrogen peroxide. Microchim Acta 186:2–9.

Su S, Han X, Lu Z, et al (2017) Facile synthesis of a MoS2--Prussian blue nanocube nanohybrid-based electrochemical sensing platform for hydrogen peroxide and carcinoembryonic antigen detection. ACS Appl Mater Interfaces 9:12773–12781

Tanner JJ, Parsons ZD, Cummings AH, et al (2011) Redox Regulation of Protein Tyrosine Phosphatases : Structural and Chemical Aspects. 15:

Tian L, Xia K, Hu W, et al (2017) A wide linear range and stable H2O2 electrochemical sensor based on Ag decorated hierarchical Sn3O4. Electrochim Acta 231:190–199

Verma S, Singh A, Shukla A, et al (2017) Anti-IL8/AuNPs-rGO/ITO as an Immunosensing Platform for Noninvasive Electrochemical Detection of Oral Cancer. ACS Appl Mater Interfaces 9:27462–27474.

Wu Z-L, Li C-K, Yu J-G, Chen X-Q (2017) MnO2/reduced graphene oxide nanoribbons: facile hydrothermal preparation and their application in amperometric detection of hydrogen peroxide. Sensors Actuators B Chem 239:544–552

Xu X, Jia J, Yang X, Dong S (2010) A Templateless , Surfactantless , Simple Electrochemical Route to a Dendritic Gold Nanostructure and Its Application to Oxygen Reduction. 26:7627–7631.

Ye W, Yan J, Ye Q, Zhou F (2010) Template-Free and Direct Electrochemical Deposition of Hierarchical Dendritic Gold Microstructures : Growth and Their

Multiple Applications. 15617–15624

Zhu Y, Chandra P, Shim Y-B (2012) Ultrasensitive and selective electrochemical diagnosis of breast cancer based on a hydrazine--Au nanoparticle--aptamer bioconjugate. Anal Chem 85:1058–1064

Chapter # III

Direct co-electrodeposition of hierarchical novel bimetallic Au-Cu dendritic nanostructures for biomolecular sensing in human urine

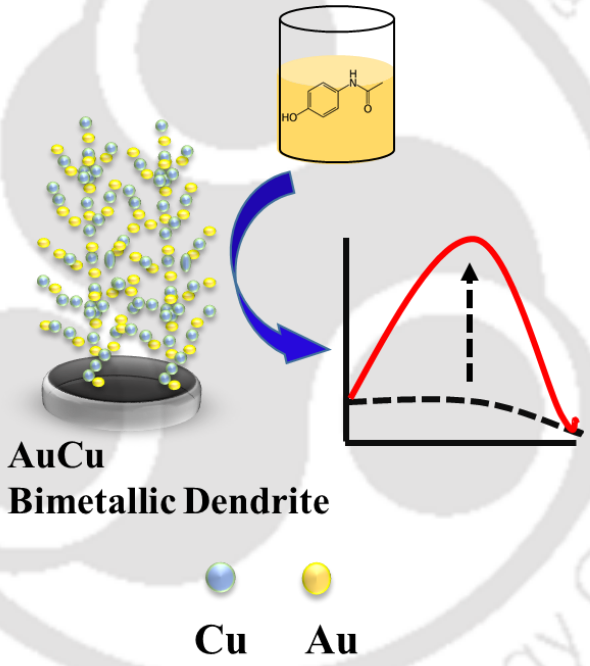

Status:

Manuscript submitted

1. Introduction

In the second objective, we attempted to develop a dendritic system for the detection of molecules of clinical importance. One such molecule of high clinical interest is acetaminophen (N-acetyl-p-aminophenol, AP), commonly used as antipyretic and analgesic medicine. A therapeutically acceptable dose of AP doesn't cause any harm in the body, as most of them are metabolized in liver and excreted through urine. When over dosed, however AP is found to cause inflammation in pancreases, nephrotoxicity, and hepatotoxicity (Chun et al. 2009; Hinson et al. 2010; Reddy et al. 2018). Liver is the most affected organ by AP toxicity, and a major portion of acute liver failure cases is due to AP over dosage (Chun et al. 2009; Bernal et al. 2010). Therefore, a sensitive detection of AP is necessary for the treatment of such cases. So far, Several analytical techniques have been used for the detection of AP including spectrophotometry(Moreira et al. 2005), spectrofluorometric (Moreira et al. 2005), high-performance liquid chromatography(Nebot et al. 2007; Gioia et al. 2008), gas chromatography, thermos gravimetric analysis (Burgot et al. 1997), NMR(Sun et al. 2008), and chemiluminescence. Although these techniques are sensitive, they include a very complicated, high cost and time consuming methods for the detection of AP.

Biosensors are analytical devices, which can be used for the detection of such analytes at very low concentrations. Electrochemical biosensors, a class of biosensor, most widely used due to its simple, low cost, more sensitive, and time saving methods for the detection of analytes(Kumar et al. 2019b). Recently reported electrochemical sensors integrate a wide range of nonmaterial to attain unique catalytic activity, enhance

their sensitivity, and reduce fouling effects owing to their enhanced physical and chemical behavior than their bulk material. Their opto-electronic and electro-catalytic properties are widely used in the development of various biosensing methodologies to achieve higher sensitivity, and signal amplification for the detection of several biomarkers. Novel metallic nanoparticles, carbon dots, quantum dots, graphene are being widely reported to develop innovative biosensing matrices. Metallic dendrites (MD), a class of nanoparticles are a self-assembled hierarchical arrangement of primary, secondary, and tertiary branches with a very high density of sharp tips, edges, and ridges possess very high catalytic activity (Naveen et al. 2016). Exploiting the electro-catalysis nature, various types of monometallic dendritic structures have been employed for the biosensor fabrication *i.e.* Au (Nesbitt et al. 2018), Ag (Ham et al. 2017), Pt (Wu et al. 2014), Cu (Zhang et al. 2008), Co(Fan et al. 2009) etc.

Among all MDs, gold-based dendritic structures (AuND) have been widely studied due its excellent optimizable shape and size dependent catalytic property, excellent biocompatibility (Xu et al. 2010), surface enhanced Raman scattering (SERC)(Lu et al. 2007), and photoluminescence (PL) (Hu et al. 2007). Though there are other form of Au based structures like flower shaped, urchin like, mushroom developed and studied, dendrites offer more promises due to its excellent catalytic activity. However, bimetallic/ multi-metallic dendrites have been reported to exhibit better catalytic activity than monometallic nanoparticles due to their synergistic effect (Zhang et al. 2009; Liu et al. 2011; Li et al. 2013).Several combinations of Au-based metallic dendritic systems *viz.* Ni (Wang et al. 2016b; Naveen et al. 2016), Pt (Liu et al. 2011), TiO_2 (Wang et al.

2016c), etc. have been reported as biosensing matrices, due to their altered/unique catalytic and electronic behavior than their individual state.

Another transition metal, copper (Cu) is one of the most commonly used catalyst in a wide range of chemical reactions. However, to the best of our knowledge, there is no report of AuCu dendritic structures been developed for its biosensing application in biological samples. Though Cu dendrites (CuND) are also reported for their catalytic activity (Decan et al. 2014; Wang et al. 2016a; Ojha et al. 2017). Therefore, it is interesting to use Cu as dopant in Au based bimetallic system, which may offer excellent electro-catalysis due to the synergistic effect of both Au and Cu to be used in biosensing applications.

The synthesis of Au based MD has been achieved by various methods, which includes surfactant-mediated synthesis, galvanic replacement synthesis, and electrochemical synthesis. In addition to this, Au-dendrites have also been synthesized using small molecules like poly(N-vinyl-2-pyrrolidone), β-cyclodextrin, cysteine(Lin et al. 2011) etc. These synthetic process of MD are time consuming, costly and follows many complex protocols eventually making the fabrication process tedious and multistep. To overcome these limitations, electrochemical-based procedures have been widely adopted for facile and robust MD synthesis, which facilitate the direct and uniform deposition of dendritic structures (Shu et al. 2014). In this process of dendrite formation, the growth rate and branching over the surface can also be controlled easily by fine tuning few parameters *viz.* applied potential, salt concentration, deposition time etc. (Shu et al. 2014).

In the second objective, we developed a bimetallic hierarchical Au-Cu dendritic like nanostructure over GCE by tuning the electrodeposition parameters for enhanced catalytic as well as bioelectronics property for the detection of AP. The sensor probe was physically characterized by SEM, TEM, EDX, and SAED to access its morphological and crystal property. The electrochemical characterization includes LSV, EIS, and chronoamperometry to access its electronic property. After the physical and electrochemical characterization studies, the analytical performance of the sensor probe was evaluated to sense AP by using DPV in terms of linear dynamic range (LDR) and lower limit of detection (LOD). The clinical applicability of the AuCuND sensor was also evaluated by sensing AP in human urine samples by spike and recovery method. Interference due to commonly found molecules and long term stability of the sensor was also evaluated. **Figure 3.1** shows the graphical representation of the work.

2. Experimental

2.1. Chemicals and Instruments

Potassium chloride (KCl), potassium ferricyanide [$K_3Fe(CN)_6$], potassium ferrocyanide [$K_4Fe(CN)_6$], sodium monophosphate and sodium bisphosphate were purchased from Himedia Pvt. Ltd., India. Chloroauric acid ($HAuCl_4$) and AP was obtained from Sigma-Aldrich Chemical Co. (USA). Sodium chloride (NaCl), citric acid, ascorbic acid, uric acid, d-glucose, urea, l-glycine, l-alanine, l-glutamic acid, l-cysteine, dopamine, serotonin was purchased from SRL Pvt. Ltd, India. All aqueous solutions were prepared in doubly distilled water obtained from a Milli-Q water purifying system (18 MΩ cm). all other chemicals used in this study were of standard grade.

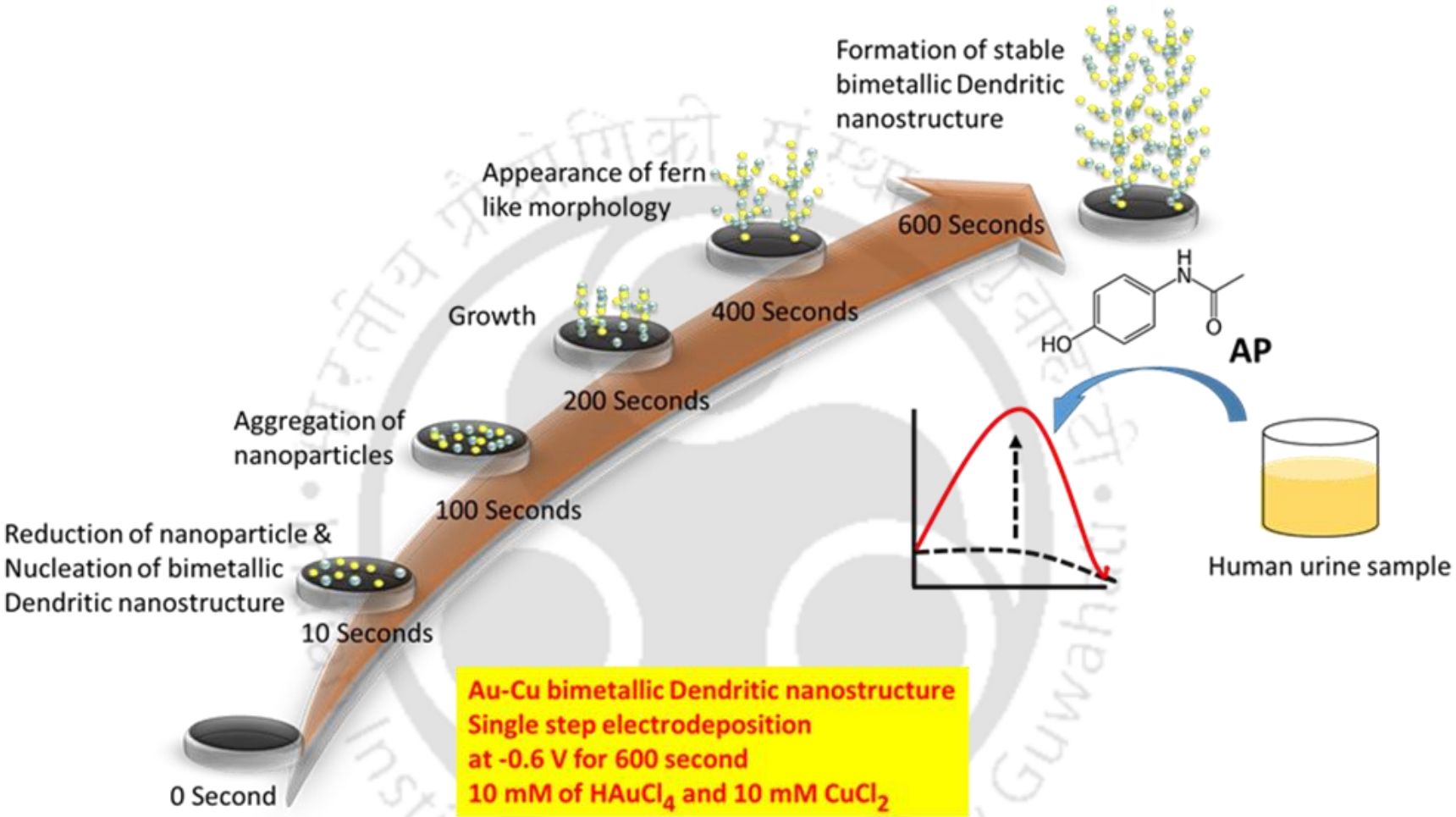

Figure 3.1. Schematic representation of AuCuND sensor fabrication and its application in AP biosensing in human urine samples.

Synthesis of the AuCu, Au, Cu dendritic nanostructures by the direct electrochemical method was performed by an electrochemical workstation (Metrohm Autolab) using three electrode based electrochemical cell. Glassy carbon electrode (GCE), platinum (Pt) wire, and Ag/AgCl (saturated with KCl) were used as the working, counter, and reference electrodes, respectively. Morphology of the thus formed dendrite was evaluated at different magnification at an operating voltage of 3.0 KV at different magnification by using a field emission scanning electron microscope (FESEM) (Zeiss, Gemini). The elemental composition of the developed MD was accessed by performing energy dispersive x-ray spectroscopy (EDX) mode in FESEM. Transmission electron microscope (TEM) images and selected area electron diffractogram (SAED) were obtained from field emission transmission electron microscope (FETEM) (JEOL, 2100F) to study the morphology and structural features.

2.2. Preparation of final AuCuND nanoprobe

The GCE electrode was cleaned to a mirror-like finish with alumina powder on a polishing cloth and rinsed several times in MilliQ water to remove any trace of ions or salt over its surface. For the synthesis of the bimetallic AuCuND over the GCE, 0.1 M KCl electrolysis solution was used containing 10 mM $HAuCl_4$ and 10 mM $CuCl_2$. The applied potential for the synthesis of the alloy dendrite was optimized to be -0.6 V for 600 seconds. This is very interesting to note that the GCE/AuCuND probe development follows a single step, facile, robust electrode synthesis procedure with a total fabrication time of 10 minutes. As control experiment, electrodes modified with monometallic Au and Cu three dimensional dendrites were prepared separately in a 0.1 M KCl solution containing 10mM $CuCl_2 \cdot 6\ H_2O$ or 10 mM $HAuCl_4$ salt for comparative electro-catalysis

study. The dendritic surfaces were cleaned with ethanol and distilled water prior to electrochemical studies.

2.3. Analytical studies of the AuCuND probe

The electrochemical studies of the sensor probe were carried out in phosphate buffer (PBS, pH 7.0 and 0.9% NaCl) and PBS containing 5 mM $[Fe(CN)_6]^{-3/-4}$ (Zobell's solution (ZS)) by using CV, LSV, and EIS methods. The impedance spectra were recorded at an open circuit voltage between 100 Hz and 1 MHz with a sampling rate of five points per decade. For the, detection of AP, DPV responses were recorded by scanning the potential from +0.30 to +0.50 V vs. Ag/AgCl at a scan rate of -0.005 V/s, with pulse potential -0.025 V and pulse time-0.05 s. The real sample analysis of AP was carried out in urine collected from three healthy individuals. The urine was diluted 10 times in PBS before analysis without any other treatment.

3. Result and discussion

3.1. Preparation of the AuCuND probe

The electrodeposition of the AuND and CuND were optimized to form a dendritic film over the electrode surface at -0.3 V, and -0.6 V, respectively. The change in current response in chronoamperometry with increase in electrolysis time is the first indication of the formation of a conducting layer, mostly due to the dendrite formation under optimized conditions. Then the AuCuND was prepared by the chronoamperometry method, where an increase in the current response after applying a fixed voltage shows the first indication of the dendrite formation. The applied potential and time was optimized to be -0.6 V and 600 seconds, respectively. The applied potential between 0.2 V and -0.8 was tested for the synthesis of the bimetallic dendrite, where the -0.6 V shows

the best electron transfer activity. We optimized the electrodeposition time between 100 s and 600 s, where the decrease in the Rct value in EIS responses in 5.0 mM PBS with time indicates the initiation and growth of the dendritic structure. Interestingly, no change after 600 s of Rct value with further increase in the electrodeposition. Also, after 600 s of electrodeposition time, the AuCuND film become so thick that it no longer adhere to the electrode surface and fall into the electrolyte solution. The increase in the current response in the chronoamperometry method with the electrodeposition time, may be due to the co-deposition of the Au and Cu on to the electrode surface.

The red circles in figure 3.2 (A) shows the oval shaped nucleation site where the formation of AuCuND starts. The blue rectangles show the sites of aggregation of oval shaped materials to form bigger structures. The size of aggregated materials increased with increase in electrolysis time. The first distinguishable AuCuND structure was formed at 100 s, where smaller aggregates of the nanoparticles in form of rods and small sphere are clearly visible. The size of the dendrite structure increased exponentially in 200 s, whereas at 400 s the dendrites become well defined. The final probe with electrolysis time of 600 s shows the minimum Rct value, used for further electrochemical characterization and analytical performances.

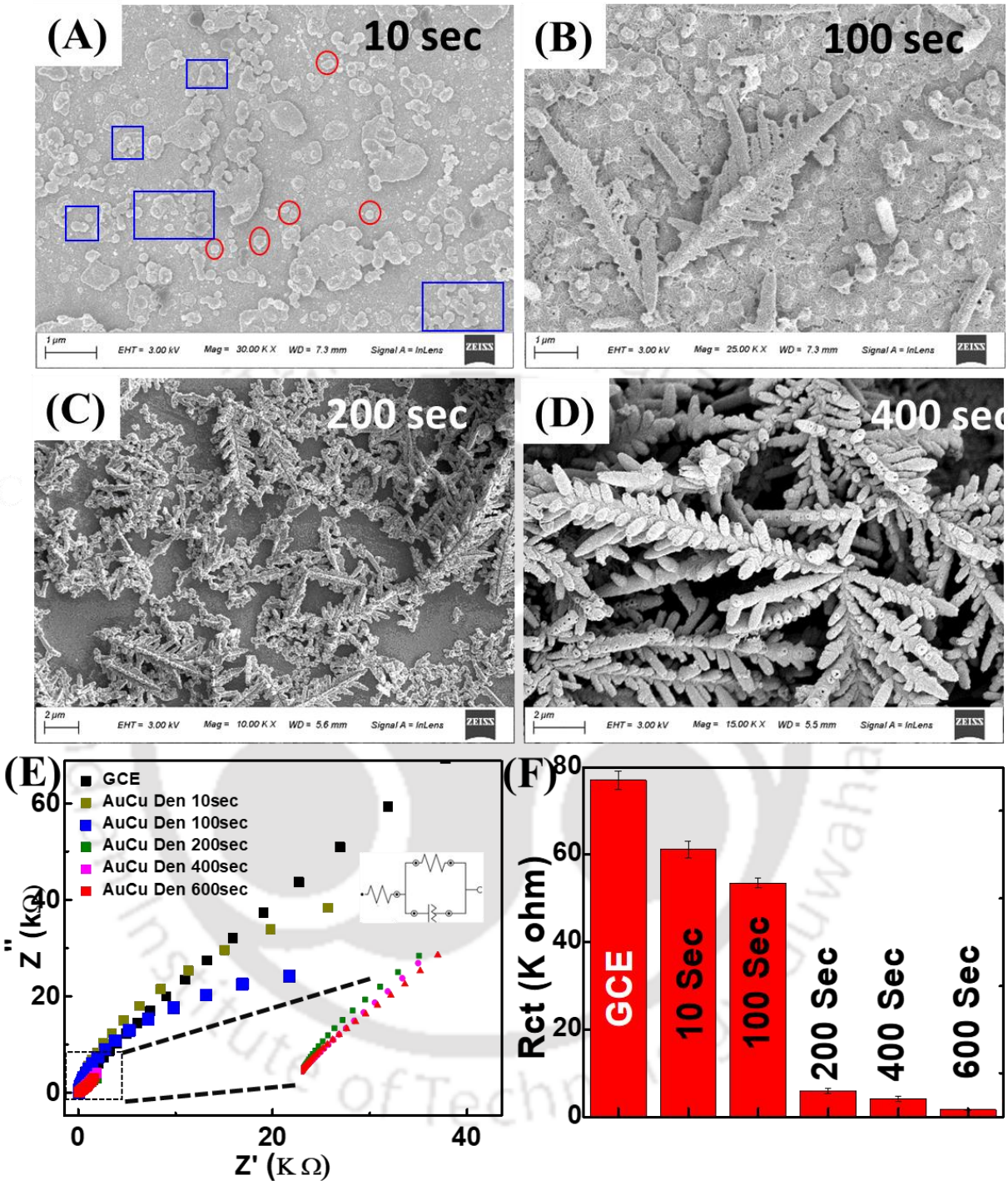

Figure 3.2. SEM micrographs of AuCuND with electrolysis time of (A) 10 s, (B) 100 s, (C) 200 s, and (D) 600 s, respectively. (E) Shows the corresponding Nyquist plot in PBS; (F) Histogram shows the Rct values of the electrodes.

3.2. Physical characterization of final GCE/AuCuND sensor probe

The nano-composite utilized in the sensor fabrication has been systematically characterized using various techniques. SEM, EDX, TEM, SAED, and elemental mapping analysis were performed to access both morphological as well as chemical composition. For SEM and EDX analysis, an ultra-cleaned ITO was used as electrode surface to deposit the dendritic structure. The ITO was activated in a solution containing NH_4OH: H_2O_2: H_2O in the ratio of 1:1:5 for homogeneous growth of the dendrite, and followed the same electrodeposition protocol as mentioned earlier in both precursor salts. **Figure 3.2 (A)** shows a leaf like dendritic patterned structure with prominent primary and secondary branches. The smaller secondary branches are grown over the much thicker primary branches. The length of the secondary branches is around 2-4 µm and tertiary branches are around 0.5 µm, with different µm thickness. However, the primary branch is much more in length (> 5 µm) and much thicker in thickness. EDX analysis of the same structure was performed further to confirm the composition of the structure (**figure 3.2. B**). A multipoint EDX analysis shows the Cu content to be 12 % and Au content to be 87 %. The same chemical composition of Au and Cu follows at every point in the primary and secondary branches all over the dendritic material. To verify the bimetallic formation, we conducted two set of control experiments. In the first set, we followed the electrodeposition protocol as mentioned previously in the 0.1 M KCl solution, with an exception of without adding both Au and Cu salts. The SEM analysis shows no structures formed over the GCE surface. In the second set of experiment, we performed the electrodeposition with only Au or Cu salt as mentioned in the section 2.2. The SEM analysis shows formation of Au and Cu dendrite (image not shown). The morphological feature of bimetallic dendrite is different than both Au and

Cu dendrite. The EDX analysis of these two structures also confirms the presence of only one predominate element.

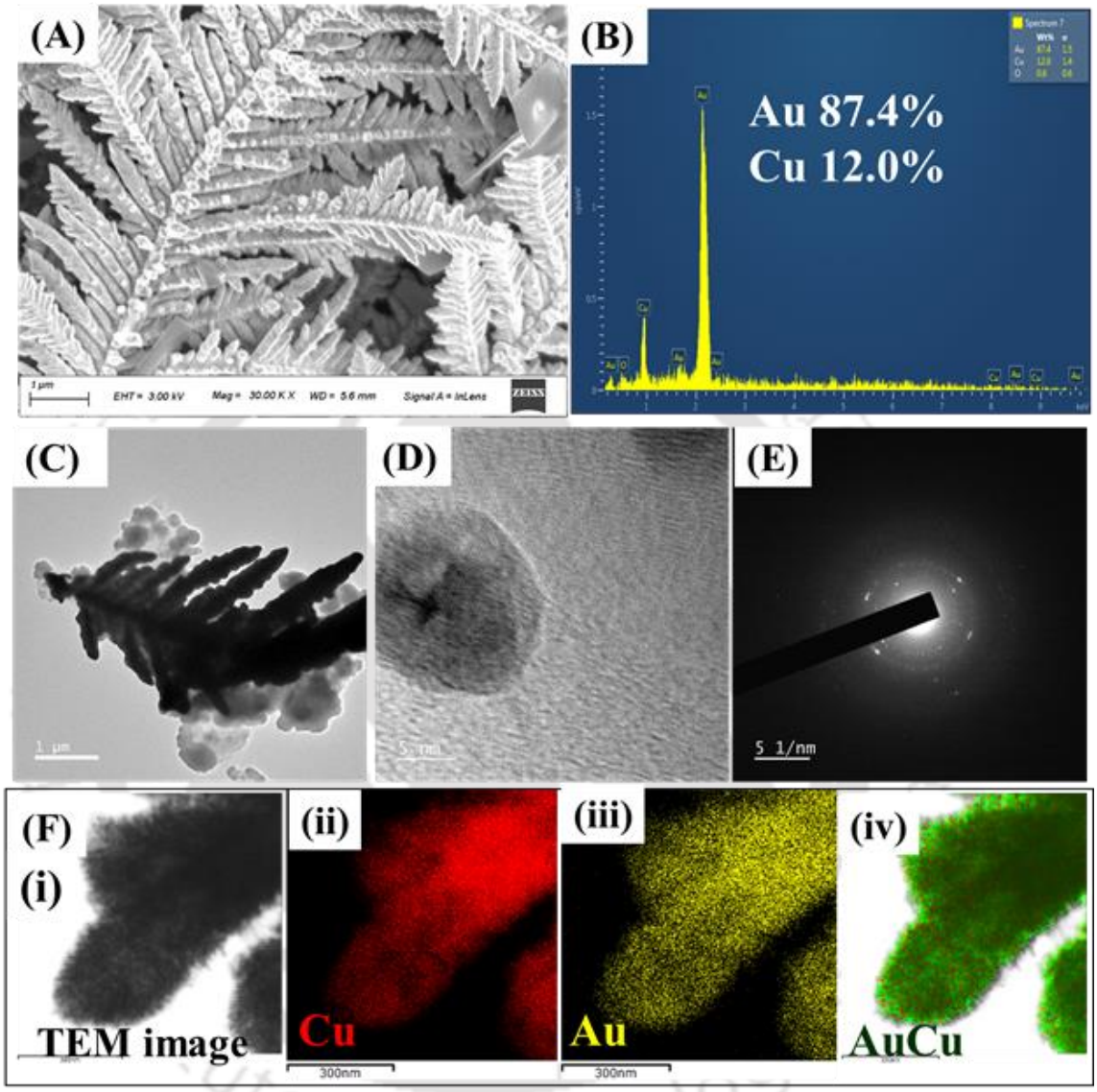

Figure 3.3. (A) SEM image of AuCuND with electrolysis time of 600 s showing characteristics dendritic pattern; (B) EDX analysis of the AuCuND structure showing chemical composition; (C) TEM image, (D) d spacing pattern, and (E) SAED pattern of the of AuCuND; (F) Shows the elemental mapping of bimetallic electrode with (i) dark field image, (ii) Cu element (red), (iii) Au element (yellow), (iv) merged image showing an equal distribution of both Au and Cu element over the surface.

The AuCuND was further characterized by TEM analysis, where the sample was collected and dried over TEM grid after sonicating the scratched material in ethanol for 1 min. The obtained TEM image shows a typical dendrite like structure as found in the SEM image **figure 3.3 (C)**. In the SAED analysis, the diffraction pattern indicates the crystalline nature of AuCu dendrite (fig 3.3. E). **Figure 3.3 (F)** shows elemental mapping images, which shows (ii) Cu element (red), and (iii) Au element (yellow) distribution over the surface. The TEM image in dark field (i) shows tip region of a typical dendrite process, where the Au and Cu element are distributed equally all over the structure. The elemental mapping confirms the co-electrodeposition of AuCu dendrites, in other words the Au and Cu element might affect the electrodeposition of one another. This also refers that the dendrites don't accumulate clumps of Au and Cu, which might have led to uneven pattern of electro catalysis. The comparative XRD analysis of AuND, CuND, and bimetallic AuCuND confirms the formation of an alloy of Au and Cu (**figure 3.4**).

3.3. Electrochemical characterization of the GCE/AuCuND sensor probe

The developed sensor probe GCE/AuCuND was further characterized electrochemically to evaluate its bioelectronics properties. The first characterization of the sensor involves LSV analysis in 5 mM ZS as shown in figure 2.A with a potential range of -0.8 to 0.8V and a scan rate of 50 mV/S. The LSV responses shows a typical voltammogram formed due to the redox reaction of the $[Fe(CN_6)]^{3-/4-}$ element of ZS. The LSV response of AuCu bimetallic dendrite (blue curve) were found to have higher cathodic peak than the bare GCE (black curve).

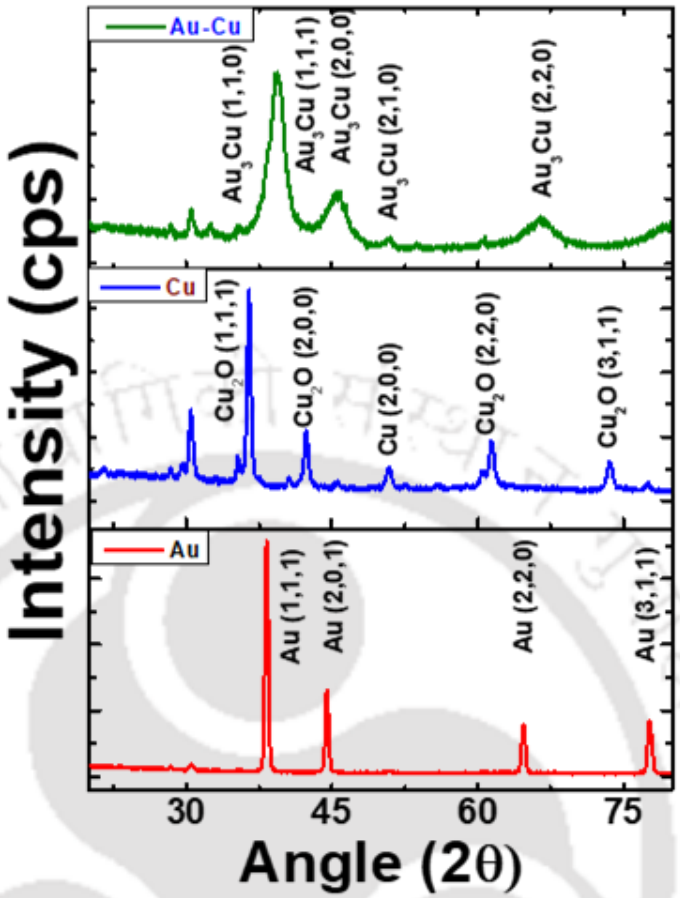

Figure 3.4. XRD analysis of the AuCu (green), Cu (blue), and Au (red) dendrites shows the crystal plane.

It is interesting to note that, the LSV responses of the control electrodes i.e. Au (red curve) and Cu (green curve) monometallic dendrite less than GCE/AuCuND electrode. The increased current response in the bimetallic dendrite surface than dendrite with its individual constituent element, signifies the synergistic effect of both Au as well as Cu in the structure. Also, the LSV peak value of GCE/CuND is less than the bare GC. The decrease in current value might be due to the formation of copper oxide dendrite. The metal oxides are known to be less conducting and in the presence of a negatively charged surface (of copper oxide), the charged elements of ZS got repelled resulting in the decrease in the LSV responses (Nasibi et al., 2012).

The increase in charge transfer capacity of the electrodes was evaluated quantitatively by comparing the diffusion coefficient of the bare GEC, GCE/AuND, GCE/CuND and GCE/AuCuND surface by using Randles-Sevcik's model (equation 1) (Bard et al. 1980).

$$I_p = \left(2.69\times10^5\right) n^{3/2} ACD^{1/2} v^{1/2} \quad \ldots \textbf{Equation 1}$$

Where, Ip is the peak current (in ampere), n is the number of electrons transferred in redox process (here n=1), A is the electrode surface area (in cm^2), C is the concentration of electroactive species (in mole cm^{-3}), D is the diffusion coefficient (in $cm^2\ s^{-1}$), and v is the scan rate (in Vs^{-1}).

The diffusion coefficient (*D*) values for bare GCE, GCE/AuND, GCE/CuND, and GCE/AuCuND electrode surfaces were found to be 3 x 10^{-6} cm^2s^{-1}, 2.61 x 10^{-6} cm^2s^{-1}, 4.2 x 10^{-6} cm^2s^{-1}, and 7.2 x 10^{-6} cm^2s^{-1}, respectively. The maximum D value of GCE/AuCu dendrite refers to the highest efficiency in electron transfer than other surfaces. In order to further evaluate the stability and charge transfer behaviour of the final sensor probe, LSV responses were recorded in 10-100 mV/S^{-1} scan rates in 5 mM ZS (**figure 3.5. C**). The cathodic (Ipc) peak currents (f**igure 3.5. D**) were found to be directly proportional to the square root of the scan rate, with correlation coefficient of 99.9 %. This shows the higher stability of the bimetallic surface as well as diffusion controlled charge transfer process at the electrode surface.

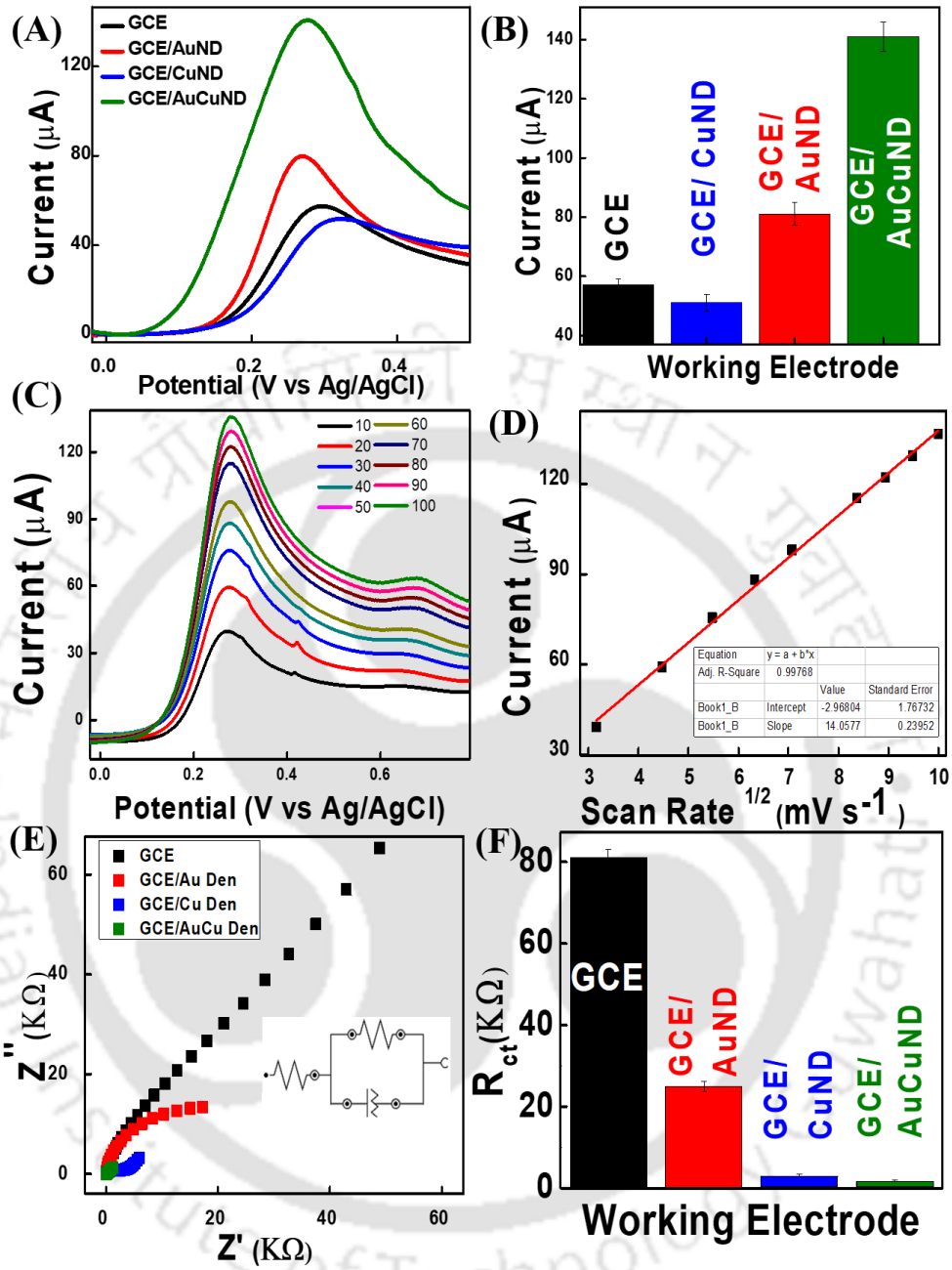

Figure 3.5 (A) shows the maximum LSV responses of bimetallic AuCuND surface than control monometallic sensor fabrication in ZS, and (B) comparative histogram shows corresponding peak values; (C) The scan rate dependent study of GCE/AuCuND surface in ZS with the scan rate of 10-100 mV/s, and the peak value following linearity showing stability of the sensor (D); Nyquist plot of the AuCuND sensor surfaces was evaluated

in PBS (E), and the corresponding Rct value (F) shows the bimetallic probe showing least resistance.

A complementary experiment to CV, electrochemical impedance spectroscopy (EIS) was performed to measure the resistance of the electrode surfaces in PBS **(figure 3.5 E)**. The Rct values of bare GCE (black curve), GCE/AuND (red curve), GCE/CuND (green curve), and GCE/AuCuND (blue curve) electrode were found to be 80.2 (±2.2), 24.3 (±1.2), 2.9 (±0.4), and 1.6 (±0.3) KΩ (histogram shown in **figure 5.3 F**). The EIS data corroborates the LSV responses showing that the AuCu surface showed the least resistance and maximum charge transfer capacity, ideal for a fabricated sensor surface to use for sensing application.

Larger surface area of GCE/AuCuND surface is not the only reason for its excellent electronic behaviour, as both Au and Cu dendritic surface have also large active surface area with equally concentrated distribution of edges and tips. It is here to note that, both Au and Cu are the among the best conducting metals with excellent charge transfer capacity. The higher charge conducting capacity of the bimetallic dendrite than both these elements, shows the electronic potential of this surface for future applications.

3.4. Analytical performance of GCE/AuCuND sensing probe

The potential of the developed GCE/AuCuND surface was evaluated for biosensing application taking AP as a model molecule. Various electrochemical studies were performed to access the clinical potential of the electrode. First, LSV responses of final bimetallic AuCuND sensor surface was recorded by sweeping the potential between 0 – 0.6 V in blank PBS, where no peak was observed as expected in the absence of any

redox molecule. Then one more LSV sweep was recorded with the same experimental set up in the presence of 1 x 10^{-4} M of acetaminophen. In the presence of AP, however a sharp peak appeared at -0.38 V (green curve of **figure 3.6**). LSV peak of AP near this potential due to catalysis of AP was earlier reported, showing the catalytic potential of the GCE/AuCuND (Kumar et al. 2019a). We further tested other electrodes in the same experimental setting in the presence/ absence of AP. No signal or peak was observed in blank PBS for bare GCE, GCE/AuND, or GCE/CuND dendritic electrode. However, in the presence of AP all the three control electrode developed peak current around -0.4 V. This control experiment further signifies the importance of the final probe in two ways. It is interesting to note that, the peak current in the GCE/AuCu electrode is significantly higher in magnitude than all the three electrodes (**figure 3.6 B).** Secondly, the catalysis peak of AP shifted towards lesser potential, showing the capacity of the electrode to catalyse AP at lower potentials.

Further to validate the peak at 0.37 V was exclusively due to the reduction of AP, we performed two more control study of the final electrode by sweeping the potential in same range. The first control study was a concentration dependent study, where the LSV responses of the final sensor probe was measured in a relatively higher concentration 10 x 10^{-6} to 1x 10^{-4} of AP in 5 mM PBS, where an increase in AP concentration leads to a linear increase in the current response. The peak current increases as a function of increased concentration of the AP with a co-relation co-efficient of 0.97, shows the ability of the final sensor probe to oxidise AP.

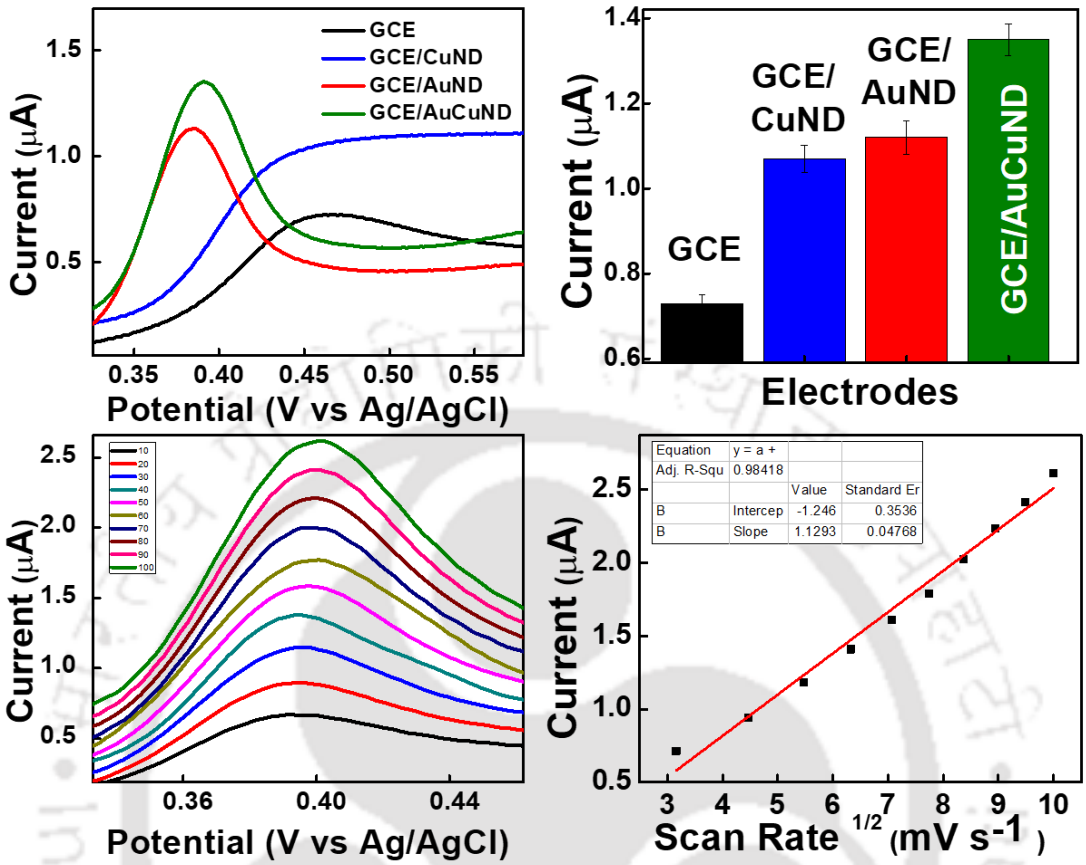

Figure 3.6 (A) shows the LSV responses at different electrode in 10 µM of AP in PBS, (B) shows the comparative LSV peak values; (C) scan rate of GCE/Au-Cu bimetallic dendrite probe in 10 µM of AP in PBS, and corresponding peak currents following linearity (D).

In the second control study, we performed a scan rate dependent study with the final probe in presence at 10 µM AP between 10 and 100 mV/S^{-1} (**figure 3.6 C).** LSV responses were found to be directly proportional with the square root of the scan rate, which was due to the catalysis of AP on the sensor surface. Both these control studies concluded that the final probe is stable and capable of sensing AP precisely.

DPV, another electrochemical method, is a more sensitive technique than the LSV to detect analyte at very low concentration(Bard et al. 1980). So, we choose DPV over LSV, for studying the analytical potential of the final probe to detect the minimum concentration of AP in PBS. **Figure 3.7 (A)** shows the calibration curve developed from DPV responses of the final GCE/AuCuND sensor at different concentration of AP in PBS.

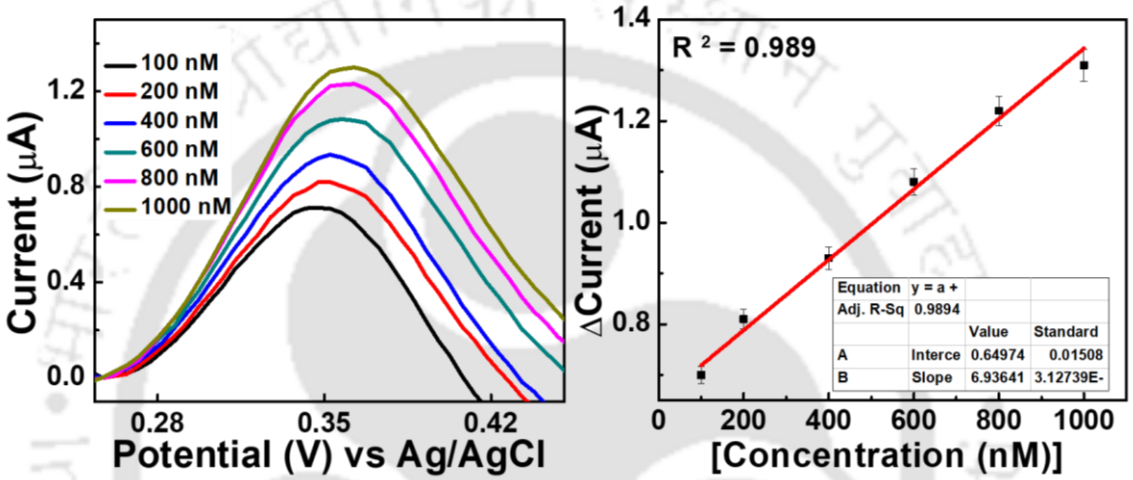

Figure 3.7 (A) shows the dose dependent curve shows the detection range of 100-1000 nM of AP, and (B) Corresponding calibration plot of AP in PBS.

The linear regression equation of AP sensing based on the calibration curve is expressed as follows:

$$\Delta I\ (A) = 0.64\ (0.01)\ X\ 10^{-6} + 6.93\ (0.31)\ X\ 10^{-4}\ Conc.\ [AP\ (nM)] \quad \ldots \textbf{Equation2}$$

With correlation coefficient of 0.989. The LOD of AP on the final electrode surface was calculated to 8.5 (±0.03) nM (RSD < 4.3%, n = 3) using equation:

$$LOD = 3\ \sigma_b / m \qquad \ldots \textbf{Equation 3}$$

Where, σ_b is standard deviation of blank and m is slope of the calibration curve.

The reported LOD and LDR by the AuCuND sensor surface is comparable to the recently reported AP sensor as shown in the Table 3.1. To further validate the sensing capacity of the bimetallic probe, the sensor probe was applied to detect AP in biological fluid and in the presence of some commonly found molecules.

3.5. Selectivity assay

The commercial and clinical applicability can be investigated by evaluating the sensitivity of the sensor towards the analyte in the presence of other co-existing molecule in biological matrix. Hence, a wide range of commonly co-existing molecules and drug molecules *viz.* glucose, cysteine, ascorbic acid, urea, uric acid, dopamine, aspirin, and chloramphenicol were selected, to evaluate their effect of potential interfering molecules by final electrode probe. All the potentially interfering molecules were tested at a higher concentration than usually found in body fluids.

Figure 3.8. shows the comparative DPV response of the final probe in the presence of the interfering molecules, where negligible or no current response for these molecules was observed. It is interesting to note that the final probe is even capable of sensing the AP in a mixed solution containing a high concentration of interfering molecules with an accuracy of 96%.

$$K\ sel = (Signal)\ Interfering\ molecules\ /\ (Signal)\ AP \quad \textbf{……4}$$

Where K sel is the coefficient of selectivity, Signal interfering molecules is the signal strength shown by the probe when treated with the interfering molecules, and Signal $_{AP}$ *is the signal strength corresponds to AP.*

SI No.	Electrode Fabrication	LDR	LOD	Real Sample	References
1	WMCNT-PDDA-FPS/GCE	3 - 1100 µM	0.6 µM	Urine samples	(Chen et al. 2018)
2	Carbon Nanoballs/ GCE	8.0×10^{-8} - 2.3×10^{-4} M	8.0 nM	Natural water	(Raymundo-Pereira et al. 2017)
3	CeO_2-SPEs	0.09 – 7.0 µM	0.05 µM	Human serum	(Khairy et al. 2018)
4	MWCNT/ β-cyclodextrin/ GCE	0.05 - 300 µM	11.5 nM	Water	(Alam et al. 2018)
5	ZKAKC/GCE	0.01–20 µM	0.004 µM	Human urine	(Kim et al. 2018)
6	Fe3O4/N/C @MWCNT/GCE	0.5 – 1355.0 µM	0.14 µM	Human serum and urine	(Yuan et al. 2019)
7	Au/ZIF-L/GCE	0.056–0.56 mM	1.02 µM	Pharmaceutical samples	(Wang et al. 2018)
8 **9**	Co-Ni/Copper foam	0.01 - 0.1 mM	2.7 µM	Pharmaceutical sample	(Premlatha and Bapu 2018)
10	**AuCuND/GCE**	**100-1000 nM**	**8.5 nM**	**Human Urine sample**	**This work**

Table 3.1. A comparison of the developed nanoprobe with previously reported AP sensors and their analytical performance.

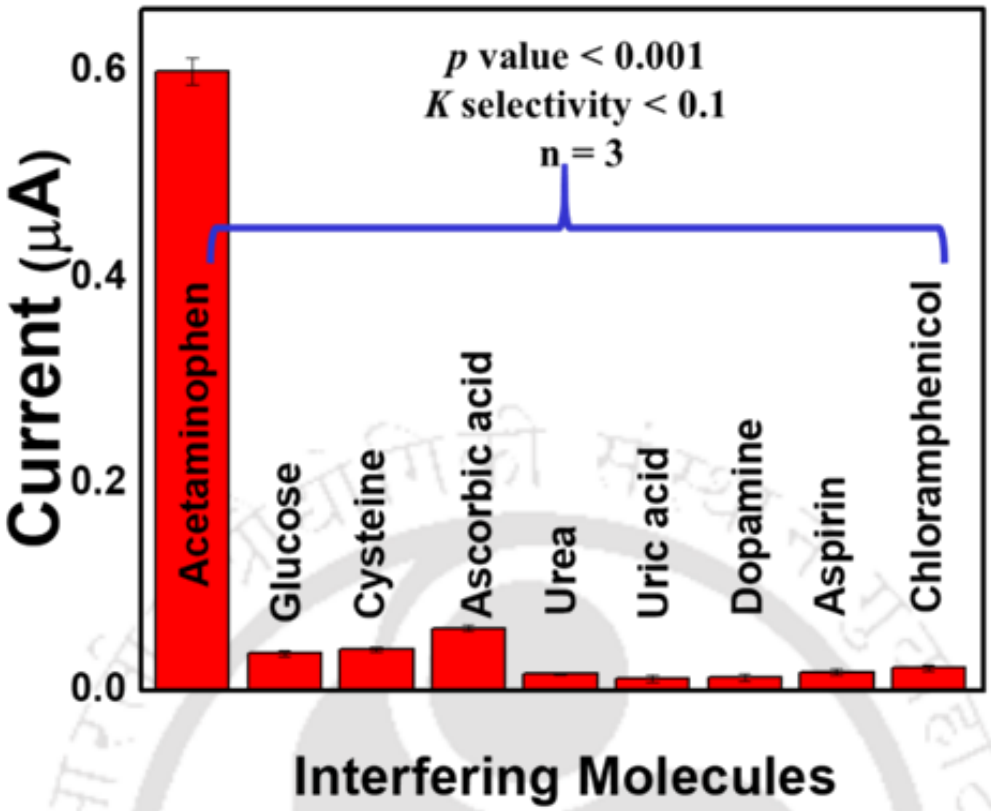

Figure 3.8. Interference study showing negligible current response by interfering molecules.

The k selectivity value of the interfering molecules was found to be negligible (K sel <<1), reflecting high selectivity of the final sensor probe towards AP. No electrochemical response in the absence of AP was seen, possibly due to the electrochemical inactive nature of interfering species and /or the selected potential where other electroactive molecules are not readily oxidised. The statistical significance of the result was calculated by t-test and the p-value against the interfering molecules were found to be negligible (<<0.001, n=3). To evaluate the activity of the final sensor to detect AP in a combination of other molecules, AP sensing by the final AuCuND electrode was tested in a mixed sample containing all the above mentioned molecules. The final probe was capable of detecting AP with a 93.6 % recovery as compared to the standard buffer solution. This result clearly

shows the ability of the GCE/AuCuND sensor probe to further detect AP in complex biological fluids.

3.6. Real sample analysis

We selected urine as a model real biological sample matrix to evaluate the practical applicability of our sensor to detect different concentrations of AP in model clinical settings. DPV responses were recorded in the 10 times diluted urine in PBS by adding different concentration of AP. The sensor was capable of detecting AP in urine, without any filtration or pre-treatment. The AP concentration was measured taking the previously developed calibration plot as a standard reference and expressed in terms of % recovery using equation 4.

$$\% \text{ Recovery} = [S]_{AP} - [B]_{AP} / [SS]_{AP} \quad \text{.....} \quad \textbf{equation 4}$$

Where, $[S]_{AP}$ and $[B]_{AP}$ are the analytical responses of AP in the spiked and blank blood samples, respectively; and $[SS]_{AP}$ is the analytical response of A in the standard buffer solutions.

The recoveries of AP in urine at each concentration has been calculated and found to be in between 91 and 97% as compared to the original calibration plot, showing the clinical potential of the developed sensor probe (figure 3.9).

The negligible decrease in the current response may be due to the matrix effect or handling error. The urine contains many unknown molecules which are not tested in the interference study, still the sensor is capable of sensing AP with high precision showing its clinical potential.

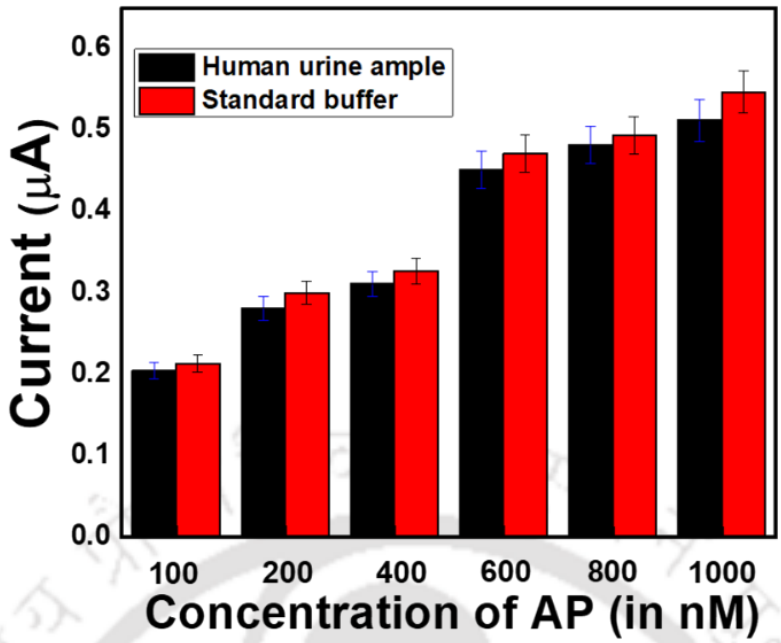

Figure 3.9 shows the high % recovery of AP in the real sample urine in comparison to standard samples.

3.7. Reproducibility and stability assay

To check the long term stability of the final GCE/Au-Cu probe, DPV responses were recorded for 12 weeks, periodically taking measurements once a week. The retention of signal was found to be 89-96%. This shows that the sensor system is stable for sensing applications for 12 weeks. We also checked the reproducibility of the sensing matrix by taking five different GCE/Au-Cu surface and recorded the DPV responses. The variation in peak current was found to be negligible ($p < 0.001$). The variations found in peak current may be due to minor handling error or fluctuation in other experimental conditions. High stability and reproducibility of the developed GCE/Au-Cu sensor shows its potential in sensing application.

4. Conclusions

A facile, simple bimetallic dendritic like nanostructure sensing surface has been developed by tuning the electrodeposition parameters for enhanced bioelectronics property. The sensor surface was thoroughly characterized using SEM, EDX, TEM, SAED, CV, EIS, DPV. The LOD was found to be 8.5 (±0.03) nM with a LDR of 100-1000 nM. The sensor is highly stable for up to 12 weeks and found to be capable of detecting AP efficiently in the presence of various interfering molecules commonly found in biological samples. To the best of our knowledge, this is the first report of Au-Cu bimetallic dendritic nanostructure developed by simple electrodeposition method with enhanced bioelectronics properties. The fabrication of the whole sensor surface takes only 10 minutes showing its possibility for other catalytic application. The synthesis procedure follows a very simple, facile, and low cost steps which can be further optimised for other biomolecular analysis.

4. References

Alam AU, Qin Y, Howlader MMR, et al (2018) Electrochemical sensing of acetaminophen using multi-walled carbon nanotube and B-cyclodextrin. Sensors Actuators, B Chem 254:896–909.

Bard AJ, Faulkner LR, Leddy J, Zoski CG (1980) Electrochemical methods: fundamentals and applications. wiley New York

Bernal W, Auzinger G, Dhawan A, Wendon J (2010) Acute liver failure. Lancet 376:190–201.

Burgot G, Auffret F, Burgot J-L (1997) Determination of acetaminophen by thermometric titrimetry. Anal Chim Acta 343:125–128

Chandra P, Son NX, Noh H-B, et al (2013) Investigation on the downregulation of dopamine by acetaminophen administration based on their simultaneous determination in urine. Biosens Bioelectron 39:139–144

Chen Y, Liu X, Wu T, et al (2018) Enhanced electrochemical sensitivity towards acetaminophen determination using electroactive self-assembled ferrocene derivative polymer nanospheres with multi-walled carbon nanotubes. Electrochim Acta 272:212–220.

Chun LJ, Tong MJ, Busuttil RW, Hiatt JR (2009) Acetaminophen hepatotoxicity and acute liver failure. J Clin Gastroenterol 43:342–349

Decan MR, Impellizzeri S, Marin ML, Scaiano JC (2014) Copper nanoparticle heterogeneous catalytic 'click'cycloaddition confirmed by single-molecule spectroscopy. Nat Commun 5:4612

Fan N, Yu H, Ju Z, et al (2009) Structure and magnetic properties of hierarchical cobalt dendrites. Mater Lett 63:551–553.

Gioia MG, Andreatta P, Boschetti S, Gatti R (2008) Development and validation of a liquid chromatographic method for the determination of ascorbic acid, dehydroascorbic acid and acetaminophen in pharmaceuticals. J Pharm Biomed Anal 48:331–339

Ham YS, Choe S, Kim MJ, et al (2017) Electrodeposited Ag catalysts for the electrochemical reduction of CO 2 to CO. Appl Catal B Environ 208:35–43.

Hinson JA, Roberts DW, James LP (2010) Mechanisms of acetaminophen-induced liver necrosis. In: Adverse drug reactions. Springer, pp 369–405

Hu Y, Pan N, Zhang K, et al (2007) Fabrication of dendrite-like Au nanostructures and their enhanced photoluminescence emission. Phys status solidi 204:3398–3404.

James LP, Mayeux PR, Hinson JA (2003) acetaminophen-induced hepatotoxicity. Drug Metab Dispos 31:1499–1506.

Khairy M, Mahmoud BG, Banks CE (2018) Simultaneous determination of codeine and its co-formulated drugs acetaminophen and caffeine by utilising cerium oxide nanoparticles modified screen-printed electrodes. Sensors Actuators, B Chem 259:142–154.

Kim D, Kim JM, Jeon Y, et al (2018) Novel two-step activation of biomass-derived carbon for highly sensitive electrochemical determination of acetaminophen. Sensors Actuators, B Chem 259:50–58.

Kumar A, Purohit B, Mahato K, et al (2019a) Gold-Iron Bimetallic Nanoparticles Impregnated Reduced Graphene Oxide Based Nanosensor for Label-Free Detection of Biomarker Related to Non-Alcoholic Fatty Liver Disease. Electroanalysis elan.201900337.

Kumar A, Purohit B, Maurya PK, et al (2019b) Engineered Nanomaterial Assisted Signal-amplification Strategies for Enhancing Analytical Performance of Electrochemical Biosensors. Electroanalysis 31:1615–1629.

Li Z, Li R, Mu T, Luan Y (2013) Ionic liquid assisted synthesis of Au-Pd bimetallic particles with enhanced electrocatalytic activity. Chem - A Eur J 19:6005–6013.

Lin TH, Lin CW, Liu HH, et al (2011) Potential-controlled electrodeposition of gold dendrites in the presence of cysteine. Chem Commun 47:2044–2046.

Liu J, Cao L, Huang W, Li Z (2011) Preparation of AuPt alloy foam films and their superior electrocatalytic activity for the oxidation of formic acid. ACS Appl Mater Interfaces 3:3552–3558.

Lu G, Li C, Shi G (2007) Synthesis and characterization of 3D dendritic gold nanostructures and their use as substrates for surface-enhanced Raman scattering. Chem Mater 19:3433–3440.

Moreira AB, Oliveira HPM, Atvars TDZ, et al (2005) Direct determination of paracetamol in powdered pharmaceutical samples by fluorescence spectroscopy. Anal Chim Acta 539:257–261

Nasibi M, Golozar MA, Rashed G. Nano iron oxide (Fe_2O_3)/carbon black electrodes for electrochemical capacitors. Mater Lett. 2012;85:40–3.

Naveen MH, Gurudatt NG, Noh H-B, Shim Y-B (2016) Dealloyed AuNi Dendrite Anchored on a Functionalized Conducting Polymer for Improved Catalytic Oxygen Reduction and Hydrogen Peroxide Sensing in Living Cells. Adv Funct Mater 26:1590–1601.

Nebot C, Gibb SW, Boyd KG (2007) Quantification of human pharmaceuticals in water samples by high performance liquid chromatography--tandem mass spectrometry. Anal Chim Acta 598:87–94

Nesbitt NT, Ma M, Trześniewski BJ, et al (2018) Au Dendrite Electrocatalysts for CO 2 Electrolysis. J Phys Chem C 122:10006–10016.

Ojha NK, Zyryanov G V, Majee A, et al (2017) Copper nanoparticles as inexpensive and efficient catalyst: a valuable contribution in organic synthesis. Coord Chem Rev 353:1–57

Premlatha S, Bapu GNKR (2018) Fabrication of Co-Ni alloy nanostructures on copper foam for highly sensitive amperometric sensing of acetaminophen. J Electroanal Chem 822:33–42

Raymundo-Pereira PA, Campos AM, Mendonça CD, et al (2017) Printex 6L Carbon Nanoballs used in Electrochemical Sensors for Simultaneous Detection of Emerging Pollutants Hydroquinone and Paracetamol. Sensors Actuators, B Chem 252:165–174.

Reddy YVM, Bathinapatla S, Łuczak T, et al (2018) An ultra-sensitive electrochemical sensor for the detection of acetaminophen in the presence of etilefrine using bimetallic Pd--Ag/reduced graphene oxide nanocomposites. New J Chem 42:3137–3146.

SEEFF LB (1986) Acetaminophen Hepatotoxicity in Alcoholics. Ann Intern Med 104:399.

Shu H, Cao L, Chang G, et al (2014) Direct electrodeposition of gold nanostructures onto glassy carbon electrodes for non-enzymatic detection of glucose.

Electrochim Acta 132:524–532.

Sun J, Schnackenberg LK, Holland RD, et al (2008) Metabonomics evaluation of urine from rats given acute and chronic doses of acetaminophen using NMR and UPLC/MS. J Chromatogr B Anal Technol Biomed Life Sci 871:328–340.

Wang C, Ciganda R, Salmon L, et al (2016a) Highly efficient transition metal nanoparticle catalysts in aqueous solutions. Angew Chemie Int Ed 55:3091–3095

Wang J, Chen F, Jin Y, Johnston RL (2016b) Highly active and stable AuNi dendrites as an electrocatalyst for the oxygen reduction reaction in alkaline media. J Mater Chem A 4:17828–17837.

Wang L, Meng T, Fan Y, et al (2018) Electrochemical study of acetaminophen oxidation by gold nanoparticles supported on a leaf-like zeolitic imidazolate framework. J Colloid Interface Sci 524:1–7

Wang Z, Zhang H, Xu L, et al (2016c) Laser-induced fabrication of highly branched Au@TiO2nano-dendrites with excellent near-infrared absorption properties. RSC Adv 6:83337–83342.

Wu T, Zhou HM, Xia BY, et al (2014) Facile synthesis of 3 D platinum dendrites with a clean surface as highly stable electrocatalysts. ChemCatChem 6:1538–1542.

Xu X, Jia J, Yang X, Dong S (2010) A Templateless , Surfactantless , Simple Electrochemical Route to a Dendritic Gold Nanostructure and Its Application to Oxygen Reduction. 26:7627–7631.

Yuan S, Bo X, Guo L (2019) In-situ insertion of multi-walled carbon nanotubes in the Fe 3 O 4 /N/C composite derived from iron-based metal-organic frameworks as a catalyst for effective sensing acetaminophen and metronidazole. Talanta 193:100–109.

Zhang X, Li D, Bourgeois L, et al (2009) Direct Electrodeposition of Porous Gold Nanowire Arrays for Biosensing Applications. 3800:436–441.

Zhang X, Wang G, Liu X, et al (2008) Copper dendrites: Synthesis, mechanism discussion, and application in determination of L-tyrosine. Cryst Growth Des 8:1430–1434.

Chapter # IV

Engineered Gold Dendrites and a Multi-Walled Carbon Nanotube Nanohybrid for Detection of Acetaminophen in Human Urine Samples

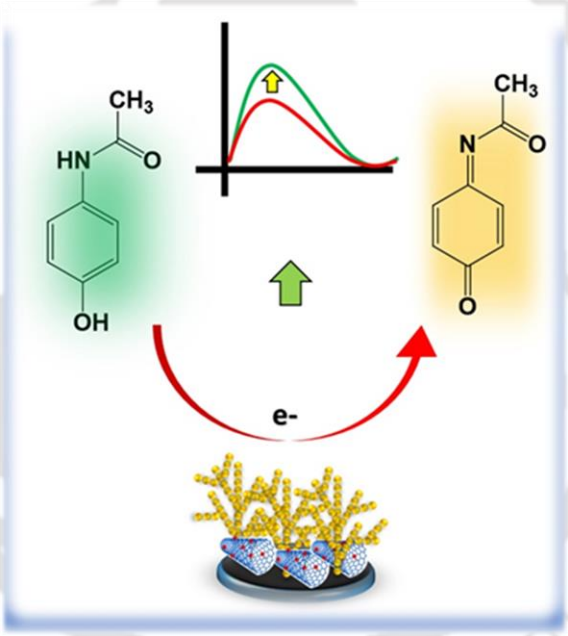

Status:

Published in Electroanalysis (2019)

1. Introduction

In this work, we attempted to develop a bimetallic nanodendrites with enhanced catalytic activity, and to study its potential for the development of non-enzymatic electrochemical biosensing of clinically important molecules. Metallic dendrites, as discussed earlier, are a class of nanomaterial, which resembles with fern like morphology reported to have enhanced catalytic activities due to the presence of the relatively larger active surface area contributed by its three dimensional protruded structures (Shu et al. 2014). Metallic dendrites are less prone to fouling by biological molecules due to the spatial structures and enormously larger active surface area (Cheng et al. 2010). In this context, many monometallic dendrites based on Au, Ag, Pt, Cu, Co, Ni etc. have been synthesized and evaluated for their catalytic behavior (Qiu et al. 2009; Noh et al. 2012; Muthukumar and Chetty 2018). Au based dendritic structures, however have been widely studied and used in biosensing application, due to their excellent biocompatibility (Shu et al. 2014; Naveen et al. 2016). The synthesis of Au dendrites (AuDN) has been achieved by various methods, which includes surfactant-mediated synthesis, galvanic replacement synthesis, and electrochemical synthesis (Lim and Xia 2011; You et al. 2013; Ataee-Esfahani and Skrabalak 2015). The electrochemical deposition is the most facile, robust, and cost-effective method, where the dendritic structures are developed directly over the electrode surface, and can be easily controlled by optimizing the parameters like the precursor salt concentration, time of deposition, applied potential etc.

Part of the work has been published as: Purohit et al., (2019) Novel Sensing Assembly Comprising Engineered Gold Dendrites and MWCNT-AuNPs Nanohybrid for Acetaminophen Detection in Human Urine. Electroanalysis. DOI: 10.1002/elan.201900551.

Although, the development of Au dendrites has been thoroughly investigated, but its integration with other nanostructure materials have been rarely attempted. Such integrative study may not only offer improved analytical performance of sensors, but it can also pave the way for developing novel nanohybrid comprising dendrites and other nanomaterials. Various metallic nanoparticles, carbon dots, quantum dots, graphene are being widely used to develop innovative biosensing matrices (Kumar et al. 2019d). Among all types of nanomaterials, carbon based nanomaterials, especially MWCNTs are greatly used in biosensor development due to its high conductivity, enormous surface area, chemical stability, significant mechanical strength, and high catalytic activity (Su et al. 2013; Li et al. 2015). The MWCNT based electrodes are generally modified with various metallic nanoparticles, which offers enhanced optoelectronic characteristics due to their synergistic behavior (Jiang and Zhang 2010; Wu et al. 2010). Among all type of metallic nanoparticles, AuNPs have been widely studied due their high conductivity, facile synthesis, stability, biocompatibility etc. (Tan et al. 2014; Assah et al. 2018; Zheng et al. 2019) Therefore, conjugate comprising MWCNT and AuNPs would be interesting to integrate with the nanostructured dendrites. In order to investigate the electro-catalytic behavior of any nanohybrid, sensing of electrochemically active molecules are performed at first stage (Kumar et al. 2019a; Purohit et al. 2019).

Among various electrochemically active molecules, acetaminophen (N-acetyl-p-aminophenol, AP) has been widely tested in various matrices (Kumar et al. 2019b), so it can be considered as a proof-of-concept model molecule to investigate the sensing behavior of novel nanohybrids. Though, it is considered safe for clinical uses in therapeutic doses, over doses of AP found to cause various clinical symptoms including hepatotoxicity (Chun et al. 2009; Hinson et al. 2010). 46% of all the acute liver failure cases in the United States are due to AP over dosages, which causes even worse health conditions in alcoholics

(SEEFF 1986; James et al. 2003; Bernal et al. 2010). The detection of AP in the early stage is very crucial for the effective treatment for such cases. Therefore, fast detection of AP in wider dynamic ranges is of high clinical importance. In view of this, several analytical techniques have been used for the detection of AP including spectrophotometry (Moreira et al. 2005), high-performance liquid chromatography (Nebot et al. 2007; Gioia et al. 2008), gas chromatography, thermogravimetric analysis (Burgot et al. 1997), NMR (Sun et al. 2008), and chemiluminescence. Though these techniques are powerful and are able to detect AP, they include a very complicated, high cost and time consuming methods for the detection of AP. In contrast, electrochemical techniques are simple, low cost, equally or more sensitive, time saving method for the detection of analytes [24,25]

In the objective 4, we tried to develop AuDN over a MWCNT-AuNPs nanohybrid for AP detection. The sensor probe was thoroughly characterized by SEM, TEM, EDX, CV, EIS, LSV, and DPV. Thereafter, the dose-dependent detection of AP was performed using the fabricated sensor probe to assess its analytical performance, *i.e.* LDR and LOD using DPV. The practical applicability of the fabricated sensor was examined by testing AP in urine samples collected from healthy individuals using spike and recovery method. Interference due to various commonly found components in urine and other biological matrices, and long-term stability of the designed sensor was also evaluated.

2. Experimental

2.1. Chemicals and instruments

Potassium chloride (KCl), potassium ferricyanide [$K_3Fe(CN)_6$], potassium ferrocyanide [$K_4Fe(CN)_6$], sodium monophosphate (NaH_2PO_4) and sodium bisphosphate (Na_2HPO_4) were purchased from Himedia Pvt. Ltd., India. Chloroauric acid ($HAuCl_4$), MWCNT, indium tin oxide (ITO) coated glass, and AP was obtained from Sigma-Aldrich Chemical

Co. (USA). Sulfuric acid (H_2SO_4), nitric acid (HNO_3), sodium chloride (NaCl), citric acid, uric acid, glucose, urea, glycine, alanine, glutamic acid, cysteine was purchased from SRL Pvt. Ltd, India. All aqueous solutions were prepared in doubly distilled water obtained from a Milli-Q water purifying system (18 MΩ cm). All chemicals used in this study were of standard analytical grade.

Synthesis of the Au dendritic nanostructures (AuDN) was performed using an electrochemical workstation (Metrohm Autolab) using three electrode based electrochemical cell system. For that, GCE, platinum (Pt) wire, and Ag/AgCl (saturated with KCl) were used as the working, counter, and reference electrodes, respectively. Surface morphological Imaging and EDX were performed using Field Emission Scanning Electron Microscope (FESEM) (Zeiss, Gemini). TEM imaging were obtained from Field Emission Transmission Electron Microscope (FETEM) (JEOL, 2100F). The preparation of the TEM samples of AuDN, MWCNT-AuNPs/AuDN, the probe materials were sonicated in ethanol for 10 minutes and then 20 µl of the solution was placed over the carbon coated copper grid for well dispersal. The grid was placed in an oven at 37 ˚C for 12 hours to remove the moisture.

2.2. Fabrication of GCE/MWCNT-AuNP/AuND sensor probe

The preparation of MWCNT-AuNPs were prepared based on previously reported method with slight modifications (Zhang and Wang 2007; Zhu et al. 2010). Briefly, the pretreated MWCNT was mixed with separately prepared colloidal gold solution (1:1) by sonication for 5 min to get a homogenous suspension. The as mixed solution was kept for 2 hrs at room temperature. Thereafter, the resulting solution was centrifuged at 2000 rpm. The supernatant was discarded and the deposited MWCNT-AuNPs composite was stored at 4 °C for further use for sensing probe preparation. At first, the GCE was polished to a mirror finish with alumina slurry and rinsed in a bath sonicator for 10 s to remove the adsorbed

alumina particles and other impurities; followed by washing of electrode surface with double distilled water and ethanol, respectively. The MWCNT-AuNPs composite was coated over the cleaned GCE, and further used as a support for Au dendritic growth. The dendrites were grown on to the GCE/MWCNT-AuNPs surface from a 10 mM $HAuCl_4$ solution prepared in 0.1 M KCl using chronoamperometry by applying a constant potential of -0.30 V vs. Ag/AgCl for 1500 s. The dendritic surface was gently cleaned using DI water prior to electrochemical studies. The final sensing probe was termed as GCE/MWCNT-AuNPs/AuDN. The sensor probe fabrication and sensing application are shown schematically in **figure 4.1**.

2.3. Electrochemical characterization of GCE/MWCNT-AuNP/AuND sensor probe

The electrochemical characterization of the sensor probe was carried out in phosphate buffer saline (PBS pH 7.0 and 0.9% NaCl) and PBS containing 5 mM $[Fe(CN)_6]^{-3/-4}$ (Zobell's solution (ZS)) by using CV, LSV, and EIS methods. The impedance spectra were recorded at an open circuit voltage between 100 Hz and 1 MHz with a sampling rate of five points per decade. For the, detection of AP, DPV responses were recorded by scanning the potential from +0.30 to +0.50 V vs. Ag/AgCl at a scan rate of 0.005 V/s, with pulse potential 0.025 V, and pulse time 0.05 s. The real sample analysis of AP was carried out in urine collected from three healthy volunteers of the laboratory. The urine was diluted 10 times in PBS before analysis with no other pretreatment steps.

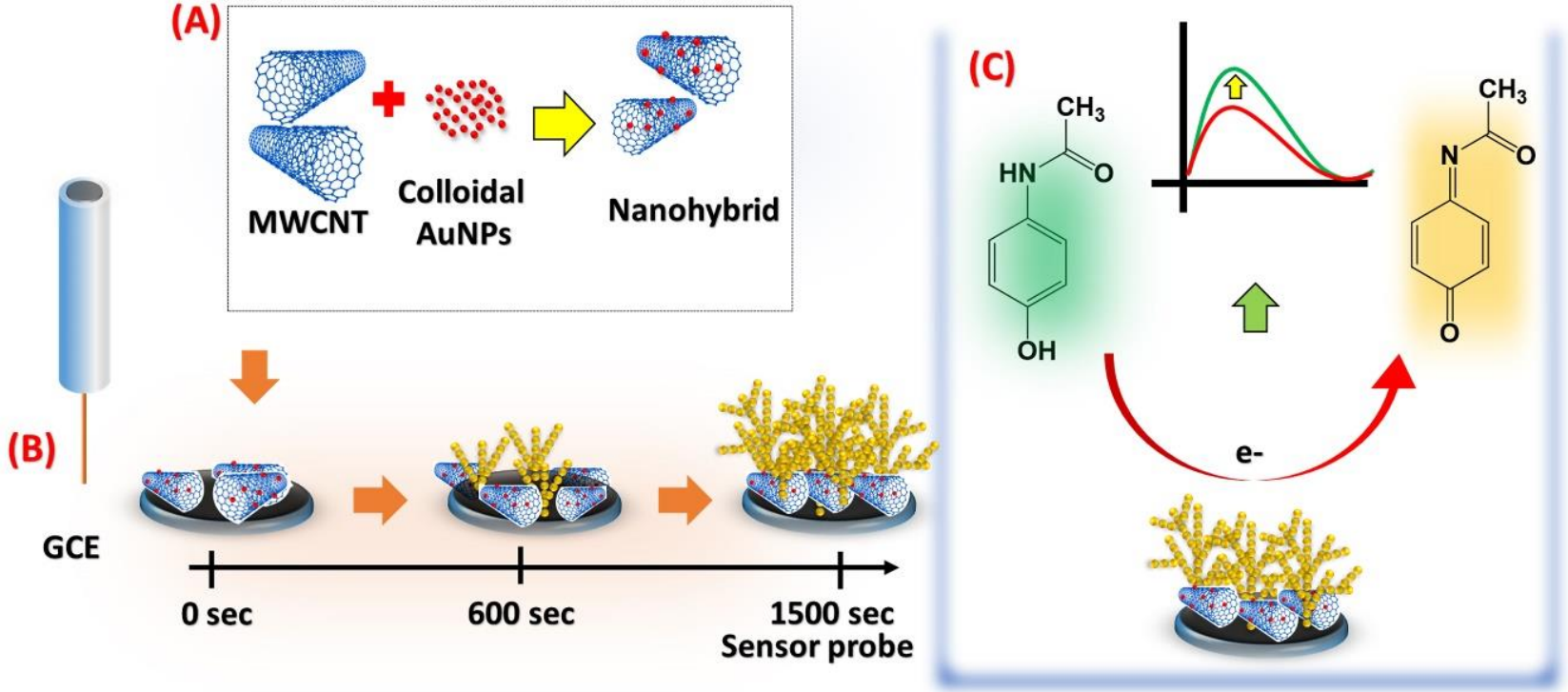

Figure 4.1. Schematic representation of sensor probe fabrication, (A) nanohybrid preparation, (B) dendrite deposition, and (C) AP sensing.

3. Result and Discussion

3.1. Preparation of the AuDN over GCE/MWCNT-AuNPs

The synthesis of Au dendrite is governed by many factors *viz.* the concentration of precursor molecules in the electrolyte solution, electrodeposition time, and potential applied. In the present study, 10 µl of the prepared MWCNT-AuNPs nanohybrid was coated over the GCE, and air dried before the electrodeposition of AuDN. The applied potential between 0.2 V and -0.6 V was tested for the synthesis of the Au dendrite, where the -0.3 V showed the best dendrite formation and maximum electron transfer ability of the surface (data not shown). The electrodeposition time between 100 s and 1500 s was also investigated, where the CV shows a linear increase in the current responses in 5.0 mM ZS between 100 s and 1500 s, which indicates the initiation and growth of the dendritic structure and a moderately optimized time. The increase in the current response in the chronoamperometry method with the increasing electrodeposition time is most likely due to the deposition of Au onto the electrode surface.

3.2. Physical characterization of sensor probe

The nano-composite utilized in the sensor fabrication has been systematically characterized using various techniques. At first, the separately prepared MWCNT-AuNPs nanohybrid was characterized by TEM and EDX analysis. The TEM micrograph of the MWCNT-AuNPs nanohybrid shows clear tube shaped structures with the dark spherical spots indicating the successful formation of MWCNT- AuNPs hybrid system (**Figure 4.2 (A)**). In order to confirm the formation of this nanohybrid, we performed elemental mapping, where Au (yellow area) and C (green area) were obtained, confirming the formation of MWCNT-AuNPs. The elemental map shown in **Figure 4.2 (B-D)** clearly suggests that the presence of the AuNPs on to the surface of MWCNTs.

The elemental compositions were also confirmed by EDX analysis, where carbon was found to be the most abundant element with 92.4 % followed by Au (6.7 %) (**Figure 4.2 (E)**) Thereafter, dendrites were grown onto the GCE/MWCNT-AuNPs and was also physically characterized in details using various techniques.

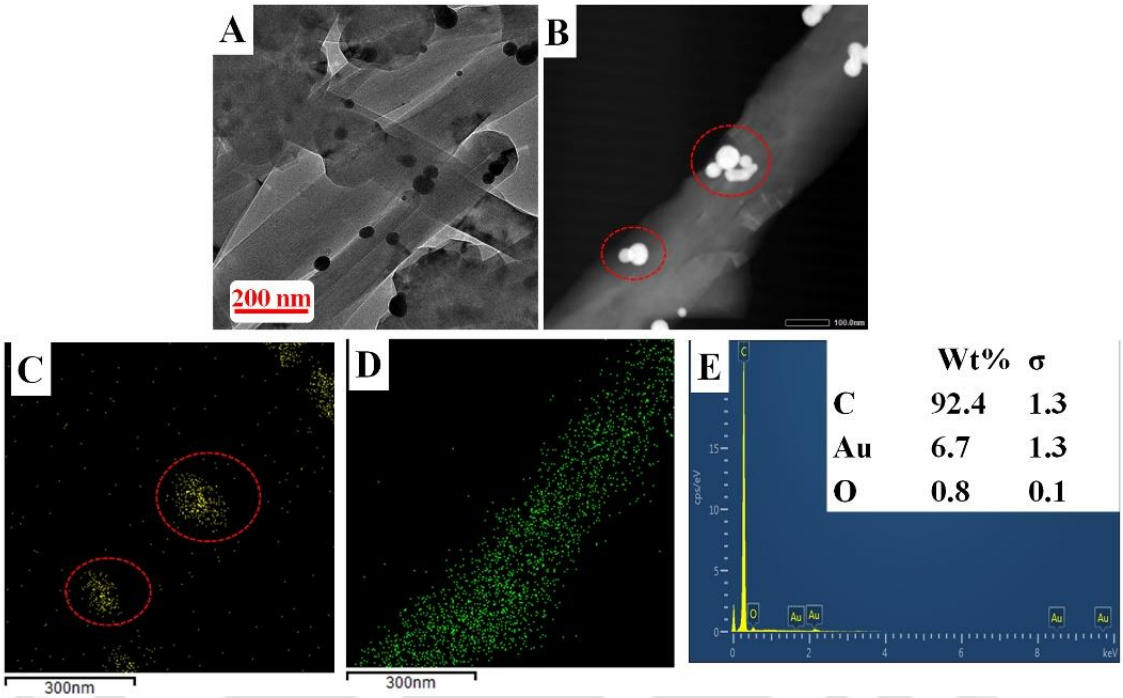

Figure 4. 2. (A) TEM micrograph of MWCNT-AuNPs composite showing rod like MWCNT embedded with spherical AuNPs; Elemental mapping studies (B) show the Dark field TEM image of MWCNT-AuNPs nanohybrid, (C) shows the Au component (encircled in red dotted line) and (D) shows the carbon component of the nanohybrid; (E) EDX analysis showing the presence of carbon, oxygen and gold.

The visible color change of the GCE electrode was observed with subsequent electrodeposition reaction forming a brown film, indicating the deposition of Au over the active surface, which has been confirmed by the SEM and EDX analysis of the surface. For these studies, the same protocol mentioned above was followed, while an ultra-cleaned ITO was used as electrode surface. **Figure 4.3 (A)** shows the MWCNT-AuNPs/AuDN coated electrode, where a clear hierarchical fern like structured over the MWCNT was observed. The structures show a typical dendrite like structure with

multiple secondary and tertiary branches over the primary branch at the MWCNT-AuNPs/ AuDN electrode surface. **Figure 4. 3 (B) and (C)** shows the magnified images of MWCNT-AuNPs and AuDN, respectively. **Figure 4.3. (D)** shows a well-defined dendritic nanostructure with primary, secondary and tertiary branches. In order to further confirm these structures, elemental mapping of the electrode prepared was performed. **Figure 4.3 (E)**, shows the distribution of Au (green color) in the region where the Au dendrites were grown, while the carbon element (red) is prominent in the area where MWCNT-AuNPs was the presence of AuNPs in the nanohybrid.

3.3. Electrochemical characterization of the GCE/MWCNT-AuNPs/AuDN sensor probe

The GCE/MWCNT-AuNPs/AuDN sensor surface was further characterized for its electro-catalytic behavior. An increase in chronoamperometric responses while electrodeposition in the $HAuCl_4$ solution refers to the formation of dendritic structures (Qiu et al. 2009). The first step of electrochemical characterization involves the CV analysis of GCE, GCE/AuDN, GCE/MWCNT/AuDN and GCE/MWCNT-AuNPs/AuDN electrodes in 5 mM ZS prepared in PBS. For this purpose, the CV responses were recorded in the potential range between -0.2 and 0.7 V at a scan rate of 50 mV/s in ZS (**figure 4.4 A**). As expected, a classical voltammogram due to the redox process of $[Fe(CN)_6]^{3-/4-}$ was observed at bare GCE electrode (black curve). The anodic (Ipa) and cathodic (Ipc) peak currents were found to be increased after AuDN deposition in GCE/AuDN (red curve) as well as in GCE/MWCNT/AuDN (green curve).

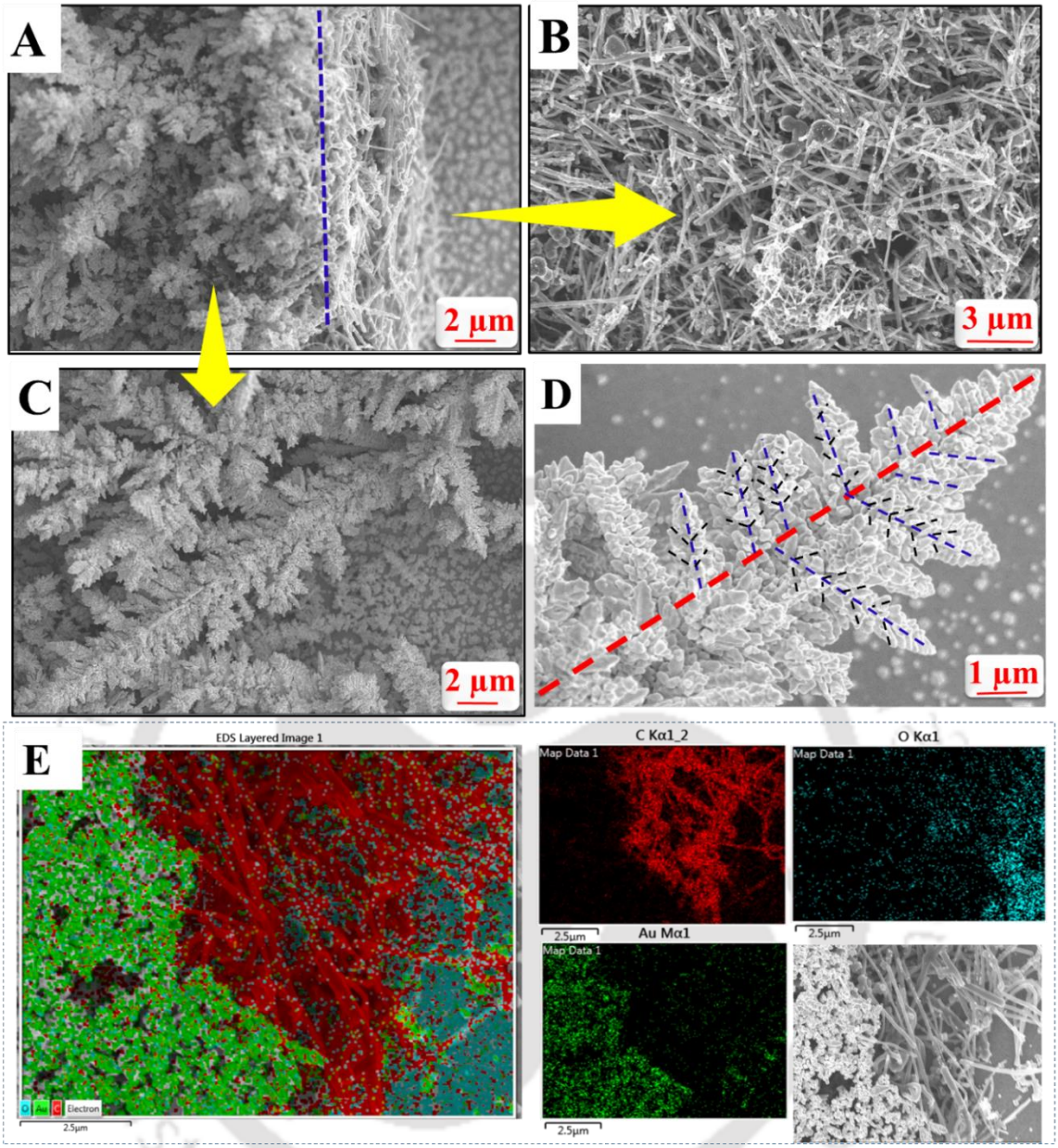

Figure. 4.3. (A) SEM micrograph showing the growth of Au dendritic nanostructures over the MWCNT-AuNP nanocomposite; (B) Magnified image of the MWCNT-AuNPs nanocomposite; (C) Au dendritic nanostructure grown over the MWCNT-AuNPs nanocomposite; (D) Shows an Au dendrite with hierarchical primary (red line), secondary (blue lines) and tertiary branches (black lines); (E) Elemental mapping shows the distribution of Au (green), carbon (red), and Oxygen (blue) in the Au dendritic nanostructure over the MWCNT-AuNPs.

The redox peak current was further amplified at GCE/MWCNT-AuNPs/AuDN (blue curve) surface. This was most likely due to the coating of MWCNT-AuNPs nanohybrid onto the bare GCE prior to the electrodeposition of AuDN, offering higher surface area and increased conductivity through enhanced charge transfer (**figure 4.4 B**). The increase in charge transfer capacity of the electrodes was evaluated quantitatively by comparing the diffusion coefficient of the bare GCE, GCE/AuDN, and GCE/MWCNT-AuNPs/AuDN surface using Randles-Sevcik's model (equation 1) (Bard et al. 1980; Verma et al. 2017).

$$I_p = \left(2.69\times10^5\right) n^{3/2} ACD^{1/2} v^{1/2} \quad \text{..... Equation 1}$$

Where, Ip is the peak current (in ampere), n is the number of electrons transferred in redox process (here n=1), A is the electrode surface area (in cm^2), C is the concentration of electroactive species (in mole cm^{-3}), D is the diffusion coefficient (in $cm^2\ s^{-1}$), and v is the scan rate (0.05 Vs^{-1}).

The diffusion coefficient (*D*) values for bare GCE, GCE/MWCNT/AuDN, GCE/AuDN, GCE/MWCNT-AuNPs/AuDN electrode surfaces were found to be 3.1 x 10^{-6} cm^2s^{-1}, 3.8 x 10^{-6} cm^2s^{-1}, 4.65 x 10^{-6} cm^2s^{-1}, and 5.29 x 10^{-6} cm^2s^{-1}, respectively. It is interesting to note that, the maximum diffusion coefficient was observed for of GCE/MWCNT-AuNPs/AuDN surface, which was 1.7, 1.4, and 1.2 times higher compared to the bare GCE, GCE/MWCNT/AuDN, and GCE/AuDN, respectively. These results clearly indicate the importance of AuDN as well as MWCNT-AuNPs nanohybrid in the sensing matrix.

In order to further evaluate the sensor stability and charge transfer behavior of the final sensor probe, CV responses were recorded at the scan rate between 10 and 100 mV/s^{-1} in 5 mM ZS (**figure 4.4 C**). The anodic (Ipa) and cathodic (Ipc) peak currents (**figure 4.4**

D) were found to be directly proportional to the square root of the scan rate, with the correlation coefficient of 0.99. This shows the higher stability as well as diffusion controlled charge transfer process at the electrode surface. The regression equations for Ipa and Ipc are expressed as follows (in **equation 2 and 3**);

Ipa (GCE/MWCNT-AuNPs/AuDN) = [-9.638 µA (s mV^{-1}) (± 3.065) x scan rate (mVs^{-1})] – 15.08 (± 0.541) µA, R^2 = 0.999 ……**Equation 2**

Ipc (GCE/MWCNT-AuNPs/AuDN) = [-6.174 µA (s mV^{-1}) (± 2.868) x scan rate (mVs^{-1})] – 10.81 (± 0.49) µA, R^2 = 0.999 ……. **Equation 3**

In order to validate the CV results in terms of highest charge transfer ability of the GCE/MWCNT-AuNPs/AuDN sensor probe, we performed a complementary experiments based on EIS and charge transfer resistance (Rct) were recorded for GCE, GCE/AuDN, GCE/MWCNT/AuDN, and GCE/MWCNT-AuNPs/AuDN in separate experiments. The Rct values were calculated based on the Nyquist plot, as shown in **figure 4.4 (E)**. The Rct values of bare GCE (black curve), GCE/MWCNT/AuDN (green curve), GCE/AuDN (red curve), and GCE/MWCNT-AuNPs/AuDN (blue curve) electrode surfaces were found to be 61.7 ± 2.1, 36 ± 1.1, 34 ± 1.2, and 29 ± 1.1 kΩ (histogram shown in **figure 4.4 (F)**. The EIS data corroborates the CV responses validating that the GCE/MWCNT-AuNPs/AuDN surface possess lowest resistance and maximum charge transfer capacity compared to other electrodes, hence ideal sensing matrix for electrochemical sensing of diverse targets.

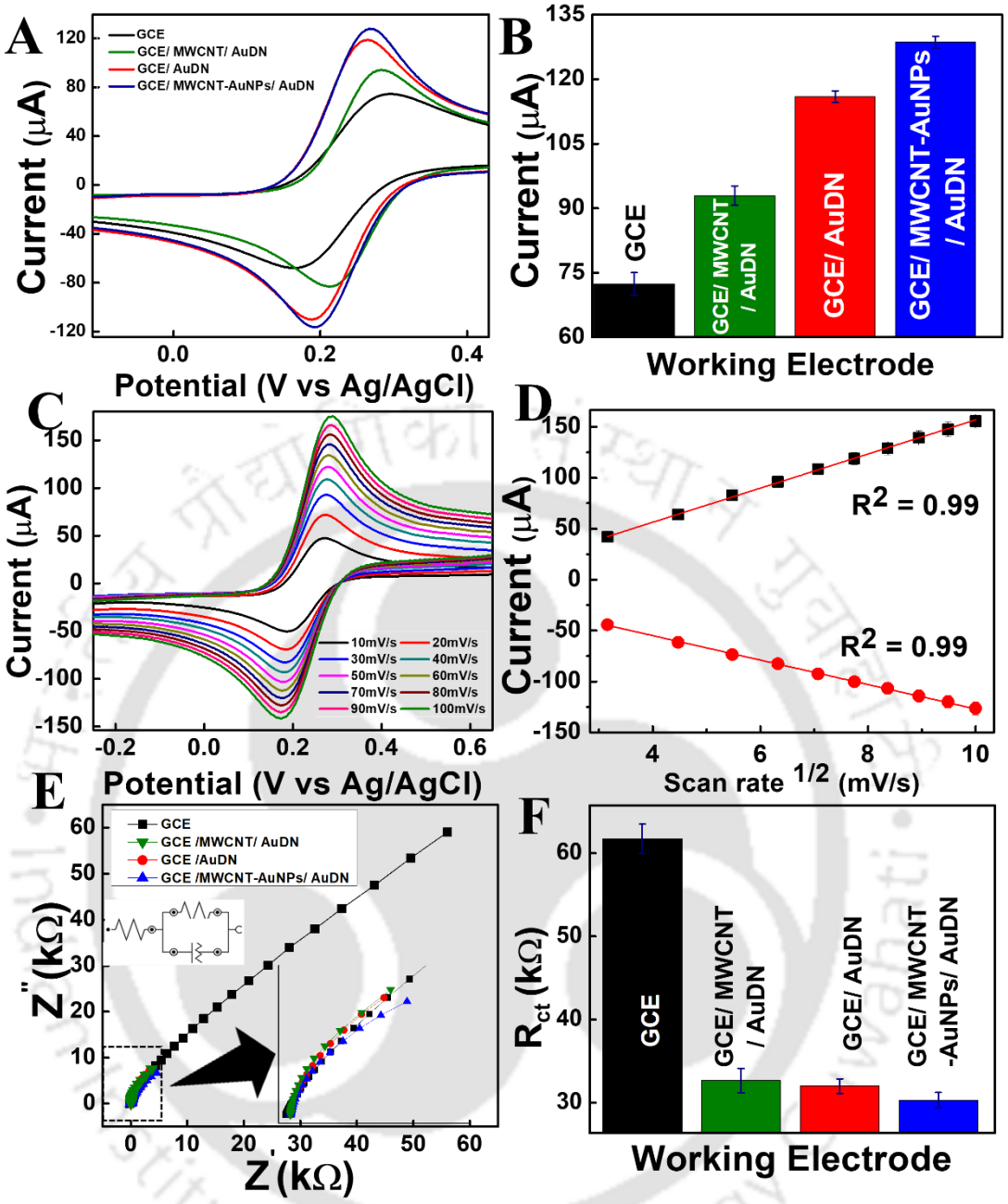

Figure 4.4. (A) CV responses at bare GCE (black), GCE/MWCNT/AuDN (green), GCE/AuDN(red), GCE/MWCNT-AuNPs/AuDN (blue) in ZS (5mM, pH 7.0, Scan rate: 50 mV/s); (B) Shows corresponding cathodic peak currents o the electrodes; (C) CV responses of GCE/ MWCNT-AuNPs/ AuDN at different scan rate (10-100 mV/s) in ZS, and (D) shows corresponding the peak currents following linearity; (E) Nyquist plot of bare GCE (black), GCE/MWCNT/AuDN (green), GCE /AuDN (red), and GCE/MWCNT-AuNPs/AuDN (blue) in 5.0 mM PBS buffer; (D) Comparative histogram showing Rct values in the different surfaces.

3.4. Analytical performance of GCE/MWCNT-AuNPs/AuDN sensing probe

The analytical performance of the GCE/MWCNT-AuNPs/AuDN dendritic surface was assessed by detecting AP, which is an important analyte related to various physiological dysfunctions including hepatotoxicity. LSV at the final GCE/MWCNT-AuNPs/AuDN sensor surface was recorded by sweeping the potential between 0 and 0.6 V in blank PBS, where no peak was observed as expected in the absence of any redox molecule either in the measuring solution or at the electrode surface. Another LSV was recorded at bare GCE under the same experimental conditions in the presence of 100 µM of AP. In this case a redox peak at 0.47 V vs. Ag/AgCl was observed most likely due to the direct electron transfer behavior of AP at the electrode surface (black curve) as shown in **figure 4.5 (A)**. Thereafter, GCE/MWCNT-AuNPs/AuDN electrode was tested for AP detection, where an amplified current response at a lower potential of 0.38 V was observed (blue curve). This was most likely due to the catalytic effect of MWCNT-AuNPs/AuDN nanohybrid sensing matrix. Comparable redox peak potential for AP has also been reported earlier (Kumar et al. 2019b).

In order to further validate that the peak at 0.38 V was exclusively due to the redox activity of AP in our experimental settings, we performed two more control experiments. The first control study was a preliminary AP concentration dependent study, where the responses of the final sensor probe was measured at 10 to 50 µM AP in 5 mM PBS. **Figure 4.5 (B)** shows the LSV curves, where current response increases with higher concentrations of AP. The corresponding linear plot is shown in **figure 4.5 (C).** The linear regression equation for the AP preliminary analysis is expressed as follows:

$$\Delta I\ (\mu A) = 0.081\ (\pm 0.047) + 0.063\ (\pm\ 0.001)\ \text{Conc. [AP (µM)]}$$ ……. **Equation 4**

with co-relation coefficient of 0.99. This result, clearly shows the ability of the final sensor probe to detect AP efficiently.

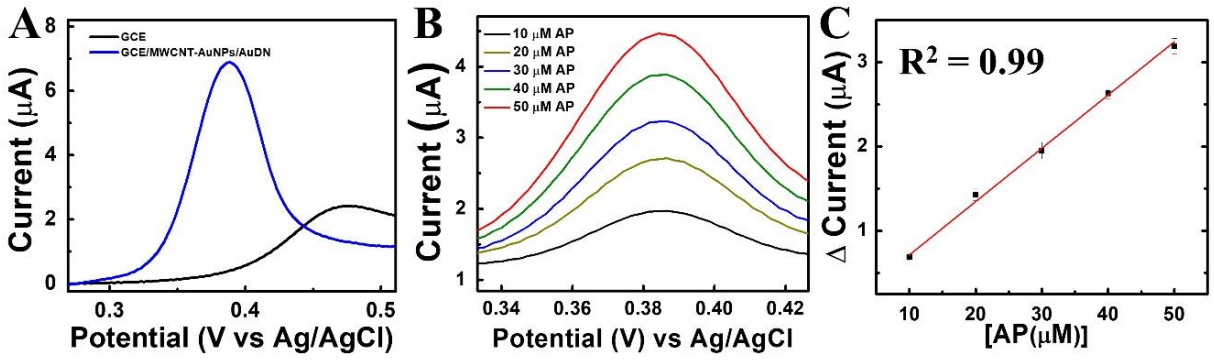

Figure 4.5. (A) Comparative LSV responses of Bare GCE (black), and GCE/MWCNT-AuNPs/AuDN (blue) at 100 µM of AP in PBS; (B) LSV responses of GCE/MWCNT-AuNPs/AuDN modified electrode surface at different concentrations of AP; (C) Calibration plot obtained from the LSV responses at GCE/MWCNT-AuNPs/AuDN sensor surface.

In the second control study, a scan rate dependent study was performed at 10 µM AP between 10 and 100 mV/s^{-1} (figure not shown). In this case, the peak currents were found to be directly proportional to the square root of the scan rate, which was merely due the electro-catalysis of AP. The results found from both the control experiments validate that the developed GCE/MWCNT-AuNPs/AuDN nanoprobe is stable and is able to detect AP accurately.

We further evaluated the analytical performance of developed GCE/MWCNT-AuNPs/AuDN probe using DPV for the detection of various concentrations of AP in 5.0 mM PBS. DPV is considered to be a very sensitive technique compared to LSV because it is capable of detecting analytes at low concentrations (Bard et al. 1980). So, we selected DPV to further study the analytical performance of the GCE/MWCNT-AuNPs/AuDN sensor probe. **Figure 4.6 (A)** shows the representative DPV responses where the current

responses increase with the increase in AP concentrations. The signals obtained at lower concentrations of AP (100-1000 nM) has been shown in **figure 4.6 (B)**. Based on the DPV signals, a calibration plot was obtained with the dynamic range between 100 and 7500 nM (**figure 4.6 (C)**).

The linear regression equation of AP sensing based on the calibration curve is expressed as follows:

$\Delta I\ (A) = 0.08\ (\pm\ 0.0072) \times 10^{-6} + 2.19\ (\pm\ 0.024) \times 10^{-4}$ Conc. [AP (nM)] **Equation 5**

The lower limit of detection (LOD) of AP was calculated to be 2.12 (±0.03) nM (RSD < 4.1%, n = 3) using equation 6.

$$DL = 3\ \sigma_b / m \ldots\ldots\ldots$$ **Equation 6**

Where, σ_b is standard deviation of blank and m is slope of the calibration curve.

This is interesting to note that, the GCE/MWCNT-AuNPs/AuDN sensor probe shows a wider LDR and low LOD compared to other recently reported AP sensors as shown in the table 4. To further validate the clinical applications, the GCE/MWCNT-AuNPs/AuDN sensor probe was applied to detect AP in biological fluid and in the presence of some commonly found molecules.

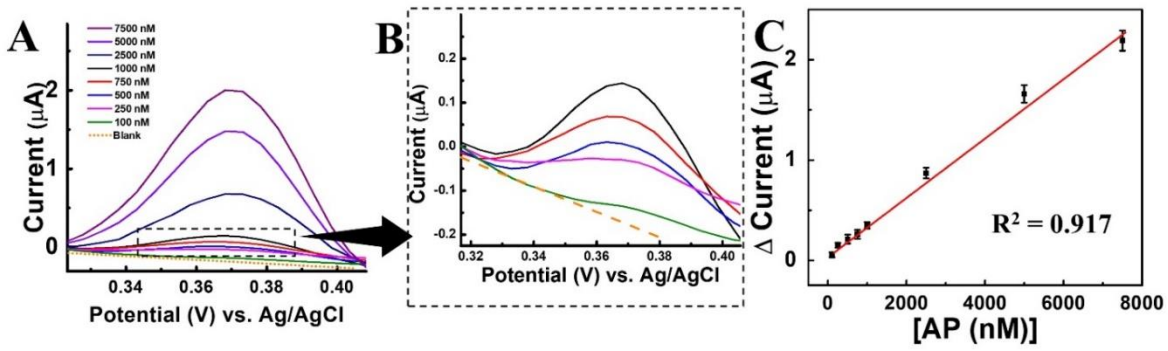

Figure 4.6. (A) Dose dependent DPV responses obtained from GCE/MWCNT-AuNPs/AuDN sensor probe at various concentrations (100-7500 nM) of AP; (B)

Magnified image of DPV responses at the lower concentration of AP; (C) Calibration plot obtained from the DPV responses at GCE/MWCNT-AuNPs/AuDN sensor surface.

3.5. Selectivity assay

To evaluate the commercial potential of any sensor, it is important to investigate the selectivity of a sensor towards various possible interfering molecules (Bansal et al. 2017; Kumar et al. 2019c) . A wide range of commonly co-existing molecules viz. glycine, alanine, glutamine, glucose, urea, and uric acid were selected for interference analysis in separate experiments. All the potentially interfering molecules were tested at a higher concentration (1 mM) than usually they are found in body fluids. **Figure 4.7** shows the recorded signal responses of the final probe in the presence of the interfering molecules, where negligible or no current were observed for these molecules. The selectivity of the final probe is estimated mathematically by using equation 7.

$$K_{sel} = (Signal)_{Interfering\ molecules} / (Signal)_{AP} \ldots\ldots\ldots \textbf{Equation 7.}$$

Where K_{sel} is the coefficient of selectivity, (Signal $_{interfering\ molecules}$ is the signal strength shown by the probe when treated with the interfering molecules, and $(Signal)_{AP}$ is the signal strength corresponding to AP.

The k_{sel} value for all the interfering molecules were found to be negligible (K_{sel} <<1), reflecting high selectivity of the final sensor probe towards AP. No electrochemical response for the interfering molecules were observed possibly due to the electrochemically inactive behavior of the compounds (e.g. glucose) and /or the analytical potential where other electroactive molecules (e.g. ascorbic acid or dopamine) do not oxidize or reduce.

SI. NO.	PROBE DESIGN	LDR	LOD	REAL SAMPLE	REF
1.	GCE/GR/NiO-CuO	4 – 400 µM	1.33 µM	Pharmaceutical samples	(Liu et al. 2016)
2	GCE/AuNP-PGA/SWCNT	50 - 300 µM	15 µM	Pharmaceutical samples	(Lee et al. 2016)
3.	GCE/CNT/PMB	50 – 500 µM	1.6 µM	Pharmaceutical samples	(Hosu et al. 2017)
4.	GCE/P-rGO	1.5 – 120 µM	0.36 µM	Pharmaceutical tablet	(Zhang et al. 2018)
5.	Lcc-TiO_2/CPE	8 – 120 µM	1 µM	Pharmaceutical samples	(Thomaz et al. 2018)
6.	GCE / MWCNT-PDDA-FPS	3 – 1100 µM	0.6 µM	Urine	(Chen et al. 2018)
7.	GCE/CSS	0.37 – 7.52 µM	0.12 µM	Saliva, sweat, urine	(Campos et al. 2018)
8.	GCE/NCD	0.5 to 600 µM	157 nM	Pharmaceutical samples	(Fu et al. 2018)
9.	ITO/F–NGQDs /BiOBr	0.01 –20.0 µM	3.33 nM	Pharmaceutical samples	(Gao et al. 2019)
10.	GCE/MWCNT-AuNPs/AuDN	100-7500 nM	2.12 nM	Urine	This work

Table 4.1. A comparison of the analytical performance of the GCE/MWCNT-AuNPs/AuDN sensor with recently reported AP sensors

The statistical significance of the result was calculated by t-test and the p-value against the interfering molecules were found to be negligible (<<0.001, n=3). In real world, AP in urine samples co-exists with the interfering molecules, hence mixed sample analysis is worthy to be investigated. For this purpose, all the interfering molecules along with AP were prepared as a mixed sample and data were collected. It is interesting to note that the final probe is also capable of detecting AP over 94% compared to the standard conditions in this case This result clearly shows the ability of the GCE/MWCNT-AuNPs/AuDN sensor probe to detect AP in complex biological fluids.

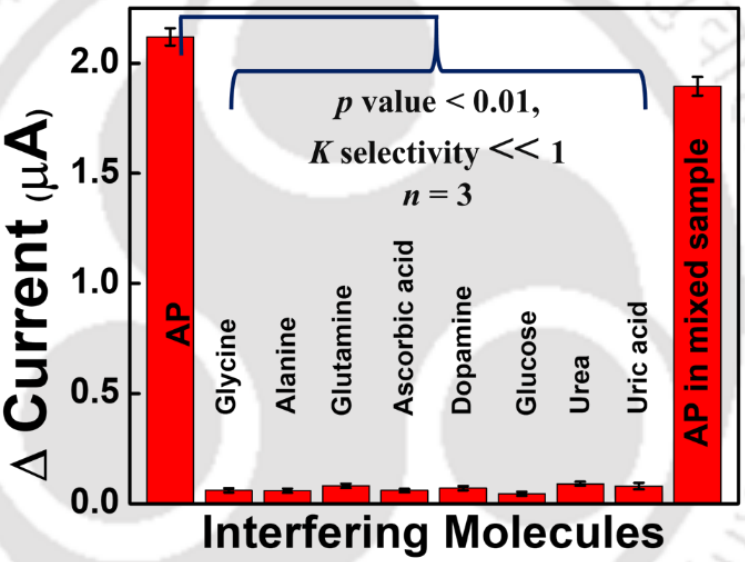

Figure 4.7 Interference study showing high selectivity of the sensor towards AP with negligible current response by interfering molecules.

3.6. Real sample analysis

Most of the AP molecule taken as a drug to relieve fever or pain are digested by the body and their digested/ semi digested product excreted out in the urine. Several previous reports also attempted to detect AP in urine samples due the clinical rational (Chandra et al. 2013; Kumar et al. 2019b). Therefore, we selected urine as a model sample matrix to analyze the practical applicability of our sensor to detect different concentrations of AP in clinical settings. DPV responses were recorded in the

equilibrated urine sample (10:1 in PBS) by spiking different concentration of AP. The sensor was capable of detecting AP in urine, without any pretreatment. The DPV responses at different concentrations of AP spiked in the real sample were compared with the standard conditions, as shown in **figure 4.8**. The recoveries of AP in the real sample at each concentration has been calculated and found between 92 and 96% of original calibration plot, showing the clinical potential of the developed sensor probe. The % recoveries of AP concentrations in the real samples were calculated using equation 8.

$$\% \text{ Recovery} = [S]_{AP} - [B]_{AP} / [SS]_{AP} \quad \text{..... } \textbf{Equation 8}$$

Where, $[S]_{AP}$ and $[B]_{AP}$ are the analytical responses of AP in the spiked and blank urine samples, respectively; and $[SS]_{AP}$ is the analytical response of AP in the standard buffer solutions.

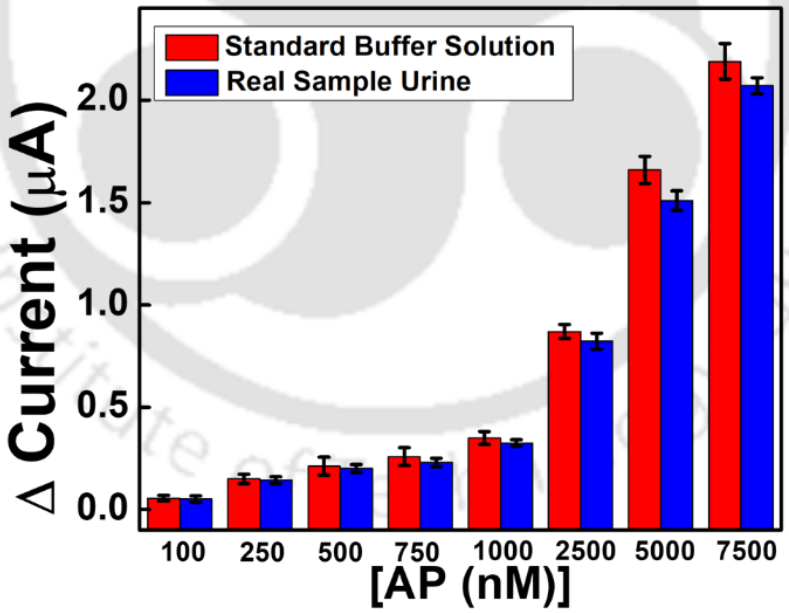

Figure 4.8 Shows a comparative values of signal in standard sample and the real sample urine indicating a high % recovery of AP.

The marginal variation in current response in the urine samples was most likely due to matrix effect or handling errors. This study validates the potential of the

GCE/MWCNT-AuNPs/AuDN sensor probe to detect AP effectively in biological samples under clinical settings.

3.7. Reproducibility and stability assay

To test the prospective of the developed sensor as an efficient tool for AP detection in clinics as well as other systems, its reproducibility and stability was investigated. To check the long term stability of the final GCE/MWCNT-AuNPs/AuDN probe, the electrode was stored in ambient condition and DPV responses were recorded for 8 weeks, periodically taking measurements thrice a week. The retention of signal was found to be 90-96%, which shows that the sensor system was stable for sensing applications for 8 weeks (RSD 4.7%, n= 3). We also tested the ability of a single electrode to detect AP in buffer medium, and found that there was no significant loss in signals up to four consecutive analyses. In another set of experiment, we also checked the reproducibility of the sensing matrix by testing five different GCE/MWCNT-AuNPs/AuDN surface at the same concentration of AP. The variation in peak current was found to be negligible in this case indicating high electrode to electrode reproducibility. The negligible variations found in peak current may be most likely due to minor handling error or fluctuation in other experimental conditions.

4. Conclusions

A simple GCE/MWCNT-AuNPs/AuDN sensor has been developed by tuning the electrodeposition parameters for enhanced bioelectronics property. The sensor surface was thoroughly characterized, and found to detect AP in clinically significant range. The sensor was able to detect AP with a wide LDR of 100-7500 nM and a LOD of 2.12 (±0.03) nM. The sensor was highly selective towards AP with

negligible effect of co-existing interfering molecules. To evaluate the clinical possibilities of the sensor, real sample analysis in urine was performed by spike and recovery method, where 92-96 % recovery of AP signal was obtained. To the best of our knowledge, this is the first report where a MWCNT-AuNPs and AuDN nanohybrid has been used for the quantitative detection of AP. In addition to this, the enhanced conductivity and catalytic property of GCE/MWCNT-AuNPs/AuDN modified electrode surface than the bare electrode surface indicates its significance as a potential electrode material. The sensor follows an easy fabrication process, and can be applied for rapid, label free, and low cost sensing. This system can be further developed for real time AP measurements in urine, serum, and other biological fluids in clinical settings.

5. References

Assah E, Goh W, Zheng XT, et al (2018) Rapid colorimetric detection of p53 protein function using DNA-gold nanoconjugates with applications for drug discovery and cancer diagnostics. Colloids Surfaces B Biointerfaces 169:214–221.

Ataee-Esfahani H, Skrabalak SE (2015) Attachment-based growth: Building architecturally defined metal nanocolloids particle by particle. RSC Adv 5:47718–47727.

Bansal S, Jyoti A, Mahato K, et al (2017) Highly Sensitive in vitro Biosensor for Enterotoxigenic Escherichia coli Detection Based on ssDNA Anchored on PtNPs-Chitosan Nanocomposite. Electroanalysis 29:2665–2671

Bard AJ, Faulkner LR, Leddy J, Zoski CG (1980) Electrochemical methods: fundamentals and applications. wiley New York

Bernal W, Auzinger G, Dhawan A, Wendon J (2010) Acute liver failure. Lancet 376:190–201.

Burgot G, Auffret F, Burgot J-L (1997) Determination of acetaminophen by thermometric titrimetry. Anal Chim Acta 343:125–128

Campos AM, Raymundo-Pereira PA, Mendonça CD, et al (2018) Size Control of Carbon Spherical Shells for Sensitive Detection of Paracetamol in Sweat, Saliva, and Urine. ACS Appl Nano Mater 1:654–661.

Chandra P, Son NX, Noh H-B, et al (2013) Investigation on the downregulation of dopamine by acetaminophen administration based on their simultaneous determination in urine. Biosens Bioelectron 39:139–144

Chen Y, Liu X, Wu T, et al (2018) Enhanced electrochemical sensitivity towards acetaminophen determination using electroactive self-assembled ferrocene derivative polymer nanospheres with multi-walled carbon nanotubes. Electrochim Acta 272:212–220.

Cheng TM, Huang TK, Lin HK, et al (2010) (110)-Exposed gold nanocoral electrode as low onset potential selective glucose sensor. ACS Appl Mater Interfaces 2:2773–2780.

Chun LJ, Tong MJ, Busuttil RW, Hiatt JR (2009) Acetaminophen hepatotoxicity and acute liver failure. J Clin Gastroenterol 43:342–349

Fu L, Wang A, Lai G, et al (2018) A glassy carbon electrode modified with N-doped carbon dots for improved detection of hydrogen peroxide and paracetamol. Microchim Acta 185.

Gao K, Bai X, Zhang Y, Ji Y (2019) N–doped graphene quantum dots embedded in BiOBr nanosheets as hybrid thin film electrode for quantitative photoelectrochemical detection paracetamol. Electrochim Acta 318:422–429.

Gioia MG, Andreatta P, Boschetti S, Gatti R (2008) Development and validation of a liquid chromatographic method for the determination of ascorbic acid, dehydroascorbic acid and acetaminophen in pharmaceuticals. J Pharm Biomed Anal 48:331–339

Hinson JA, Roberts DW, James LP (2010) Mechanisms of acetaminophen-induced liver necrosis. In: Adverse drug reactions. Springer, pp 369–405

Hosu O, Barsan MM, Cristea C, et al (2017) Nanocomposites based on carbon nanotubes and redox-active polymers synthesized in a deep eutectic solvent as a new electrochemical sensing platform. Microchim Acta 184:3919–3927.

James LP, Mayeux PR, Hinson JA (2003) ACETAMINOPHEN-INDUCED HEPATOTOXICITY. Drug Metab Dispos 31:1499–1506.

Jiang LC, Zhang W De (2010) A highly sensitive nonenzymatic glucose sensor based on CuO nanoparticles-modified carbon nanotube electrode. Biosens Bioelectron 25:1402–1407.

Kumar A, Purohit B, Mahato K, et al (2019a) Design and Development of Ultrafast Sinapic Acid Sensor Based on Electrochemically Nanotuned Gold Nanoparticles and Solvothermally Reduced Graphene. 1–12.

Kumar A, Purohit B, Mahato K, et al (2019b) Gold-Iron Bimetallic Nanoparticles Impregnated Reduced Graphene Oxide Based Nanosensor for Label-Free Detection of Biomarker Related to Non-Alcoholic Fatty Liver Disease. Electroanalysis elan.201900337.

Kumar A, Purohit B, Mahato K, Chandra P (2019c) Advance Engineered Nanomaterials in Point-of-care Immunosensing for Biomedical Diagnostics. In: Immunosensors. pp 238–266

Kumar A, Purohit B, Maurya PK, et al (2019d) Engineered Nanomaterial Assisted Signal-amplification Strategies for Enhancing Analytical Performance of Electrochemical Biosensors. Electroanalysis 31:1615–1629.

Lee SH, Lee JH, Tran VK, et al (2016) Determination of acetaminophen using functional paper-based electrochemical devices. Sensors Actuators, B Chem 232:514–522.

Li Z, Liu Z, Sun H, Gao C (2015) Superstructured Assembly of Nanocarbons: Fullerenes, Nanotubes, and Graphene. Chem Rev 115:7046–7117.

Lim B, Xia Y (2011) Metal nanocrystals with highly branched morphologies. Angew Chemie - Int Ed 50:76–85.

Liu B, Ouyang X, Ding Y, et al (2016) Electrochemical preparation of nickel and copper oxides-decorated graphene composite for simultaneous determination of dopamine, acetaminophen and tryptophan. Talanta 146:114–121.

Mahato K, Purohit B, Bhardwaj K, et al (2019) Novel electrochemical biosensor for serotonin detection based on gold nanorattles decorated reduced graphene

oxide in biological fluids and in vitro model. Biosens Bioelectron 142:111502.

Moreira AB, Oliveira HPM, Atvars TDZ, et al (2005) Direct determination of paracetamol in powdered pharmaceutical samples by fluorescence spectroscopy. Anal Chim Acta 539:257–261

Muthukumar V, Chetty R (2018) Electrodeposited Pt–Pd dendrite on carbon support as anode for direct formic acid fuel cells. Ionics (Kiel) 24:3937–3947. 2

Naveen MH, Gurudatt NG, Noh HB, Shim YB (2016) Dealloyed AuNi Dendrite Anchored on a Functionalized Conducting Polymer for Improved Catalytic Oxygen Reduction and Hydrogen Peroxide Sensing in Living Cells. Adv Funct Mater 26:1590–1601.

Nebot C, Gibb SW, Boyd KG (2007) Quantification of human pharmaceuticals in water samples by high performance liquid chromatography--tandem mass spectrometry. Anal Chim Acta 598:87–94

Noh H, Lee K, Chandra P, et al (2012) Electrochimica Acta Application of a Cu – Co alloy dendrite on glucose and hydrogen peroxide sensors. Electrochim Acta 61:36–43.

Purohit B, Mahato K, Kumar A, Chandra P (2019) Sputtering enhanced peroxidase like activity of a dendritic nanochip for amperometric determination of hydrogen peroxide in blood samples. Microchim Acta 186:658.

Qiu R, Cha HG, Noh HB, et al (2009) Preparation of dendritic copper nanostructures and their characterization for electroreduction. J Phys Chem C 113:15891–15896

SEEFF LB (1986) Acetaminophen Hepatotoxicity in Alcoholics. Ann Intern Med 104:399.

Shu H, Cao L, Chang G, et al (2014) Direct electrodeposition of gold nanostructures onto glassy carbon electrodes for non-enzymatic detection of glucose. Electrochim Acta 132:524–532.

Su DS, Perathoner S, Centi G (2013) Nanocarbons for the development of advanced catalysts. Chem Rev 113:5782–5816.

Sun J, Schnackenberg LK, Holland RD, et al (2008) Metabonomics evaluation of urine from rats given acute and chronic doses of acetaminophen using NMR and UPLC/MS. J Chromatogr B Anal Technol Biomed Life Sci 871:328–340.

Tan YN, Lai A, Su X (2014) Interrogating Cooperative Interactions of Transcription Factors with Composite DNA Elements Using Gold Nanoparticles. Sci Adv Mater 6:1460–1466.

Thomaz DV, de Oliveira MT, Lobón GS, et al (2018) Development of Laccase-TiO2@carbon paste biosensor for voltammetric determination of paracetamol. Int J Electrochem Sci 13:10884–10893.

Verma S, Singh A, Shukla A, et al (2017) Anti-IL8/AuNPs-rGO/ITO as an Immunosensing Platform for Noninvasive Electrochemical Detection of Oral Cancer. ACS Appl Mater Interfaces 9:27462–27474.

Wu HX, Cao WM, Li Y, et al (2010) In situ growth of copper nanoparticles on multiwalled carbon nanotubes and their application as non-enzymatic glucose sensor materials. Electrochim Acta 55:3734–3740.

You H, Yang S, Ding B, Yang H (2013) Synthesis of colloidal metal and metal alloy nanoparticles for electrochemical energy applications. Chem Soc Rev 42:2880–2904.

Zhang R, Wang X (2007) One step synthesis of multiwalled carbon nanotube/gold nanocomposites for enhancing electrochemical response. Chem Mater 19:976–978.

Zhang X, Wang KP, Zhang LN, et al (2018) Phosphorus-doped graphene-based electrochemical sensor for sensitive detection of acetaminophen. Anal Chim Acta 1036:26–32.

Zheng XT, Goh WL, Yeow P, et al (2019) Ultrasensitive dynamic light scattering based nanobiosensor for rapid anticancer drug screening. Sensors Actuators B Chem 279:79–86.

Zhu Y, Son JI, Shim YB (2010) Amplification strategy based on gold nanoparticle-decorated carbon nanotubes for neomycin immunosensors. Biosens Bioelectron 26:1002–1008.

Chapter # V

Electrochemical immunosensor based on gold nanodendrites/ chitosan-reduced graphene oxide for label free detection of cancer biomarker in human serum samples

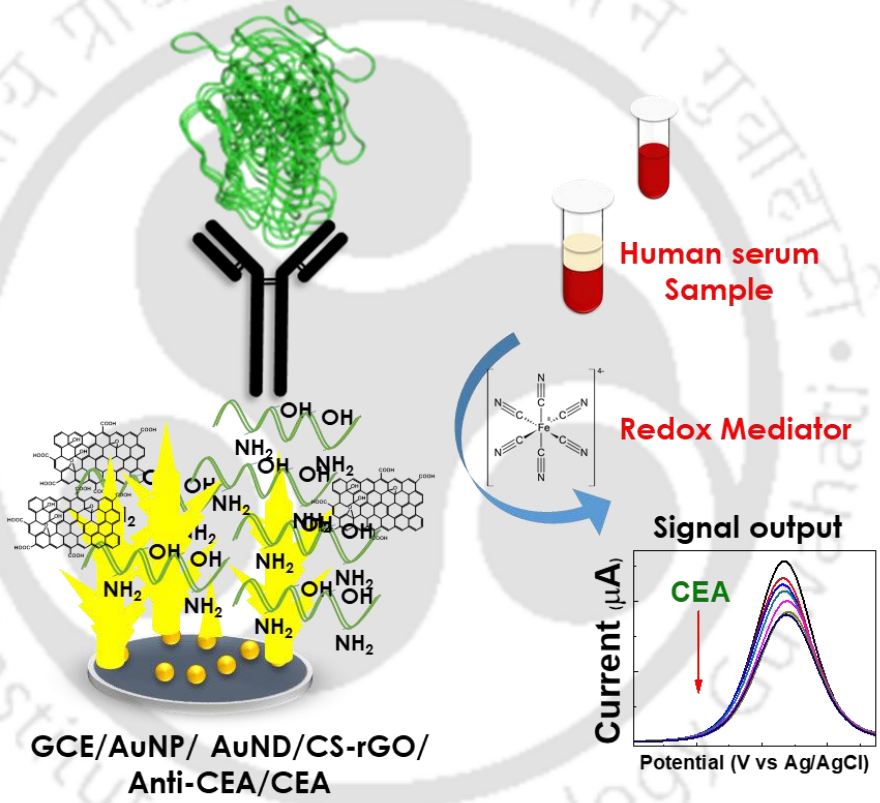

Status:

Manuscript Submitted

1. Introduction

In this part of the study, we have attempted to develop an electrochemical label-free cancer biosensing system using metallic dendrites and its composites as a sensing matrix. Carcinoembryonic antigen (CEA), a glycoprotein expressed on the cell surface is an important cancer biomarker associated is used as a model antigen (Reynoso et al. 1972; Benchimol et al. 1989; Beauchemin et al. 1999). CEA is produced in foetus at a higher level, which rapidly declines after birth. In healthy individuals, the level of CEA found in serum is <5 ng/ mL. Higher concentration of CEA (>20 ng/ mL) in blood is associated with various cancers like colon, breast, lung, pancreases, *etc.*(Beard and Haskell 1986; Berinstein 2002; Goonetilleke and Siriwardena 2007; Gu et al. 2007; Hasanzadeh and Shadjou 2017). CEA is also used as a cancer relapse marker, and used for determining the stage of disease progression (Sculier et al. 1985; Molina et al. 1995). The conventional methods to detect CEA follows the protein measurements by enzyme-linked immunosorbent assay (ELISA) and radioimmunoassay, which suffers from low sensitivity and problems of radio waste disposal, respectively (Gu et al. 2018). Also, advanced methods like colorimetry (Kim et al. 2009), fluorescence (He et al. 2013), chemiluminescence(Zhao et al. 2016), surface-enhanced Raman scattering (SERS) (Lee et al. 2011) have been used for the detection of CEA in various samples. However, these methods follow a multistep time-consuming protocol involving various labels, which hinders in fast detection of the biomarker. A fast, simple, and sensitive analytical method for the determination of analytes is important for the clinical diagnosis, where biosensors can be a possible solution. Electrochemical immunosensor, a class of electrochemical biosensor that generates an electrochemical signal as a result of the coupling of an antigen with an antibody to

form an antigen-antibody complex (Afkhami et al. 2017; Mahato et al. 2020). Electrochemical immunosensors are designed in such a way that when an antigen or antibody immobilized onto a sensing surface forms a complex with the corresponding antibody or antigen, it will generate a signal proportional to the amount of analyte. Advanced electrochemical methods are nowadays being developed utilizing nanomaterials, microfluidics, enzymes based labels, and other signal enhancement strategies to sense analyte in a very small sample volume (Wilson 2005; Kokkinos et al. 2016; Cho et al. 2018). Innovative surface engineering of the electrode with nanomaterials is an integral part of an electrochemical immunosensor to achieve higher sensitivity and selectivity.

AuND has been used for the development of sensing matrices to detect H_2O_2 and acetaminophen in the previous three works. However, the lack of functional groups over the AuND limits its applications for the development of biosensors where selective detection is important. Hence, AuND can be conjugated with various other nanomaterials with functional groups to develop immunosensor, where the AuND functions as a highly conducting matrix material, and other nanomaterials with functional group act to immobilize the bio-recognition molecules like an antibody, aptamer, or DNA probe (Mahato et al. 2020). Chitosan (CS), a biopolymer isolated from chitin (naturally present material in the exoskeleton of crustaceans, insects, and fungal cell walls) is widely used in biosensor development. CS is widely integrated in biosensor due to its excellent biocompatibility, excellent ability to form films, wide availability in different functionalized forms, and ease of controlled electro-deposition as a durable thin film on negatively charged material of sensor probe (cathodes) (Suginta et al. 2013; Baranwal et al. 2018). Also, it can retain its structural and chemical stability owing to its hydrogel-forming capacity and chemical

adaptability, an important criterion to be used as an immobilization matrix in electrochemical sensing (Ohkawa et al. 2004; Yi et al. 2005; Rinaudo 2006). CS contains an abundant number of primary amine group (-NH_2), hydroxyl (−OH), and acetanilide (−$NHCOCH_3$) throughout its chain, which can be further derivatized (sugar-modified, phosphorylated, quaternized, cyclodextrinlinked, thiolated, and sulfated) to form many linkages to immobilize biomolecules necessary for immunosensor development (Suginta et al. 2013). However, its non-conducting nature results in a decrease in the current responses in the electrochemical sensors. Thus, it has been employed in biosensor by compositing with nanomaterials to achieve higher sensitive matrices. For this, reduced graphene oxide (rGO) is an excellent candidate for the preparation of nanocomposite material due to its unique properties such as large surface-to-volume ratio, easy and cost-effective synthesis and exceptional high electrical conductivity, mechanical strength, thermal stability (Afkhami et al. 2017). Also, the functional groups in the rGO are very less, so it is not going to interfere with the binding of CS to activated protein molecules. Based on these, a combination of AuND, CS, and rGO can be used for the development of an immunosensor with very high sensitivity.

In this study, we developed a CEA immunosensor based on hierarchical electrodeposited AuND by sequential electrodeposition using LSV and chronoamperometry for its excellent conductivity as a matrix material. CS, and rGO are used for immobilization of antibodies and to amplify the signal, respectively. The sensor probe was physically characterized by SEM, TEM, and EDX to access its morphological property. The electrochemical characterization includes CV, EIS, and chronoamperometry to access its electronic property.

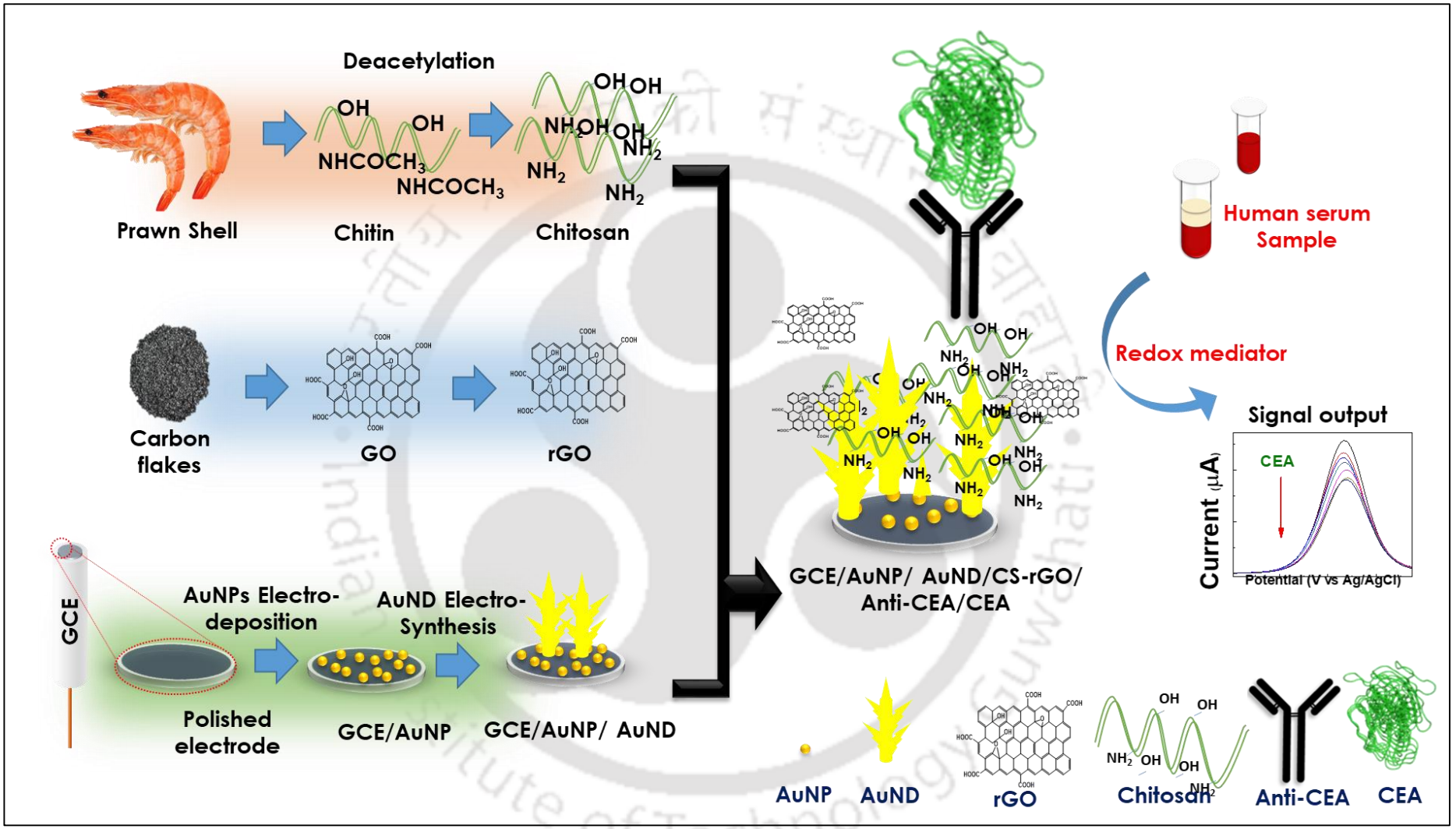

Figure 5.1. Schematic representation of the work depicting the immunosensing of a cancer biomarker, CEA by a novel AuNP/AuND/ CS-rGO electrode.

After the characterization studies, the analytical performance of the sensor probe was evaluated i.e. linear dynamic range (LDR), and low limit of detection (LOD) using DPV. The clinical applicability of the sensor was also evaluated by sensing CEA in human serum samples by spike and recovery methods. Interference due to commonly found molecules and long term stability of the sensor was evaluated. Fabrication of the biosensors and their application to detect CEA in human serum is graphically represented in **figure 5.1**.

2. Experimental

2.1. Chemicals and Instruments

Potassium chloride (KCl), potassium ferricyanide [$K_3Fe(CN)_6$], potassium ferrocyanide [$K_4Fe(CN)_6$], sodium monophosphate (NaH_2PO_4) and sodium bisphosphate (Na_2HPO_4) were purchased from Himedia Pvt. Ltd., India. Chloroauric acid ($HAuCl_4$), N-(3-dimethylaminopropyl)-N'-ethyl carbodiimide hydrochloride (EDC), N-hydroxy succinimide (NHS), indium tin oxide (ITO) coated glass was obtained from Sigma-Aldrich Chemical Co. (USA). sodium hydroxide (NaOH), hydrochloric acid (HCl), Sulfuric acid (H_2SO_4), nitric acid (HNO_3), sodium chloride (NaCl), acetic acid, citric acid, uric acid, glucose, urea, glycine, alanine, glutamic acid, cysteine was purchased from SRL Pvt. Ltd, India. All aqueous solutions were prepared in doubly distilled water obtained from a Milli-Q water purifying system (18 MΩ cm). All chemicals used in this study were of standard analytical grade.

Synthesis of the AuND was performed using an electrochemical workstation (Metrohm Autolab) using three electrode-based electrochemical cell systems. For that, GCE, platinum (Pt) wire, and Ag/AgCl (saturated with KCl) were used as the working, counter, and reference electrodes, respectively. Surface morphological

Imaging and EDX were performed using FESEM (Zeiss, Gemini). TEM imaging was obtained from FETEM (JEOL, 2100F). For the preparation of the TEM samples of CS (in acetic acid), AuND, AuND/CS-rGO, rGO the probe materials were sonicated in ethanol for 5 minutes, and then 20 µl of the solution was placed over the carbon-coated copper grid for well dispersal. The grid was placed in an oven at 37 ˚C for 12 hours to remove the moisture.

2.2. CS isolation from shrimp shell

CS was isolated from dried shrimp shells (following a previosly reported method), a waste collected from a nearby market. Dried shrimp shells were put in the hot air oven for 24 hrs to remove moisture, followed by grinding it to form a powder with minimum roughness. The powder was treated with 7% HCl at room temperature for 30 min, followed by centrifuge at 1000 rpm. The powder was washed in MilliQ water and immersed in 10% NaOH at 95 ºC for 3 hrs. The solution was then filtered to remove proteins and other residues. The solution was washed with MilliQ water two times, then in 95% ethanol, and kept at 50 ºC to dry overnight to obtain chitin (shown in Fig. 5.2.). To obtain CS, 10g of Chitin powder was deacetylated in 50% NaOH at 90 ºC for 15 min. The resultant material was washed with luke warm water 3 times and dried in the oven.

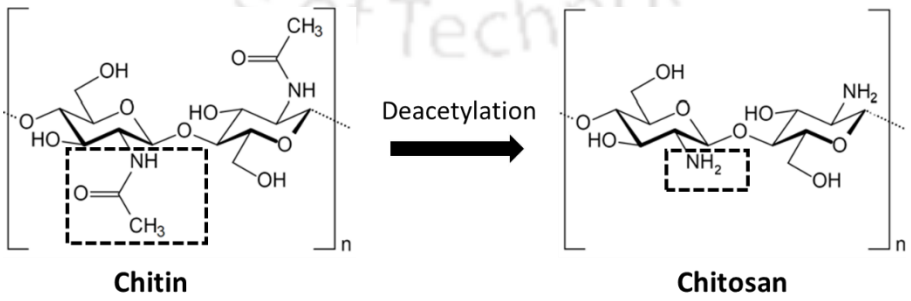

Figure 5.2. Structure of chitin and chitosan showing the change of structure after deacetylation; Chitin is isolated from shrimp shell, and then chitosan from chitin.

.2.3. Synthesis of rGO

For the synthesis of rGO, the modified hammer's method was followed using graphite flakes as a starting material (Kumar et al. 2019a). First, GO was synthesized from graphite flakes, followed by rGO synthesis from GO. Graphite flakes (0.450 g) were treated with concentrated H_2SO_4 and H_3PO_4 (9:1). Thereafter, $KMnO_4$ (2.64g) was added slowly and the solution was allowed to stir for 6 hours. After that, in order to neutralize the $KMnO_4$, 1.35 ml of H_2O_2 (30% v/v) was mixed and agitated for 10 minutes which has been followed by the addition of 10 mL of HCl (30%) and 60 mL of deionized water to the synthesized slurry. This a highly exothermic process leading to the increase of temperature, so an ice bath was used to keep the temperature in a steady state. Thereafter, the solution was centrifuged at 5000 RPM to collect the sample followed by overnight drying at 90 °C in an oven to obtain the GO powder. The obtained GO was dried and then exposed to microwaves at 900W for 60 s using a domestic microwave oven to get rGO. The rGO was then placed in an oxygen-free container to prevent further oxidation of the rGO.

2.4. Fabrication of final AuNP/AuND/CS-rGO/Anti-CEA sensing probe

In the previous three objectives, we have discussed the electrodeposition and growth pattern of Au dendrites in details. In this work, we tried to synthesize AuND in a much faster way than before, so we deposited AuND over an optimized layer of AuNP. AuNP was first electrodeposited onto the surface by sweeping the potential in a 0.1 M H_2SO_4 solution containing 0.1 mM $HAuCl_4$ salt. The number of the sweep was optimized by the current response. This surface, containing the deposited Au nanoparticles was termed as GCE/AuNP. AuND was then electrodeposited over a

GCE/AuNP surface using the previously described method with the same experimental setup of 10 mM of $HAuCl_4$ in 0.1 M KCl.

A CS solution (0.5%, w/v) was prepared to add CS powder in a 2% acetic acid solution and sonicated for 1 hr. Then, the solution was filtered to remove any impurity from the CS solution. A CS-rGO solution was prepared by adding 2 mg of rGO in 200µl of CS solution. Prior to electrode fabrication, the GCE/AuNP/AuND electrode was thoroughly rinsed with MilliQ water. Then 10 µl of CS-rGO solution was drop coated onto the GCE/AuNP/AuND electrode and incubated at ambient temperature for 15 minutes. After the fabrication, the electrode was again rinsed with MilliQ water and dried. Anti-CEA antibody (5 µl) was mixed with a freshly prepared EDC (50 mM) and NHS (50 mM) solution (10 µl) at room temperature for 15 min to activate the primary carboxylic groups of the protein. Then, the mixed solution was drop cast onto the GCE/AuND/CS-rGO electrode surface and incubated for 2 hr at 4 ˚C to form a covalent bond with the primary amine group of CS. The functionalized GCE/ AuND/ CS-rGO/ Anti-CEA was treated with a 1mg/ml BSA solution for 10 min to block unspecified sites to prevent non-specific interactions..

2.5. Electrochemical and Analytical measurements

The electrochemical characterization of the sensor probe was carried out in phosphate buffer saline (PBS pH 7.0 and 0.9% NaCl) and PBS containing 5 mM $[Fe(CN)_6]^{-3/-4}$ (Zobell's solution (ZS)) by using CV, LSV, and EIS methods. The impedance spectra were recorded at an open-circuit voltage between 100 Hz and 1 MHz with a sampling rate of five points per decade. For the detection of CEA, DPV responses were recorded by scanning the potential from 0.0 to +0.50 V vs. Ag/AgCl at a scan rate of 0.005 V/s, with pulse potential 0.025 V, and pulse time 0.05 s. The real sample analysis of CEA was carried out in human serum samples collected from

three healthy volunteers of the laboratory, using the same DPV methods as mentioned.

2.6. Real sample preparation and analysis

For real sample analysis, the human serum sample was collected in IIT Guwahati hospital, Assam, India consented with the lab volunteers. The serum sample was collected by centrifuging the collected blood at 3000 rpm for 5 min following the standard clinical protocol. The obtained serum was then equilibrated with the PBS (pH=7.0) before using it for electrochemical studies.

3. Results and Discussion

3.1. Physical Characterization

3.1.1. Characterization of Synthesized CS

Sample for SEM imaging of CS was made by putting it on carbon tape and with a layer of gold sputtering to avoid any damage due to a high energy beam. SEM image of CS in **figure 5.3 (A-B)** shows the sheet-like structure of CS. Then we performed TEM analysis of CS, where a sheet-like structure with porosity was observed. Then we performed EDX to analyze the composition of the materials. In EDX analysis, carbon (C) was found to be the most abundant material, followed by oxygen. A very faint peak of nitrogen (N) was obtained in the spectra. All these materials are characteristics of CS. Then we performed FTIR to analyze the functional groups present in its surface. The comparative FTIR analysis of commercial CS, and CS obtained from shrimp shell following the process mentioned before (figure not shown). The isolated CS exhibits the characteristic absorption bands at 3450 cm^{-1} (O-H stretching), 1870–2880 cm^{-1} (CH-stretching), 1655 cm^{-1} (Amide I), 1580 cm^{-1} (–NH2 bending), and 1320 cm^{-1} (Amide III). The presence of amide bonds confirms

that the CS element can be used as a matrix to immobilize Anti-CEA antibody to selectively bind CEA.

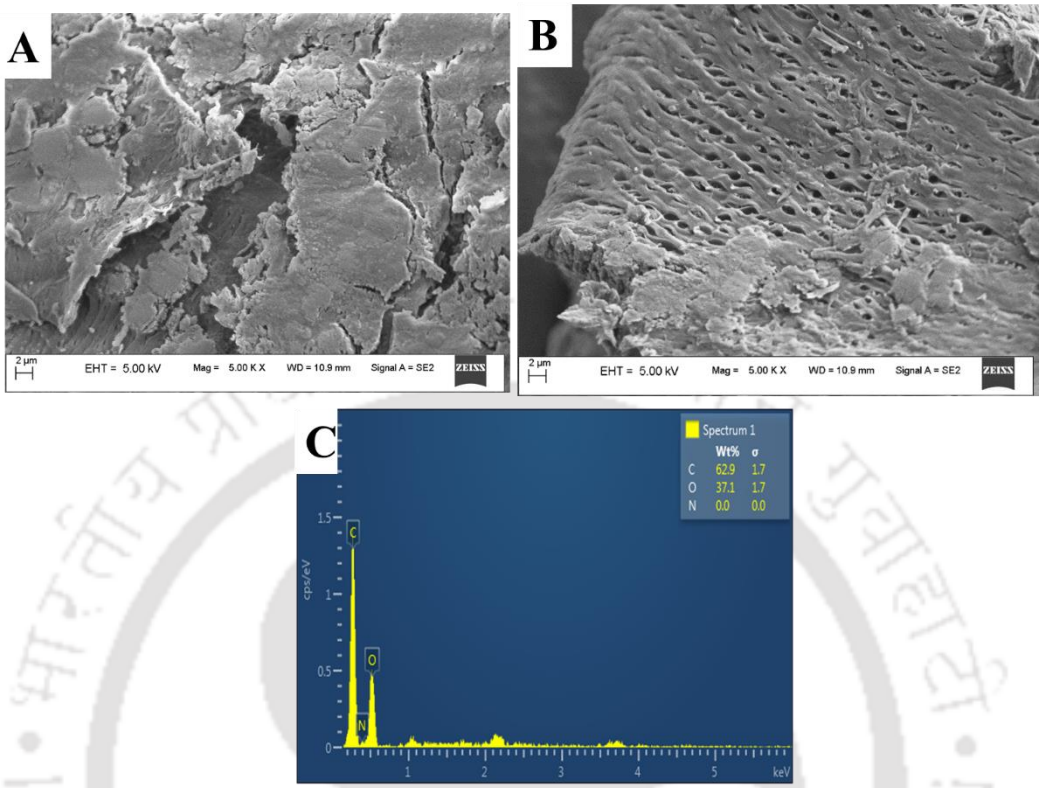

Figure. 5.3. Physical characterization of CS. SEM image of CS (A) and showing a porous characteristic in magnified image(B); (C) EDX analysis of CS showing the presence of carbon, oxygen, and nitrogen characteristics of CS.

3.1.2. Characterization of rGO

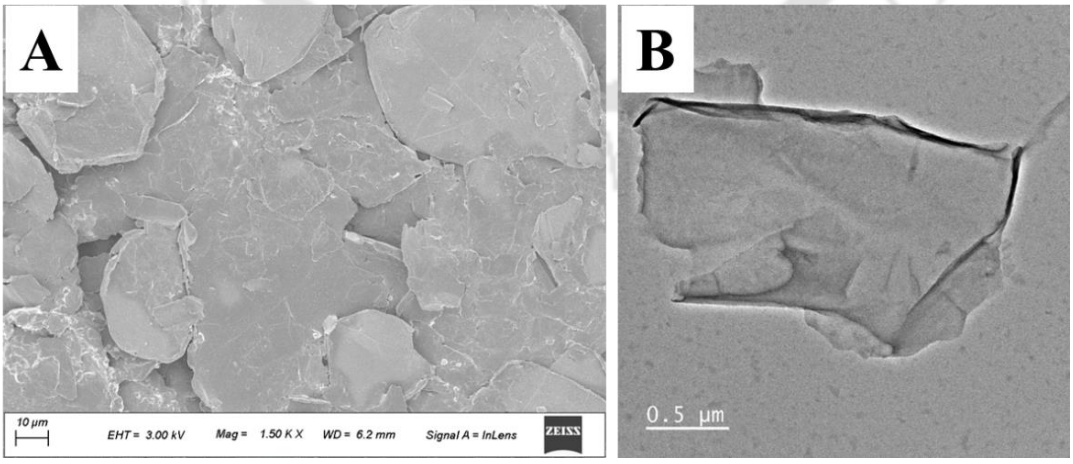

Figure. 5.4. SEM (A), and TEM (B) image of sheet like structure of rGO.

The rGO sheets were characterized using SEM, TEM and EDX. The SEM micrograph (figure 5.4 (A)) shows a sheet like arrangement of the rGO, indicating a very large surface area. The TEM micrograph shows a transparent layer of rGO (figure 5.4 (B)), showing the successful formation of rGO from graphite flakes. The EDX analysis (image not shown) confirms C and O a the most abundant element, confirming the formation of rGO.

3.1.3. Characterization of GCE/AuNP/AuND

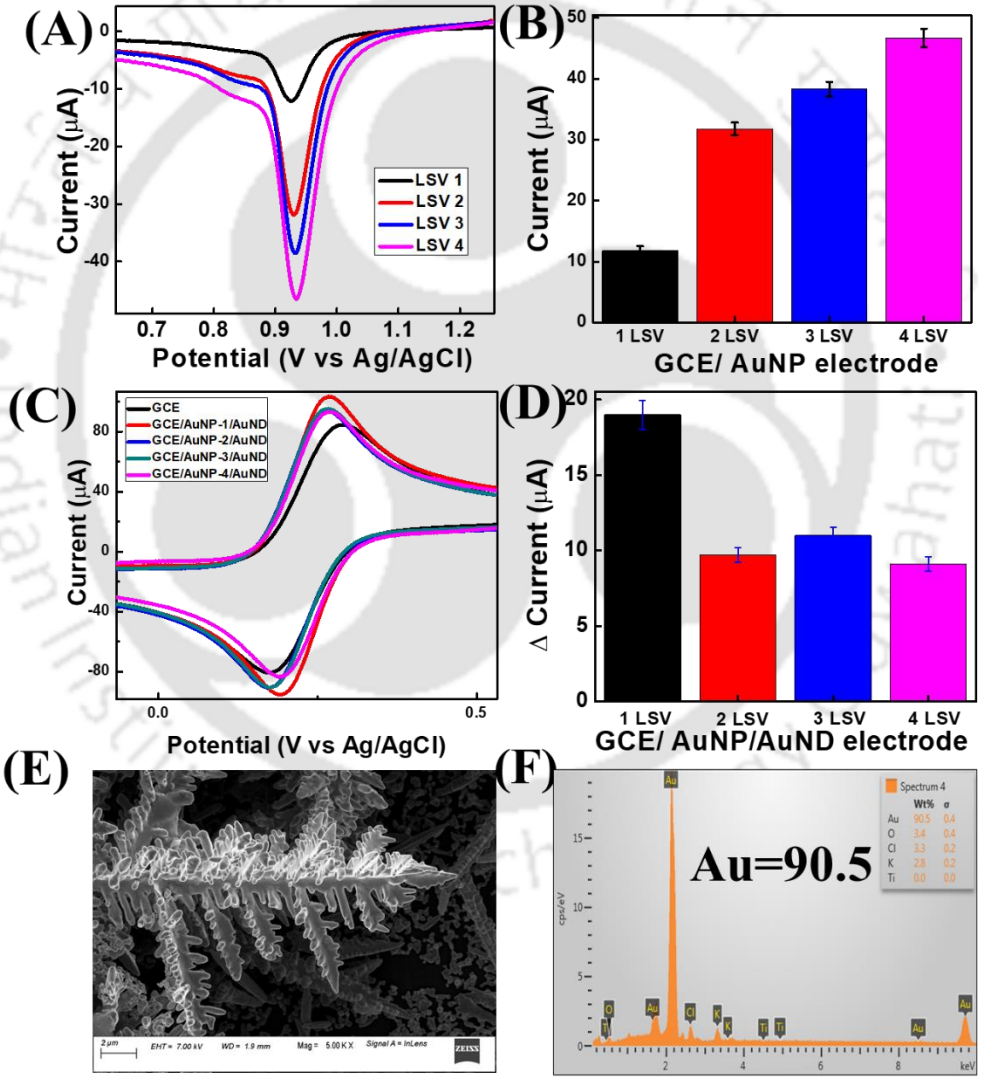

Figure 5.5. (A) LSV responses of the reduction of Au salt to form AuNP, and (B) comparative histogram of corresponding electrodes; (C) CV current responses of subsequently grown AuND over different GCE/AuNP surface, and (D) comparative

histogram of corresponding electrodes; SEM image of AuNP/AuND showing hierarchical structures (E), and EDX analysis of the same.

Electrodeposition of Au nanodendrites has been already mentioned in previous objectives, both in the presence and absence of other nanomaterials. In this objective we tried to synthesize AuND by using electrodeposited AuNP in the matrix to fasten the dendrite formation. Hence, AuNP was first electrodeposited over the GEC by LSV in an acidic solution of H_2SO_4 containing $HAuCl_4$ salt. Multiple sweep of LSV was performed to get a surface with a sufficient number of AuNP to catalyze the dendrite formation. Figure 5.5. (A-B) shows that at 4^{th} cycle, the surface shows maximum current response showing maximum AuNP formation. After AuNP formation, AuND was synthesized over the electrode surface using the same protocol as used in previous objectives. We expected the AuND formed over a surface with 4 LSV cycle would show maximum current response. However, AuND formed over the GCE with 1 LSV sweep showed maximum current response indicating highest dendrite formation. This result might be due to a moderate number of catalyzing AuNP sites over the GCE surface that leads to highest degree of dendrite formation by catalyzing the reduction of gold salts. However, when a large number of AuNP sites are available, these lead to a uniform deposition of Au all over the surface hindering dendrite formation. The SEM image of AuNP/AuND with one 1 LSV sweep shows a hierarchical arrangement (figure 5.5 (E)), with pointed edges and tips. From the SEM image, the primary branch is several m in length and wider than other secondary branches grown over it. There are smaller tertiary branches over the secondary branches giving it a fern-like appearance. We also performed the EDX analysis and found Au to be the most abundant material over the structure,

showing the dendrite is formed from Au. Further, this dendritic structure was used in combination with CS-rGO to develop the CEA immunosensor.

3.1.4. Characterization of GCE/AuNP/AuND/ CS-rGO/ Anti-CEA/CEA

The composite of CS-rGO was sonicated for several minutes prior to the preparation of a homogeneous sample for SEM and TEM analysis to physically characterize the samples. SEM (**figure 5.6.** (A)) and TEM (**figure 5.6 B**) shows a composite of sheet like rGO with the well dispersed CS all over its surface. The positively charged amino group can interact with the negatively charged carbon-based nanomaterial in a mildly acidic environment resulting in enhanced dispersity of the composite (Singh et al. 2013). The TEM analysis also confirms a well-dispersed image of CS-rGO. The CS element was also found to be porous resulting in a higher surface area. **Figure 5.6. (C),** shows the SEM micrograph of AuNP/AuND/CS-rGO, where a hierarchical dendritic material covered in CS-rGO is clearly visible. This image proves that the dendrites were still intact, even after drop-casting the CS-rGO nanocomposites, referring to the mechanical strength of the dendrite. The TEM image **(Figure 5.6. (D))** further confirms the result obtained in SEM analysis. The dendrite pattern is shown with CS-rGO. EDX analysis was performed and Au was found to be the most abundant material followed by carbon and oxygen. In the EDX analysis, a small peak of nitrogen was observed. Hence, elemental mapping imaging was performed in FETEM to confirms the presence of different characteristics elements in the same. The result as shown in **figure 5.7** corroborates with the EDX analysis. The presence of Au (yellow dots), C (green dots), N (red dots), and O (blue dots) is confirmed over its surface. SAED analysis (**figure 5.6. (F)**) shows a crystalline nature of the AuNP/AuND/CS-rGO. The dendritic composite was

electrochemically characterized to access its bioelectronics property to develop as a biosensor.

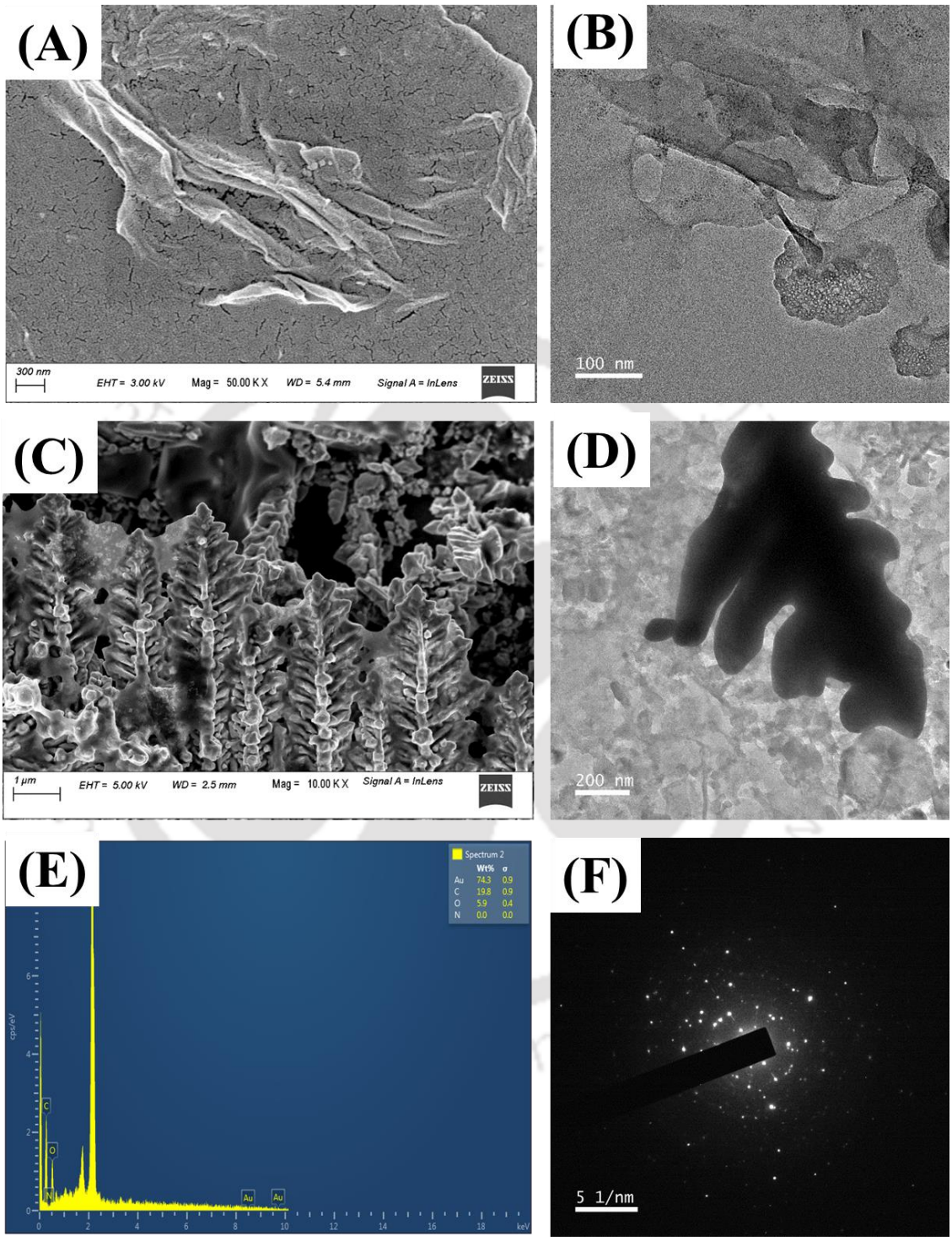

Figure 5.6. **(**A) SEM and (B) TEM of CS-rGO composite; SEM (C), (D) TEM, (E) EDX, and (F) SAED analysis of AuNP/AuND/CS-rGO.

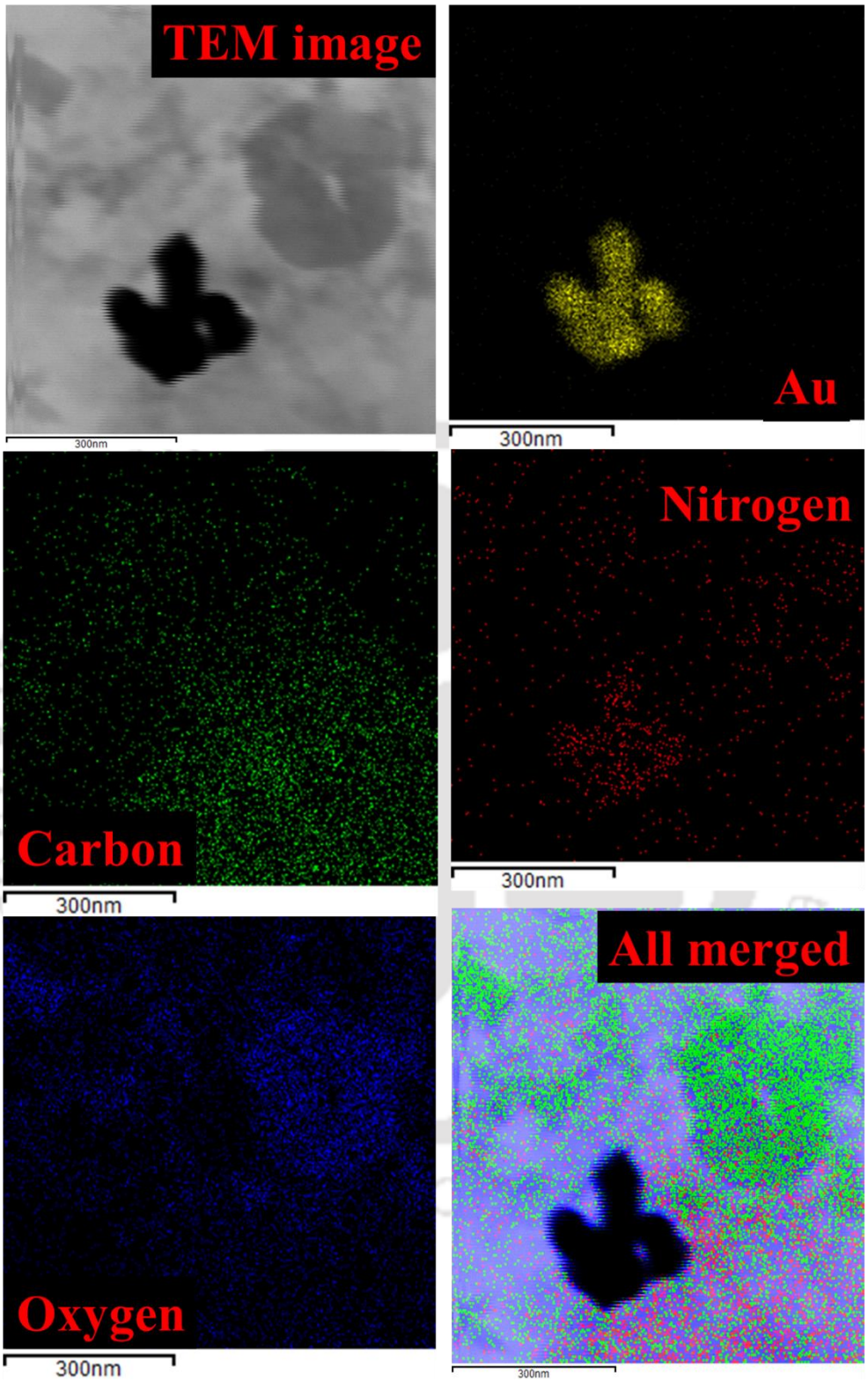

Figure 5.7. Elemental Mapping images of sonicated AuNP/AuND/CS-rGO material showing the presence of Au, C, N, O content in the material.

3.2. Electrochemical Characterization

The developed sensor probe AuND/CS-rGO was further characterized electrochemically to access its bioelectronics properties. The first characterization of the sensor involves CV analysis in 5 mM ZS as shown in **figure 5.8 (A)** with a potential range of -0.8 to 0.8V and a scan rate of 50 mV/S. The CV responses show a typical voltammogram formed due to the redox reaction of the ferro-ferri element of ZS. The CV response of AuND/CS-rGO was found to have a higher anodic and cathodic peak than the bare GCE. Further development in the sensor probe development, CS, antibody, and antigen immobilization lead to a decrease in current response due to the hindrance in charge transfer to the electrode surface. A complementary experiment to the CV responses, EIS also confirmed the data.

The GCE/AuNP/AuND/ CS-rGO/ Anti-CEA sensor surface was further characterized for its electro-catalytic behavior. The first step of electrochemical characterization is analyzing CV responses of various electrode fabrication steps of GCE, GCE/AuNP, GCE/AuNP/AuND, GCE/AuNP/AuND/ CS-rGO, GCE/AuNP/AuND/ CS-rGO/ Anti-CEA, GCE/AuNP/AuND/ CS-rGO/ Anti-CEA/CEA electrodes in 5 mM ZS prepared in PBS. For this purpose, the CV responses were recorded in the potential range between -0.2 and 0.7 V at a scan rate of 50 mV/s in ZS (**figure 5.8 A**). A characteristics patterned was obtained at bare due to the redox process of $[Fe(CN)_6]^{3-/4-}$ (black curve). CV response of GCE/AuNP (red curve), and GCE/AuNP/AuND (blue curve) shows increased anodic (Ipa) and cathodic (Ipc) peak currents as a result of deposition of conducting highly AuNP/AuND nanostructure. However, a decreased CV response obtained as expected after drop coating a layer of CS, due to non- conducting nature of CS (orange). After drop coating a composite of CS-rGO over the AuNP/AuND surface,

the current response further increased significantly (olive curve). The role of rGO is to facilitate the charge transfer between electrode surface and mediator molecule working a tunnel for charge migration. The subsequent functionalization with Anti-CEA leads to further decrease in the current response (cyan curve). The selective binding of CEA antigen over the Anti-CEA antibody leads to further decrease in the current, as it will further decrease the access of charge element to reach the electrode surface (magenta curve).

The increase in charge transfer capacity of the electrodes was evaluated quantitatively by comparing the diffusion coefficient of the bare GCE, GCE/AuND, and GCE/MWCNT-AuNPs/AuND surface using Randles-Sevcik's model (equation 1)(Verma et al. 2017; Kumar et al. 2019a).

$$I_p = \left(2.69\times10^5\right) n^{3/2} ACD^{1/2} v^{1/2} \quad \text{..... Equation 1}$$

Where Ip is the peak current (in ampere), n is the number of electrons transferred in the redox process (here n=1), A is the electrode surface area (in cm^2), C is the concentration of electroactive species (in mole cm^{-3}), D is the diffusion coefficient (in $cm^2\ s^{-1}$), and v is the scan rate (0.05 Vs^{-1}).

The diffusion coefficient (*D*) values for bare GCE, GCE/AuNP, GCE/AuNP/AuND, GCE/AuNP/AuND/ CS, GCE/AuNP/AuND/ CS-rGO, GCE/AuNP/AuND/ CS-rGO/ Anti-CEA, GCE/AuNP/AuND/ CS-rGO/ Anti-CEA/CEA electrode surfaces were found to be 3.10 x 10^{-6} cm^2 s^{-1}, 3.60 x 10^{-6} cm^2 s^{-1}, 3.83 x 10^{-6} cm^2 s^{-1}, 3.30 x 10^{-6} cm^2 s^{-1}, 3.80 x 10^{-6} cm^2 s^{-1}, 3.20 x 10^{-6} cm^2 s^{-1}, 2.97 x 10^{-6} cm^2 s^{-1}, respectively. It is interesting to note that, the maximum diffusion coefficient was observed for of GCE/AuNP/AuND surface followed by GCE/AuNP/AuND/CS-rGO. The higher D value of GCE/AuNP/AuND/CS-rGO indicates a better charge transfer rate, which is

an important requirement to develop a sensitive sensor with enhanced signal amplification (Bard et al. 1980; Kumar et al. 2019b). The role of CS in the sensing matrix is to covalent bind Anti-CEA, whereas rGO is used as a conducting material to bridge the charge transfer to get a higher signal even after using CS, a non-conducting material for its functional groups. These results clearly indicate the importance of AuND as well as CS-rGO composite in the sensing matrix.

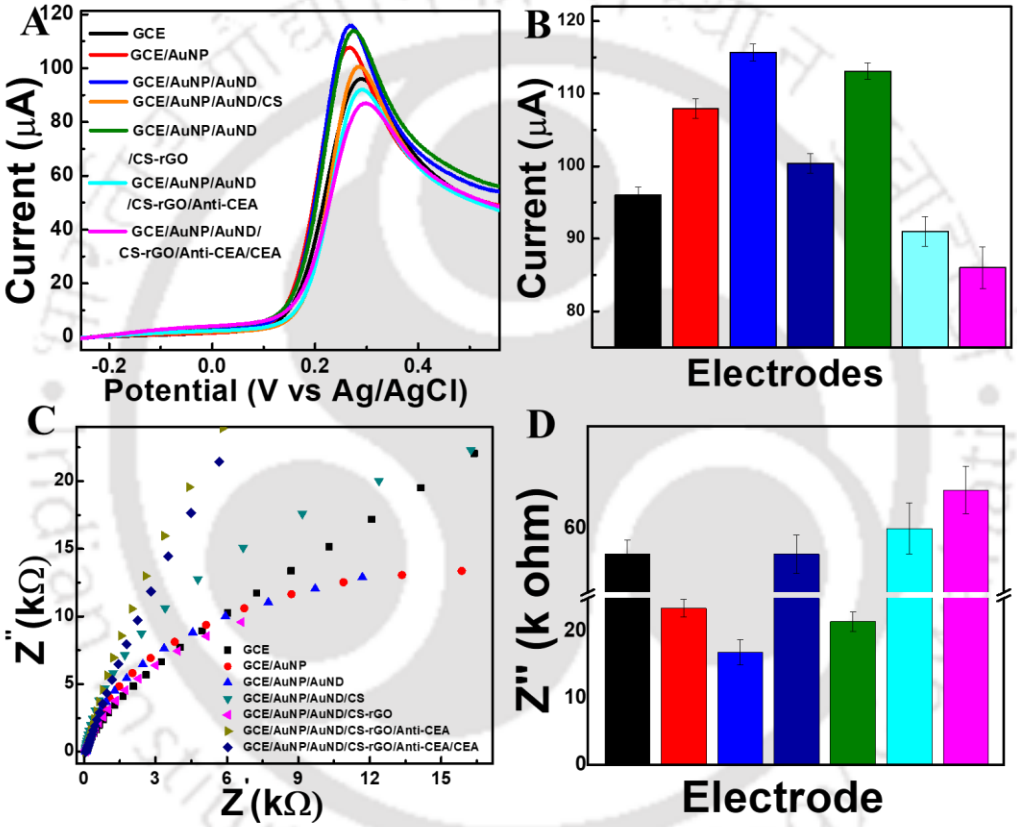

Figure 5.8. (A) CV responses of all the sensor fabrication stages in ZS. GCE (black), GCE/AuNP (red), GCE/AuNP/AuND(blue), GCE/AuNP/AuND/ CS (orange), GCE/AuNP/AuND/ CS-rGO (olive), GCE/AuNP/AuND/ CS-rGO/ Anti-CEA (cyan), GCE/AuNP/AuND/ CS-rGO/ Anti-CEA/CEA (magenta); (B) Histogram showing the comparative CV responses; (C) Nyquist plot of each step of electrode development in PBS (D) Histogram showing the comparative EIS responses.

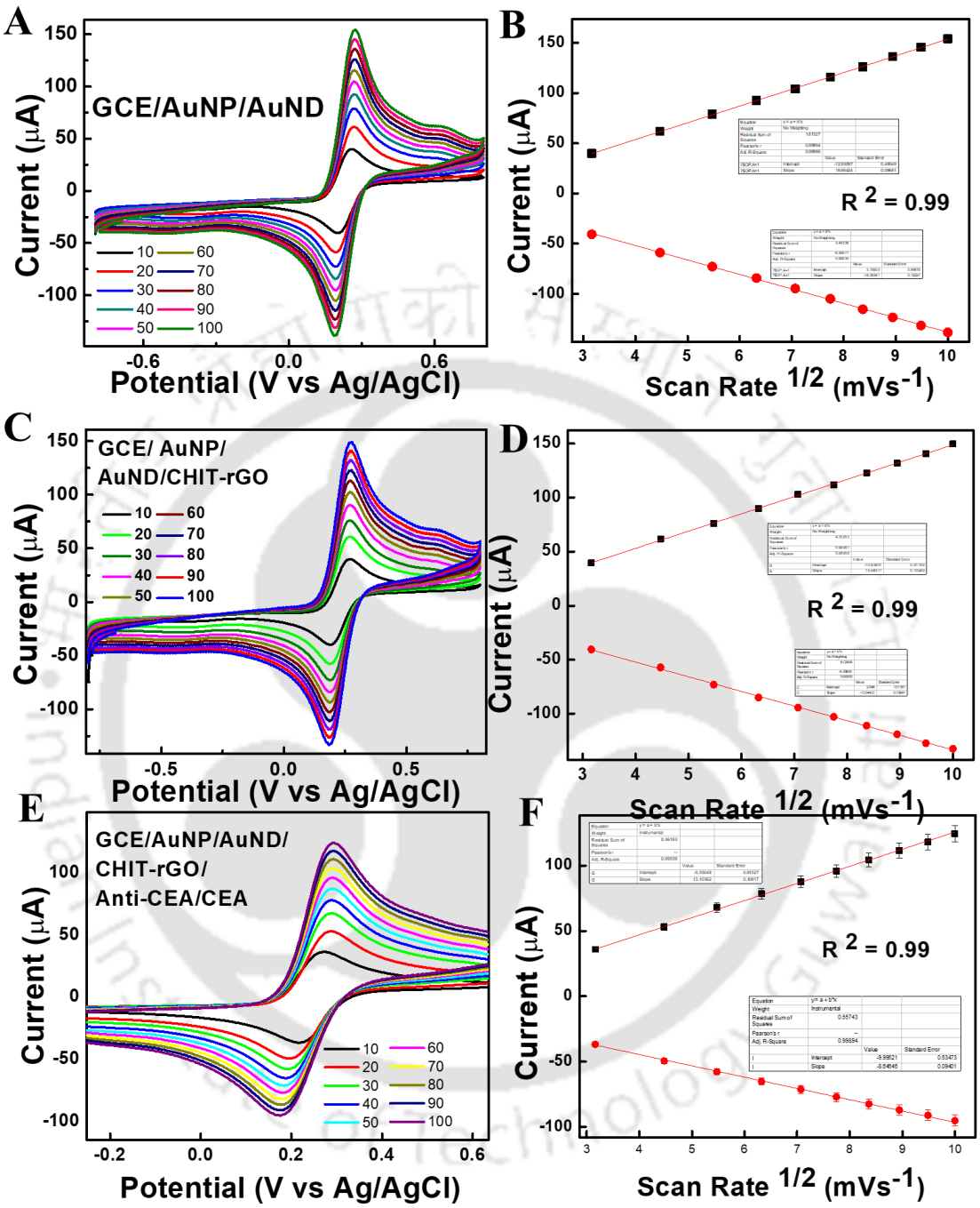

Figure 5.9. (A) CV responses of GCE/AuNP/AuND (A), GCE/AuNP/AuND/ CS-rGO (C), GCE/AuNP/AuND/ CS-rGO/ Anti-CEA (E) at different scan rate (10-100 mV/s) in ZS, and (B, D, F) shows corresponding peak currents following linearity.

A complementary experiment to CV, EIS was performed to measure the charge transfer kinetics by monitoring the change in the Nyquist plot **(figure 5.8 (C**). The Rct values were calculated based on the Nyquist plot and plotted as a comparative histogram in **figure 5.8 (D)**. The EIS data corroborates with the CV responses validating that the GCE/AuNP/AuND has the least Rct followed by GCE/AuNP/AuND/ CS-rGO. The functionalized surface possess a high charge transfer due to the presence of rGO in the matrix. The EIS data corroborates with the CV result indicating the GCE/AuNP/AuND/ CS-rGO as an efficient surface for biosensing applications.

Further, CV responses were recorded at the scan rate between10 and 100 mV/s^{-1} in 5 mM ZS to evaluate the stability of the different stage of sensor probe development. The peak currents in scan rate of all electrode fabrication step found to increase with an increased scan rate. Also, the peak currents found to be directly proportional to the square root of the scan rate indicating a diffusion-controlled reaction, with the correlation coefficient of 0.99. This shows higher stability as well as diffusion-controlled charge transfer process at the electrode surface. The regression equations for Ipa and Ipc for GCE/AuNP/AuND/expressed as follows **figure 5.9 (E-F)**.

Ipa = [13.10 µA (s mV^{-1}) (± 0.108) x scan rate (mVs^{-1})] – 5.35 (± 0.615) µA,

R^2 = 0.999 ……**Equation 2**

Ipc = [-8.64 µA (s mV^{-1}) (± 0.094) x scan rate (mVs^{-1})] – 9.99 (± 0.534) µA,

R^2 = 0.999 ……. **Equation 3**

3.3. Analytical performance of the developed sensor

The analytical performance of the GCE/AuND/CS-rGO/Anti-CEA surface was evaluated for immunosensing of CEA in 5mM ZS. DPV responses of final composite sensor surface without CEA was recorded by sweeping the potential between 0 – 0.4 V in ZS (black curve in **figure 5.10 A**), where a characteristic peak was observed as expected due to the presence of ferro-ferri elements. This response is considered as a blank response for other responses with CEA. Then a concentration-dependent DPV was recorded with the same experimental set up in the presence of 1 x 10^{-13} g/mL of CEA. In the presence of CEA, however, a decrease in the current response was found (red curve). Further increasing the CEA concentration to 1 x 10^{-12} g/mL, the value of peak current decreased more. When tried to detect the highest amount of CEA that can be monitored, we found that the peak current got saturated at 1 x 10^{-8} g/mL of CEA. The DPV responses are inversely proportional with the CEA concentration used. The decrease in the current value was plotted as a function of the concentration of CEA using equation 4. ΔI value was calculated to remove the differences between the electrodes and minimize the effect of errors in electrode fabrications.

$$\Delta I = I_i - I_O \quad \text{……Equation 4}$$

Where, I_i is the DPV current response obtained in blank electrode, and I_O is the DPV current response obtained in presence of CEA.

The linear regression equation of CEA sensing based on the calibration curve is expressed as follows:

$$\Delta I\ (A) = (-67.08)\ (\pm\ 2.306)\ x\ 10^{-6} + (-4.46)\ (\pm\ 0.083)\ x\ 10^{-4}\ Conc.\ [CEA\ (g\ ml^{-1})]$$

…. **Equation 5**

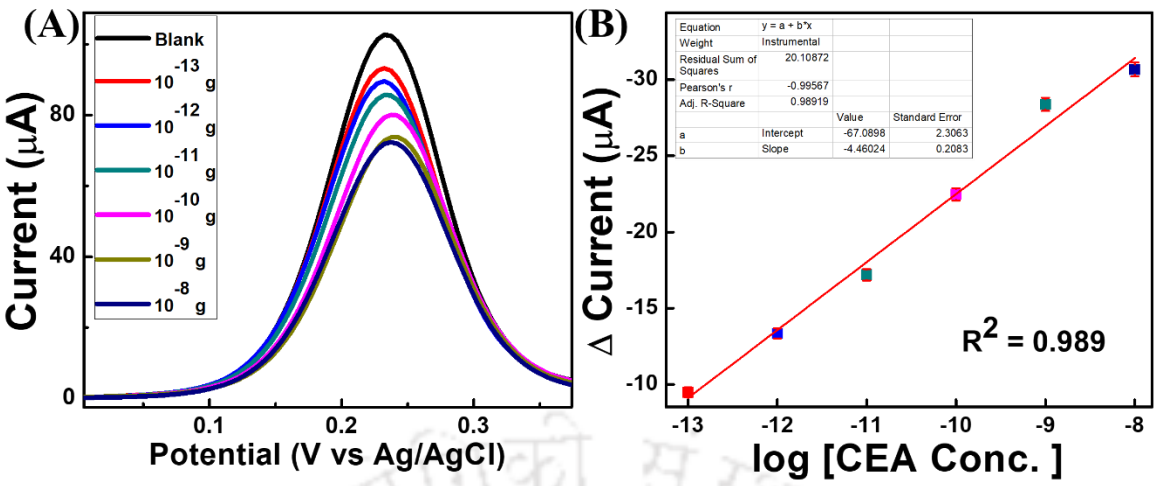

Figure 5.10. (A) shows the dose dependent DPV responses of the nanocomposite electrode in ZS, where an increase in the CEA concentration (g mL^{-1}) leads to a decrease in current responses. The developed calibration plot (B) of CEA.

The peak value was found to linearly decrease with a coefficient value of 0.989. The LOD value was calculated as 2.3 (±0.03) x 10^{-14} g mL^{-1} using **equation 6** (Mahato et al. 2019; Purohit et al. 2019b).

$$LOD = \frac{3SD_B}{Slope} = \frac{3SD_B}{\frac{dy}{dx}} = \frac{3SD_B}{\frac{dy}{d\ln x} \times \frac{d\ln x}{dx}} = \frac{3SD_B}{\frac{dy}{2.303(d\log x)} \times \frac{1}{x}}$$

…equation 6.

$$= \frac{3(2.303)SD_B x}{\frac{dy}{(d\log x)}} = \frac{3(2.303)SD_B x}{\text{slope of the semilog plot}}$$

Where, SD_B is standard deviation of blank; x is the limit of quantification or lowest concentration measured.

This is worth mentioning that this bio-nano hybrid probe possesses a very wide dynamic range, hence it can be directly used in diverse types of cancers or cancer relapse study, where CEA concentration varies greatly. It is also important to note that our nanoprobe possesses simple fabrication steps even though it offers an unprecedented LOD and a wide LDR. This clearly indicates the promise of the

developed GCE/AuNP/AuND/CS-rGO/Anti-CEA for robust and sensitive CEA detection in clinically relevant ranges in diverse real sample matrices. Importantly, the LDR and LOD in this work are significantly wider and lower, respectively compared to the most of the previously reported CEA sensors. A detailed account of the comparative analytical performances of some previously reported sensors is shown in **Table 5**.1.

3.4. Selectivity assays

The selectivity of a sensor towards the analyte in the presence of various possible interfering molecules is very important for its commercial possibilities (Kumar et al. 2019b, c). A wide range of commonly co-existing molecules in serum viz. glucose, glycine, glutamine, cysteine, citric acid, uric acid, ascorbic acid, and serum albumin were selected for interference analysis in separate experiments, and their effect on the signal generation was studied. A lung cancer biomarker, cyfra-21 was also selected to check the selectivity of the sensor. All the potentially interfering molecules were tested at a higher concentration (1 Mm of salts) than usually they are found in body fluids. **Figure 5.11** shows a comparative DPV responses of the final probe in the presence of the interfering molecules, where negligible or no current deviation was observed for these molecules. The selectivity of the final probe is estimated mathematically calculated. As the deviation in current due to interfering molecules are very less, the k_{sel} value for all the interfering molecules were found to be negligible (K_{sel} <<1), reflecting high selectivity of the final sensor probe towards CEA. The high selectivity of the final .

SI. NO.	PROBE DESIGN	LDR	LOD	REAL SAMPLE	REFERENCES
1.	AuNPs@γ-Fe2O3/Pb/Anti-CEA	25-600 ng/mL	4.31 ng/mL	Human serum sample	(Buyrac et al. 2017)
2	GCE/MoS_2-PBNCs/Anti-CEA	0.005-10 ng/mL	0.54 pg/mL	Human serum sample	(Su et al. 2017)
3.	GCE/Au@PDA/Anti-CEA and Au@PtDNs/NG/Cu+-Anti-CEA	0.5-50 ng/mL	0.167 pg/mL	Human serum sample	(Lv et al. 2018a)
4.	ITO/erGO/AuNP-P5Fln/Anti-CEA	0.0005-50 ng/mL	0.14 pg/mL	Human serum sample	(Liu et al. 2019)
5.	GCE/rGO-AuNPs/Anti-CEA and Anti-CEA/SWCNTs-GQPs	0.05-0.65 ng/mL	5.3 pg/mL	Human serum sample	(Luo et al. 2018)
6.	GCE/AuAg/3D-rGO-MWCNT	0.001-80 ng/mL	3 pg/mL	Human serum sample	(Yang et al. 2019a)
7.	Pt-PANI-AuNS-GQPs/Anti-CEA	0.5-1000 ng/mL	0.01 ng/mL	Human serum sample	(Ganganboina and Doong 2019)
8.	GCE/rGO-PDA/AuAg/Anti-CEA	0.001-80 ng/mL	0.286 ng/mL	Human serum sample	(Yang et al. 2019b)
9.	GCE/AuNPs/Anti-CEA	0.001-80 ng/mL	0.33 pg/mL	Human serum sample	(Ma et al. 2019a)
10.	GCE/AuNP/AuND/CS-rGO/Anti-CEA	0.1 pg-10 ng/mL	0.002 pg/mL	Human serum sample	This work

Table 5. A comparison of the analytical performance of the AuNP/AuND/CS-rGO/Anti-CEA sensor with recently reported CEA sensors.

GCE/AuNP/AuND/CS-rGO/Anti-CEA surface towards CEA molecules is due to the highly specific immune-complexation between CEA and Anti-CEA, where other non-specific protein molecules can't bind. The statistical significance of the obtained result was calculated by the t-test, and the p-value was found to be negligible (<<0.001, n=3).

In real samples, CEA co-exists with the interfering molecules, hence mixed sample analysis is worthy to be investigated. For this purpose, all the interfering molecules along with CEA were prepared as a mixed sample, and data were collected. It is interesting to note that the final probe was capable of detecting CEA with more than 94% compared to the standard conditions. This result clearly shows the excellent capacity of the GCE/AuNP/AuND/CS-rGO/Anti-CEA sensor probe to detect CEA in complex biological fluids.

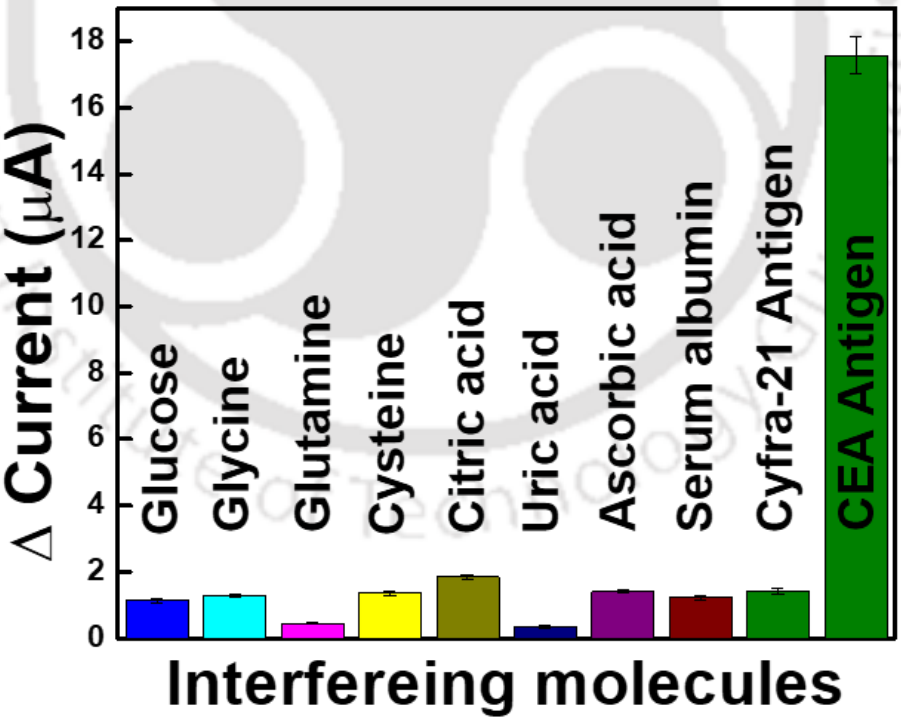

Figure 5.11. A comparative histogram shows the DPV responses in the presence of interfering molecules, where negligible current deviations were observed for other protein and coexisting molecules as compared to the response of CEA.

3.5. Real sample analysis

CEA is an important biomarker found in blood serum at a range of several ng ml^{-1} based on the severity of various diseases. Several previous reports also attempted to detect CEA in urine samples due the clinical rationale (Lv et al. 2018; Ma et al. 2019; Zhang et al. 2019). Therefore, we selected serum as a model biological fluid matrix to analyze the practical applicability of our sensor to detect different concentrations of CEA concentration in clinical settings. The serum sample was first equilibrated to facilitate the charge flow during the electrochemical studies (10:1 in PBS). Different concentrations of CEA than spiked into the equilibrated serum sample and drop cast over the developed final probe and the DPV responses were recorded following the same protocol mentioned earlier. The DPV responses at different concentrations of CEA spiked in the real sample were compared with the standard conditions, as shown in **figure 5.12**. The recoveries of CEA in the real sample at each concentration has been calculated and found between 94 and 96% of original calibration plot, showing the clinical potential of the developed sensor probe. The % recoveries of CEA concentrations in the real samples were calculated using equation 8.

$$\% \text{ Recovery} = [S]_{CEA} - [B]_{CEA} / [SS]_{CEA} \quad \text{……. } \textbf{Equation 8}$$

Where, $[S]_{CEA}$ and $[B]_{CEA}$ are the analytical responses of AP in the spiked and blank serum samples, respectively; and $[SS]_{CEA}$ is the analytical response of CEA in the standard buffer solutions.

We found variation in the peak current to be statistically negligible ($p < 0.001$). The changes in current response might be due to the hindrance in charge migration in the thick real sample matrices or handling errors.

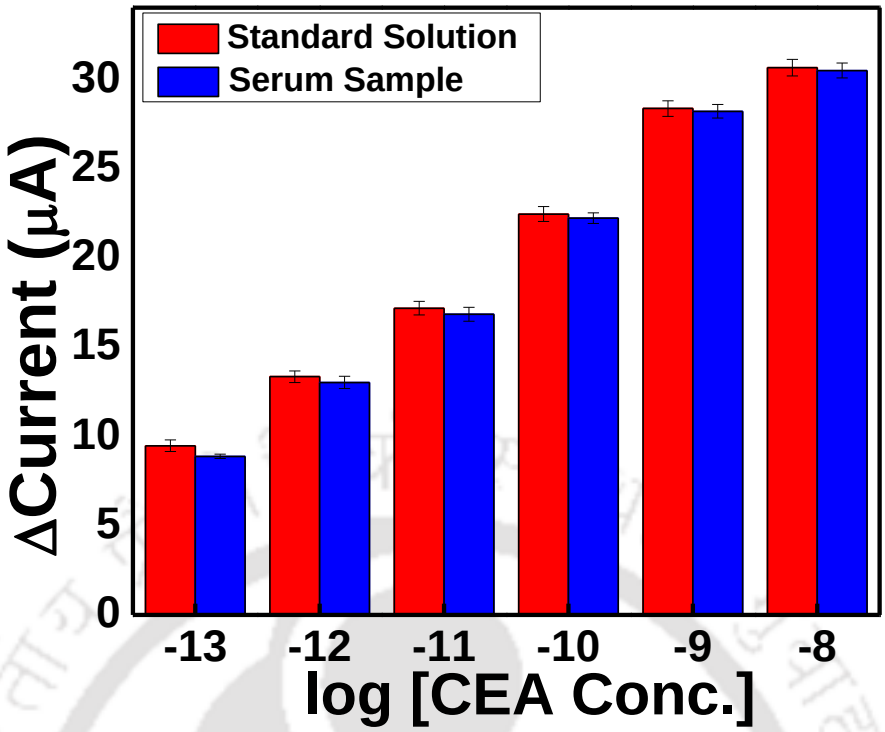

Figure 5.12. Real sample analysis shows a very high % recovery of CEA in the serum sample.

3.6. Stability and Reproducibility assay

The commercial and clinical perspective of an immunosensor largely depends on its reproducibility and stability to sense analyte in clinical samples (Mahato et al. 2018). We checked the reproducibility of the DPV responses at five different GCE/AuNP/AuND/CS-rGO/Anti-CEA surfaces in sample solution containing the same concentration of CEA. The variation in DPV responses was found to be negligible in all case indicating high electrode to electrode reproducibility. The high reproducibility of the sensor surface might be due to two factors, (i) high selectivity of the sensor for CEA due to Anti-CEA in the sensor matrix, and (ii) the stability and conductivity of the dendritic sensor matrix. The variations may be most likely due to minor handling error or fluctuation in other experimental conditions.

To check the long term stability of the GCE/AuNP/AuND/CS-rGO/Anti-CEA sensor probe, the electrodes were stored at -4 ˚C, and DPV responses were recorded for 6 weeks, periodically taking measurements twice a week. The retention of signal was found to be <90 %, which shows that the sensor system was stable for sensing applications for 6 weeks (RSD 4.7%, n= 3). This shows that the antibody immobilized over the sensor surface is intact for 6 weeks, after which there might be some degradation of the sensor matrix happening. High reproducibility and stability of the fabricated nanoprobe signify its commercial potential.

6.4. Conclusion

A novel GCE/ AuNP/ AuND/ CS- / Anti-CEA immunosensor for the detection of CEA was developed by using a composite of CS and rGO as the sensing matrix and the ZS element to monitor the concentration of the protein. CS was isolated from locally available shrimp shell and thoroughly characterized prior to use in sensor fabrications. The rGO element are used as a strategy for signal amplification for enhancing the current response even in the presence of a layer of insulating molecules. The sensor surface was thoroughly characterized using SEM, EDX, TEM, and various electrochemical methods like CV, EIS, and DPV. The sensor was found to detect CEA by forming immune complexation with Anti-CEA antibody. The sensor was able to detect CEA in the range of 1×10^{-13} - 1×10^{-7} ng with a LOD of 2.3 (±0.03) $\times 10^{-14}$ g mL^{-1}. The sensor was highly selective towards CEA, when tested in the presence of high concentration of interfering molecules commonly found in biological samples. To evaluate its clinical possibilities, real sample analysis was performed by spiking different concentrations of CEA to equilibrated serum sample, where >90% recovery of CEA was obtained. The sensor was found to be highly stable for 6 weeks showing the retention of structural and functional

features by the Anti-CEA antibody to capture CEA selectively. To the best of our knowledge, this is the first report to use dendritic electrode incorporation with a CS element to develop a immunosensor. The sensor follows an easy fabrication process, and can be applied for rapid, label free, and low cost sensing. This system can be used for immunosensing of other important biological molecules by optimizing and using other biorecognition molecules in serum or other biological fluids in clinical settings.

References:

Afkhami A, Hashemi P, Bagheri H, et al (2017) Impedimetric immunosensor for the label-free and direct detection of botulinum neurotoxin serotype A using Au nanoparticles/graphene-chitosan composite. Biosens Bioelectron 93:124–131.

Baranwal A, Kumar A, Priyadharshini A, et al (2018) Chitosan: An undisputed bio-fabrication material for tissue engineering and bio-sensing applications. Int J Biol Macromol 110:110–123.

Bard AJ, Faulkner LR, Leddy J, Zoski CG (1980) Electrochemical methods: fundamentals and applications. wiley New York

Beard DB, Haskell CM (1986) Carcinoembryonic antigen in breast cancer. Clinical review. Am J Med 80:241–245

Beauchemin N, Draber P, Dveksler G, et al (1999) Redefined nomenclature for members of the carcinoembryonic antigen family. Exp Cell Res 252:243

Benchimol S, Fuks A, Jothy S, et al (1989) Carcinoembryonic antigen, a human tumor marker, functions as an intercellular adhesion molecule. Cell 57:327–334

Berinstein NL (2002) Carcinoembryonic antigen as a target for therapeutic anticancer vaccines: a review. J Clin Oncol 20:2197–2207

Cho IH, Lee J, Kim J, et al (2018) Current technologies of electrochemical immunosensors: Perspective on signal amplification. Sensors (Switzerland) 18:1–18.

Goonetilleke KS, Siriwardena AK (2007) Systematic review of carbohydrate antigen (CA 19-9) as a biochemical marker in the diagnosis of pancreatic cancer. Eur J Surg Oncol 33:266–270

Gu P, Huang G, Chen Y, et al (2007) Diagnostic utility of pleural fluid carcinoembryonic antigen and CYFRA 21-1 in patients with pleural effusion: a systematic review and meta-analysis. J Clin Lab Anal 21:398–405

Gu X, She Z, Ma T, et al (2018) Electrochemical detection of carcinoembryonic antigen. Biosens Bioelectron 102:610–616

Hasanzadeh M, Shadjou N (2017) Advanced nanomaterials for use in electrochemical and optical immunoassays of carcinoembryonic antigen. A review. Microchim Acta 184:389–414.

He Y, Tian J, Hu K, et al (2013) An ultrasensitive quantum dots fluorescent polarization immunoassay based on the antibody modified Au nanoparticles amplifying for the detection of adenosine triphosphate. Anal Chim Acta 802:67–73

Kim D, Daniel WL, Mirkin CA (2009) Microarray-based multiplexed scanometric immunoassay for protein cancer markers using gold nanoparticle probes. Anal Chem 81:9183–9187

Kokkinos C, Economou A, Prodromidis MI (2016) Electrochemical immunosensors: Critical survey of different architectures and transduction strategies. TrAC - Trends Anal Chem 79:88–105.

Kumar A, Purohit B, Mahato K, et al (2019a) Gold-Iron Bimetallic Nanoparticles Impregnated Reduced Graphene Oxide Based Nanosensor for Label-Free Detection of Biomarker Related to Non-Alcoholic Fatty Liver Disease. Electroanalysis

Kumar A, Purohit B, Maurya PK, et al (2019b) Engineered Nanomaterial Assisted Signal-amplification Strategies for Enhancing Analytical Performance of Electrochemical Biosensors. Electroanalysis 31:1615–1629.

Kumar A, Purohit B, Maurya PK, et al (2019c) Engineered Nanomaterial Assisted Signal-amplification Strategies for Enhancing Analytical Performance of

Electrochemical Biosensors. Electroanalysis 31:1615–1629.

Lee M, Lee S, Lee J, et al (2011) Highly reproducible immunoassay of cancer markers on a gold-patterned microarray chip using surface-enhanced Raman scattering imaging. Biosens Bioelectron 26:2135–2141

Lv H, Li Y, Zhang X, et al (2018) Enhanced peroxidase-like properties of Au@Pt DNs/NG/Cu2+ and application of sandwich-type electrochemical immunosensor for highly sensitive detection of CEA. Biosens Bioelectron 112:1–7.

Ma E, Wang P, Yang Q, et al (2019) Electrochemical immunosensor based on MoS2 NFs/Au@AgPt YNCs as signal amplification label for sensitive detection of CEA. Biosens Bioelectron 142:111580.

Mahato K, Maurya PK, Chandra P (2018) Fundamentals and commercial aspects of nanobiosensors in point-of-care clinical diagnostics. 3 Biotech 8:1–14.

Mahato K, Purohit B, Bhardwaj K, et al (2019) Novel electrochemical biosensor for serotonin detection based on gold nanorattles decorated reduced graphene oxide in biological fluids and in vitro model. Biosens Bioelectron 142:111502.

Mahato K, Purohit B, Kumar A, Chandra P (2020) Clinically comparable impedimetric immunosensor for serum alkaline phosphatase detection based on electrochemically engineered Au-nano-Dendroids and graphene oxide nanocomposite. Biosens Bioelectron 148:111815.

Molina R, Zanón G, Filella X, et al (1995) Use of serial carcinoembryonic antigen and CA 15.3 assays in detecting relapses in breast cancer patients. Breast Cancer Res Treat 36:41–48

Ohkawa K, Cha D, Kim H, et al (2004) Electrospinning of chitosan. Macromol Rapid Commun 25:1600–1605

Purohit B, Kumar A, Mahato K, Chandra P (2019a) Novel sensing assembly comprising engineered gold dendrites and MWCNT-AuNPs nanohybrid for acetaminophen detection in human urine. Electroanalysis elan.201900551.

Purohit B, Mahato K, Kumar A, Chandra P (2019b) Sputtering enhanced peroxidase like activity of a dendritic nanochip for amperometric determination of hydrogen peroxide in blood samples. Microchim Acta 186:658.

Reynoso G, Chu TM, Holyoke D, et al (1972) Carcinoembryonic antigen in patients with different cancers. Jama 220:361–365

Rinaudo M (2006) Chitin and chitosan: properties and applications. Prog Polym Sci 31:603–632

Sculier JP, Feld R, Evans WK, et al (1985) Carcinoembryonic antigen: a useful prognostic marker in small-cell lung cancer. J Clin Oncol 3:1349–1354

Singh A, Sinsinbar G, Choudhary M, et al (2013) Graphene oxide-chitosan nanocomposite based electrochemical DNA biosensor for detection of typhoid. Sensors Actuators B Chem 185:675–684

Suginta W, Khunkaewla P, Schulte A (2013) Electrochemical biosensor applications of polysaccharides chitin and chitosan. Chem Rev 113:5458–5479.

Verma S, Singh A, Shukla A, et al (2017) Anti-IL8/AuNPs-rGO/ITO as an Immunosensing Platform for Noninvasive Electrochemical Detection of Oral Cancer. ACS Appl Mater Interfaces 9:27462–27474.

Wang J, Chen F, Jin Y, Johnston RL (2016) Highly active and stable AuNi dendrites as an electrocatalyst for the oxygen reduction reaction in alkaline media. J Mater Chem A 4:17828–17837.

Wilson MS (2005) Electrochemical immunosensors for the simultaneous detection of two tumor markers. Anal Chem 77:1496–1502.

Yi H, Wu L-Q, Bentley WE, et al (2005) Biofabrication with chitosan. Biomacromolecules 6:2881–2894

Zhang C, Zhang S, Jia Y, et al (2019) Sandwich-type electrochemical immunosensor for sensitive detection of CEA based on the enhanced effects of Ag NPs@CS spaced Hemin/rGO. Biosens Bioelectron 126:785–791.

Zhao M, Li H, Liu W, et al (2016) Plasma treatment of paper for protein immobilization on paper-based chemiluminescence immunodevice. Biosens Bioelectron 79:581–588

Chapter # VI

Summary and Future Work

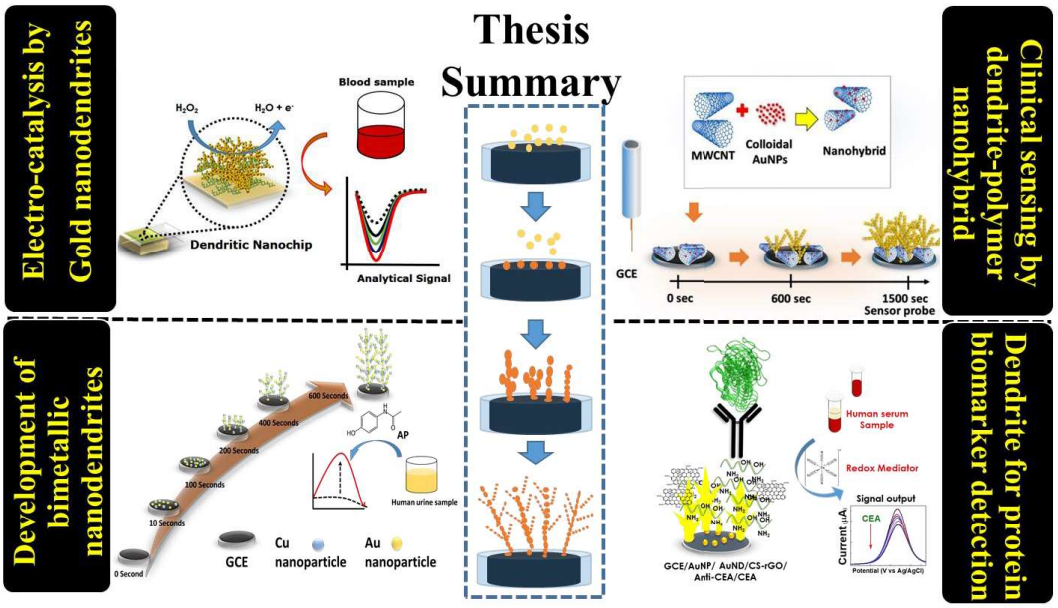

1. Summary

The thesis includes various ultrasensitive biosensing matrix development using metallic dendrites and their composites. Both direct-electron-transfer based biosensors and immunosensors development have been discussed based on the material property of dendrites. In chapter II, we have described the development of a hydrogen peroxide biosensor by using a gold dendritic nanochip after sputtered for electron microscopy imaging. The sensor chip used in the study was initially meant to throw away, making the sensor chip to be an example of making cash from the trash. This is also the first instance, where sputtering is used to enhance the peroxidase activity of a dendritic sensor chip. The nanochip showed two wider linear dynamic ranges of 10^{-12} M to 10^{-10} M and 10^{-10} M to10^{-5} M, and a limit of detection (LOD) of 9.8 (±0.02) x 10^{-13} M, which is the lowest LOD reported, to the best of our knowledge. The nanochip also had a very quick response time of ≤ 1.0 sec.

In chapter III, we have developed a bimetallic AuCu dendritic electrode for an enhanced material property than monometallic dendrite for the sensitive electrochemical detection of common drug acetaminophen in the urine sample, which over dosage is associated with various liver dysfunction. To the best of our knowledge, this is the first report of using AuCu bimetallic dendrite for biosensing activity. The sensor probe was synthesized electrochemically with minimum chemicals utilized and characterized by using various physical and electrochemical techniques. The sensor showed a wide dynamic range of a linear dynamic range of 100 – 1000 nM, with a low limit of detection of 8.5 (±0.03) nM. The stability of the sensor was found to be eight weeks. The sensor showed high selectivity towards acetaminophen when tested with a mixture of other potential interfering molecules co-existing in biological samples.

In chapter IV, we have designed the sensor surface by incorporating a multi-walled carbon-nanotube-gold nanoparticle nanohybrid with gold nanodendrite for ultrasensitive detection of acetaminophen. The nanobiosensor matrix was characterized extensively by various physical as well as electrochemical methods. The sensor matrix was utilized further for acetaminophen sensing. The probe showed excellent analytical performances with a wide linear range of 100 to 7500nM, and a low limit of detection (LOD) of 2.12 (±0.03) nM. The sensor probe showed good selectivity towards acetaminophen and exhibited negligible response towards interfering molecules commonly co-existing in biological samples. The sensor was tested in urine samples and found to recover more than 92 % of acetaminophen when spiked. The nanohybrid-dendritic electrode was found to be stable for eight weeks.

In chapter V, we developed a novel immunosensor for the detection of carcinoembryonic antigen using chitosan-reduced graphene oxide nanocomposite coated on to the Au-nanodendrites deposited over the glassy carbon electrode surface. For the first time, the growth of Au nanodendrite over the AuNP modified GCE electrode was studied and optimized for an enhanced electro-conductive property. A nanocomposite of chitosan and rGO was used for the selective immobilization of antibody, and signal amplification, respectively. The linear dynamic range for CEA detection was found to be of 1 x 10^{-12} g to 3 x 10^{-8} g mL^{-1}, which covers the CEA concentration in both healthy and diseased individuals. The limit of detection was obtained to be of 2.3 (±0.03) x 10^{-14} g mL^{-1}. The nanobiosensor was found to recover >90% of spiked CEA concentration in human blood serum. The sensor was found to be highly selective towards CEA, capable of detecting the antigen in the presence of a high concentration of co-existing molecules in real samples.

2. Future works:

The future works that may be extended to:

- The larger active surface area of dendrites may be utilized to develop miniaturized biosensors prototypes.
- The work in this thesis may lead to microelectrodes development for various biosensing purposes.
- The excellent catalysis of dendrites may further be used for the multipole analyte sensing by direct electron transfer methods, and may also be used for other catalysis activity other than biosensing.
- The method explained in objective one may be incorporated in other sensing assemblies to develop their hydrogen peroxidase activity.
- The extension of two works on urine analysis may be further developed to detect a wide range of analytes in clinical settings.
- The work done in objective 4 may be extended for the development of other immunosensors by incorporating other antibody-antigen in the sensing assembly.

Annexure

Annexure I

List of publications from thesis and associated works

1. **Buddhadev Purohit**; Kuldeep Mahato; Ashutosh Kumar; and Pranjal Chandra*. Sputtering assisted enhanced peroxidase like activity of a repurposed dendritic nanochip for label-free hydrogen peroxide detection in blood sample, *Microchimica Acta, springer Vienna*, (2019), 186, 9, 658**.**
2. **Buddhadev Purohit**; Ashutosh Kumar; Kuldeep Mahato; and Pranjal Chandra*. Novel layered sensing assembly comprising engineered gold dendrites and MWCNT-AuNPs nanohybrid for ultrafast detection of a biomarker related to hepatotoxicity, *Electroanalysis*, *Willey*, (2019).
3. **Buddhadev Purohit**; Ashutosh Kumar; Kuldeep Mahato; and Pranjal Chandra*. Smartphone assisted personalized diagnostics devices and wearable sensors, *Current Opinion in Biomedical Engineering*, *Elsevier*, (2020) 13, 42–50.
4. **Buddhadev Purohit**; Ashutosh Kumar; Kuldeep Mahato; Sharmili Roy; and Pranjal Chandra***.** Cancer Cytosensing Approaches in Miniaturized Settings Based on Advanced Nanomaterials and Biosensors, Nanotechnology in Modern Animal Biotechnology: Concepts and Applications, *Elsevier Philadelphia*, (2019), pp.133-147.
5. **Buddhadev Purohit**; Ashutosh Kumar; and Pranjal Chandra*. Electrodeposition of metallic nanostructures for biosensing applications in health care, *Journal of Scientific Research* (2020), (*Accepted, In press*)
6. **Buddhadev Purohit**; Kuldeep Mahato; Ashutosh Kumar; and Pranjal Chandra*. Repurposing of waste: developing sensors from laboratory waste materials, *Asia Pacific Biotech News* (2019), 21,12.

7. **Buddhadev Purohit**; Ashutosh Kumar; Kuldeep Mahato; and Pranjal Chandra*. Fabrication of a bimetallic nanostructured electrode for drug monitoring in human urine. (Manuscript under preparation)
8. **Buddhadev Purohit**; Ashutosh Kumar; Kuldeep Mahato; and Pranjal Chandra*. Development of a cancer biosensor using a nanocomposite of metallic nanostructures and biocompatible nanomaterials. (Manuscript under preparation)
9. **Buddhadev Purohit**; Ashutosh Kumar; Kuldeep Mahato; and Pranjal Chandra*. Development of a metallic nanodendritic assisted immunoassay to detect cancer biomarkers (Manuscript under preparation)
10. Kuldeep Mahato, **Buddhadev Purohit**, Keshav Bhardwaj, Amit Jaiswal, Pranjal Chandra*. Novel electrochemical biosensor for serotonin detection based on gold nanorattles decorated reduced graphene oxide in biological fluids and in vitro model, *Biosensors and Bioelectronics*, Elsevier, (2019), 142, 111502.
11. Kuldeep Mahato, **Buddhadev Purohit**, Ashutosh Kumar, Pranjal Chandra*. Clinically comparable impedimetric immunosensor for serum alkaline phosphatase detection based on electrochemically engineered Au-nano-Dendroids and graphene oxide nanocomposite, *Biosensors and Bioelectronics*, Elsevier. (2019), 148, 111815.
12. Ashutosh Kumar, **Buddhadev Purohit**, Pawan Kumar Maurya, Lalit M. Pandey, Pranjal Chandra*. Engineered nanomaterial assisted signal-amplification strategies towards analytical performance of biosensor. *Electroanalysis*, Wiley, (2019), 31, 9, 1615-1629
13. Ashutosh Kumar, **Buddhadev Purohit**, Kuldeep Mahato, Sharmili Roy, Pranjal Chandra*. Electrochemically nano-tuned gold nanoparticles impregnated

solvothermally reduced graphene oxide nanocomposite for efficient sensing of sinapic acid in unprocessed urine, Electroanalysis, Willey, (2019), 31, 1-12.

14. Ashutosh Kumar, **Buddhadev Purohit**, Kuldeep Mahato, Riddhipratim Mandal, Ananya Srivastava, Pranjal Chandra*. Gold iron bimetallic nanoparticles impregnated reduced graphene oxide based label-free nanosensor for acetaminophen detection in unprocessed human urine, Electroanalysis, Willey, (2019), 31, 1-13.

15. Ashutosh Kumar, Sharmili Roy, Ananya Srivastava, Mastan M Naikwade, **Buddhadev Purohit**, Kuldeep Mahato, VGM Naidu, Pranjal Chandra*. Nanotherapeutics: a novel and powerful approach in modern healthcare system. Nanotechnology in modern animal biotechnology: Concepts and applications, Elsevier Philadelphia, (2019), (pp. 133-147)

16. Ashutosh Kumar, **Buddhadev Purohit**, Kuldeep Mahato, Pranjal Chandra*. Advance engineered materials in immunosensing for point-of-care bioanalysis. Immunosensors; Detection Science Series, Royal Society of Chemistry, London. (2019), (pp. 238-266).

Annexure 2

Conferences presentations

1. Buddhadev Purohit, Kuldeep Mahato, Ashutosh Kumar, Monalisha Ghosh Dastidar, Sharmili Roy, Pranjal Chandra *. Design of engineered dendritic nanochip for electrochemical characterization of biologically important small molecules at Recent advancements in biochemical engineering and biotechnology (RABEB-2019), Indian Institute of Technology (BHU) Varanasi on 15-16 March 2019. Page number: 97-98.
2. Buddhadev Purohit, Ashutosh Kumar, Kuldeep Mahato, Pranjal Chandra*. "Electrochemical sensing of ROS Molecule in Blood Samples Using a Modified Metallic Dendritic electrode" at 6th International Conference on Advanced Nanomaterials and Nanotechnology (ICAAN2019) Indian Institute of Technology Guwahati, Guwahati on 18- 21 December, 2019. Page number:270.
3. Buddhadev Purohit, Ashutosh Kumar, Kuldeep Mahato, Pranjal Chandra* "Designing a non-enzymatic peroxidase biosensor chip using sputtered gold dendrite for clinical applications in biological samples" at Indo-US conference on bioengineering & regenerative medicine (ICBR 2020) Indian Institute of Technology (BHU) Varanasi on 27-29, February 2020.

Annexure 3

List of media coverages

1. Vigyan Prasar, Government of India

http://www.vigyanprasar.gov.in/isw/Nano-chip-made-from-laboratory-waste-can-help-in-diagnosis-of-diseases.html

2. The Hindu Business Line

https://www.thehindubusinessline.com/news/science/nano-chip-made-from-laboratory-waste-can-help-in-diagnosis-of-diseases/article29331811.ece

3. Biotecnika Times

https://www.biotecnika.org/2019/09/indian-scientists-develop-nano-chip-from-laboratory-waste-to-diagnose-diseases/

4. Down to Earth

https://www.downtoearth.org.in/news/health/nano-chip-made-from-laboratory-waste-can-help-in-diagnosis-of-diseases-66527

5. Newsroom

https://newsroom24x7.com/2019/09/04/nano-chip-made-from-laboratory-waste-can-help-in-diagnosis-of-diseases/

6. Sputnik News

https://sputniknews.com/society/201909061076737012-indian-scientists-fabricate-nano-chip-made-from-lab-waste-for-diagnosis-of-diseases/

7. The India Saga/ Daily hunt News

https://m.dailyhunt.in/news/india/english/the+india+saga-epaper-indsaga/iit+guwahati+scientists+reused+laboratory+waste+to+design+nanosensor-newsid-136393186

Media highlights of Hydrogen Peroxide paper

Media highlights of Serotonin sensor

Microchimica Acta (2019) 186: 658
https://doi.org/10.1007/s00604-019-3773-2

ORIGINAL PAPER

Sputtering enhanced peroxidase like activity of a dendritic nanochip for amperometric determination of hydrogen peroxide in blood samples

Buddhadev Purohit[1] · Kuldeep Mahato[1] · Ashutosh Kumar[1] · Pranjal Chandra[1]

Received: 23 April 2019 / Accepted: 16 August 2019 / Published online: 29 August 2019

Abstract

A nonenzymatic electrochemical nanoprobe is described for the fast determination of hydrogen peroxide (H_2O_2). A sputtered indium tin oxide electrode with a nano-hierarchical 3D gold structure is used. The nanoprobe was characterized by SEM, EDX, TEM, SAED, and electrochemical techniques. Figures of merit include (a) a fast response time (≤ 1.0 s), (b) two linear dynamic ranges that extend from 10^{-12} M to 10^{-10} M and from 10^{-10} M to10^{-5} M; and (c) a low limit of detection of 9.8×10^{-13} M. The nanoprobe works in the clinical range and was applied for trace analysis of H_2O_2 in spiked blood samples, and recoveries ranged between 90 and 96%. It has negligible response ($p < 0.001$, for $n = 3$) toward glucose, citric acid, ascorbic acid, uric acid, glycine, and alanine. The shelf-lifetime is found to be 12 weeks.

Keywords Nanoprobe · Nanozyme · Ultrafast H_2O_2 detection · Indium tin oxide · Free radicals · Nano engineering

Introduction

Hydrogen peroxide (H_2O_2) is produced as a byproduct of several oxidases including; glucose oxidase, cholesterol oxidase, glutamate oxidase, urate oxidase, lactate oxidase, *etc.* in various subcellular compartments and organelles. H_2O_2 possesses a high reduction potential and binds with the proteins in the local microenvironment at the cysteine residue forming a reversible sulfenic group and directs the signaling process of various cellular functions involved in cell proliferation, differentiation, motility, *etc* [1]. However, when present in higher concentrations, H_2O_2 forms an irreversible sulfinic and sulfonic linkage and permanently damages proteins. Thus, the altered concentrations of H_2O_2 is reported to be associated with various pathological conditions *i.e.* inflammation, aging, diabetes, cardiovascular diseases, neurodegenerative disorders, cancer, *etc* [2]. The concentration of H_2O_2 also varies in human blood and other biological fluids in various diseased conditions. However, the exact concentration of H_2O_2 in the extracellular and intracellular matrices is a matter of debate due to the severity or stage of the pathological condition, hence several authors have reported different sets of data [3].

In view of such clinical importance of H_2O_2 in diverse biological matrices, many methods have been designed to detect / quantify the concentration of H_2O_2 based on fluorescence [4], colorimetry [5], chemiluminescence [6], and spectroscopy [7]. These methods are though reliable to detect H_2O_2, they suffer due to the involvement of bulky instruments, low sensitivity, time-consuming protocols, and interference from molecules commonly found in the complex biological matrices. Among all types of analytical systems, electrochemical sensing methods are considered to be robust, selective, and have the ability of miniaturization for point-of-care analysis [8–10]. For the development of electrochemical H_2O_2 sensor, horseradish peroxidase (HRP), an oxidoreductase enzyme is commonly used due to its high specificity toward H_2O_2 [11]. However, the limitation of using an enzyme for sensing purposes lies in the complicated immobilization process, temperature dependent denaturation, effect of micro-environment, less operational stability, low shelf-life,

Electronic supplementary material The online version of this article (https://doi.org/10.1007/s00604-019-3773-2) contains supplementary material, which is available to authorized users.

✉ Pranjal Chandra
pchandra13@iitg.ac.in

[1] Laboratory of Bio-Physio Sensors and Nano-bioengineering, Department of Bioscience and Bioengineering, Indian Institute of Technology Guwahati, Guwahati 781039, India

DOI: 10.1002/elan.201900551

Novel Sensing Assembly Comprising Engineered Gold Dendrites and MWCNT-AuNPs Nanohybrid for Acetaminophen Detection in Human Urine

Buddhadev Purohit,[a] Ashutosh Kumar,[a] Kuldeep Mahato,[a] and Pranjal Chandra*[a]

Abstract: A layered nanohybrid comprising of multi walled carbon nanotubes(MWCNT)-gold nanoparticles (AuNPs) has been designed as a matrix for the development of Au dendritic nanostructures (AuDN) with enhanced catalytic activity. The developed sensor matrix was thoroughly characterized by scanning electron microscope (SEM), transmission electron microscope (TEM), and energy dispersive X-ray spectroscopy (EDX). The developed sensor probe MWCNT-AuNPs/AuDN over glassy carbon electrode (GCE) was used for the label free detection of acetaminophen (AP), a commonly used drug associated with hepatotoxicity when overdosed, as a model molecule. The final sensor probe was characterized by cyclic voltammetry (CV), electrochemical impedance spectroscopy (EIS), linear sweep voltammetry (LSV), and differential pulse voltammetry (DPV). The sensor shows excellent analytical performances with a linear dynamic range (LDR) of 100 to 7500 nM, and a low limit of detection (LOD) of 2.12 (±0.03) nM, which is better than recently reported AP sensors. The practical application / clinical possibilities of the final sensor were evaluated by real sample analysis in human urine by spike and recovery method, where the AP recoveries were found in between 92 % to 96 %. The sensor probe shows negligible response towards co-existing interfering molecules like glucose, urea, uric acid and various amino acids, which are commonly found in real samples ($p < 0.001$, $n = 3$). The shelf life of the sensor probe was evaluated and found to be stable for 8 weeks. The fabricated sensor probe using MWCNT-AuNPs/AuDN is easy to fabricate, simple, robust, and able to detect AP in urine with high recoveries shows its possibilities to be used in clinical settings.

Keywords: Au dendritic nanostructure · MWCNT · AuNPs · Acetaminophen sensing · Urine analysis

1 Introduction

Metallic dendrites are a class of nanomaterial, which resembles with fern like morphology reported to have enhanced catalytic activities due to the presence of the relatively larger active surface area contributed by its three dimensional protruded structures [1,2]. Metallic dendrites are self-assembled hierarchical arrangement of primary, secondary, and tertiary branches with a very high density of sharp tips, edges, and ridges. In addition, the lower fouling effects have also been reported due to the spatial structures and enormously larger active surface area [3]. In this context, many monometallic dendrites based on Au, Ag, Pt, Cu, Co, Ni etc. have been synthesized and evaluated for their catalytic behavior [4–6]. Au based dendritic structures, however have been widely studied and used in biosensing application, due to their excellent biocompatibility [2,7]. The synthesis of Au dendrites (AuDN) has been achieved by various methods, which includes surfactant-mediated synthesis, galvanic replacement synthesis, and electrochemical synthesis [8–10]. The electrochemical deposition is the most facile, robust, and cost-effective method, where the dendritic structures are developed directly over the electrode surface eliminating the nanoparticle transfer step and its associated errors in signal generation. Also, electrodeposition assures an equal distribution of the active surfaces and can be easily controlled by optimizing the parameters like the precursor molecules concentration, time of deposition, applied potential etc. Although, the development of Au dendrites has been thoroughly investigated, but its integration with other nanostructure materials have been rarely attempted. Such integrative study may not only offer improved analytical performance of sensors, but it can also pave the way for developing novel nanohybrid comprising dendrites and other nanomaterials.

Various metallic nanoparticles, carbon dots, quantum dots, graphene are being widely used to develop innovative biosensing matrices [11]. Among all types of nanomaterials, carbon based nanomaterials, especially MWCNTs are greatly used in biosensor development due to its high conductivity, enormous surface area, chemical

[a] B. Purohit, A. Kumar, K. Mahato, P. Chandra
Laboratory of Bio-Physio Sensors and Nano-bioengineering, Department of Biosciences and Bioengineering, Indian Institute of Technology Guwahati, Guwahati-781039, India
Fax: +91361-258-2249
Phone: +91361-2583207
E-mail: pchandra13@iitg.ac.in

Available online at www.sciencedirect.com

ScienceDirect

Current Opinion in Biomedical Engineering

Smartphone-assisted personalized diagnostic devices and wearable sensors

Buddhadev Purohit, Ashutosh Kumar, Kuldeep Mahato and Pranjal Chandra

Abstract

Personalized point-of-care (POC) devices offer an easy access for health monitoring without using sophisticated instruments. Recently, miniaturized biosensors are being widely used as POC devices because of their reliable, sensitive, and fast detection of biomolecules with portable features. The recent advances in the camera and processor of smartphones are being eagerly integrated with biosensing applications, and this can be a big boost for health-care diagnoses owing to their wider presence all over the world. In this review, we have discussed most recent developments of portable diagnostic devices and wearable sensors based on the combined features of smartphones and biosensors for POC applications. Optical, electrochemical, and wearable biosensors are discussed in detail, and their sensing mechanism using smartphones has been illustrated. To put perceptive insights into the importance of smartphone-based POC devices and wearable sensing devices, recent examples have been described including the sensor design, transduction mechanism, and smartphone integration.

Addresses

Laboratory of Bio-Physio Sensors and Nano-bioengineering, Department of Biosciences and Bioengineering, Indian Institute of Technology Guwahati, Guwahati, 781039, India

Corresponding author: Chandra, Pranjal (pchandra13@iitg.ac.in) (pranjalchandra13@gmail.com)

Current Opinion in Biomedical Engineering 2020, **13**:42–50

This review comes from a themed issue on **Biomaterials: Biosensors**

Edited by **Rama S. Verma** and **Seeram Ramakrishna**

https://doi.org/10.1016/j.cobme.2019.08.015

Keywords

Biosensor, Optical biosensor, Electrochemical biosensor, Wearable biosensor, Point of care, Smartphone.

Introduction

Point-of-care (POC) devices are used for on-site detection of pathogens/analytes in various clinical conditions for easy and reliable health monitoring. POC devices are a portable miniaturized version of analyzers that can be easily transported, can be operated by semiskilled personnel, and are able to measure the analyte in the smallest quantity without compromising the sensitivity of the detection [1]. Most of the traditional bulky, high-cost sophisticated instruments (such as high-pressure liquid chromatography, gas chromatography, and mass spectroscopy), although sensitive, cannot be relied on for POC detection. Biosensors, on the other hand, can be a possible solution for this as it can be miniaturized, transported, and designed to sense a number of analytes. The design of a biosensor for development of POC devices includes the sensor probe development, condition optimization to efficiently detect analytes, signal generation/amplification, and representation of the signal in a visual or digital mode for easy interpretation by the end user [2]. Except for the success of the glucometer and some lateral flow-based strip assays, the commercial biosensors are still unknown to the wider population. Thus, the wider application of biosensors as POC devices requires some innovative way to use them as a daily object.

The smartphone can be integrated with biosensors for development of POC devices, where the end user can perform the sensing application on-site. As of January 2019, two-thirds of the world population is accustomed to smartphones and half of the population is accustomed to the Internet, which makes them a potential bioanalysis interface (https://thenextweb.com/contributors/2019/01/30/digital-trends-2019-every-single-stat-you-need-to-know-about-the-internet/). Smartphones have been used as a detector, processor, or instrument interface for biosensing activity. Irrespective of the manufacturer, smartphones have now the most advanced complementary metal oxide semiconductor (CMOS) sensor and integrated circuits with high processing power including other features that can be used for data acquisition and processing. In addition, smartphones can be used as a medium to store the data in the cloud for future use, eliminating the need for bigger data storage devices [3].

As there has been a wider applicability of smartphone-based POC devices at end users, it is interesting to document recent advances in design and development of such devices. Considering a fascinating research interest for a wider audience, we have critically examined the role of smartphones and their conjugation with other technologies to develop better biosensing POC devices. The most commonly used biosensor types and their uses

Biosensors and Bioelectronics 148 (2020) 111815

Contents lists available at ScienceDirect

Biosensors and Bioelectronics

journal homepage: http://www.elsevier.com/locate/bios

Clinically comparable impedimetric immunosensor for serum alkaline phosphatase detection based on electrochemically engineered Au-nano-Dendroids and graphene oxide nanocomposite

Kuldeep Mahato, Buddhadev Purohit, Ashutosh Kumar, Pranjal Chandra *

Laboratory of Bio-Physio Sensors and Nano-bioengineering, Department of Biosciences and Bioengineering, Indian Institute of Technology Guwahati, Guwahati, 781039, India

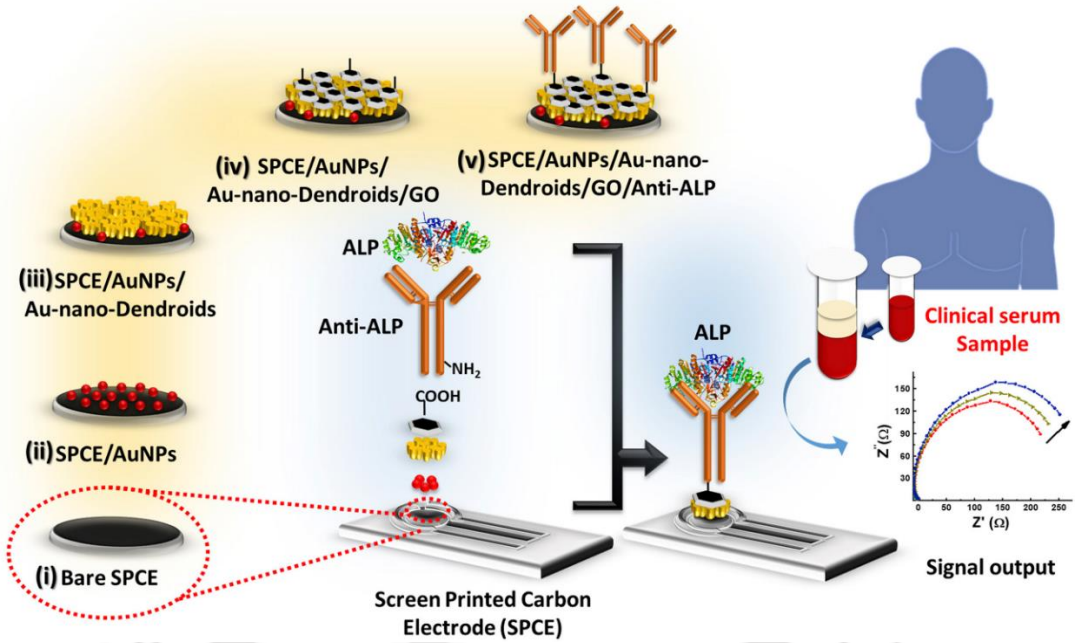

Abstract: In this work, we demonstrate label-free electrochemical impedance spectroscopy (EIS) based alkaline phosphatase (ALP) detection using gold nanoparticles (AuNPs), electrochemically engineered Au-nano-Dendroids, and graphene oxide (GO) nanocomposite. These nanomaterials were sequentially deposited on to the screen-printed carbon electrode (SPCE) and antibodies against ALP (anti-ALP) were immobilized using carbodiimide bioconjugation process. The sensor probe has been characterized extensively using TEM, EDX, SAED, XRD, FE-SEM, FTIR, DIC, and electrochemical techniques. The analytical performance of fabricated biosensor has been evaluated using EIS, where linear dynamic range and limit of detection were obtained to be 100–1000 U/L and 9.10 (±0.12) U/L, respectively. The developed biosensor showed high selectivity towards ALP with negligible interference (k_{sel} « 1; n = 3) due to coexisting molecules. The sensor probe has successfully recovered ALP between 108.84% and 172.50% (n = 3) in human serum samples. The sensor has been used to estimate ALP in clinical serum samples, where the level was found to be 83.15 U/L and was comparable with standard technique used in the hospitals. The shelf life, stability, and reproducibility have also been evaluated.

Mahato, K., **Purohit, B.**, Kumar, A., & Chandra, P. (2019). Clinically comparable impedimetric immunosensor for serum alkaline phosphatase detection based on electrochemically engineered Au-nano-dendroids and graphene oxide nanocomposite. *Biosensors and Bioelectronics*, 111815.

Biosensors and Bioelectronics 142 (2019) 111502

Contents lists available at ScienceDirect

Biosensors and Bioelectronics

journal homepage: www.elsevier.com/locate/bios

Novel electrochemical biosensor for serotonin detection based on gold nanorattles decorated reduced graphene oxide in biological fluids and *in vitro* model

Kuldeep Mahato[a], Buddhadev Purohit[a], Keshav Bhardwaj[b], Amit Jaiswal[b], Pranjal Chandra[a,*]

[a] Laboratory of Bio-Physio Sensors and Nano-bioengineering, Department of Biosciences and Bioengineering, Indian Institute of Technology Guwahati, Guwahati, 781039, India

[b] School of Basic Sciences, Indian Institute of Technology Mandi, Mandi, 175005, Himachal Pradesh, India

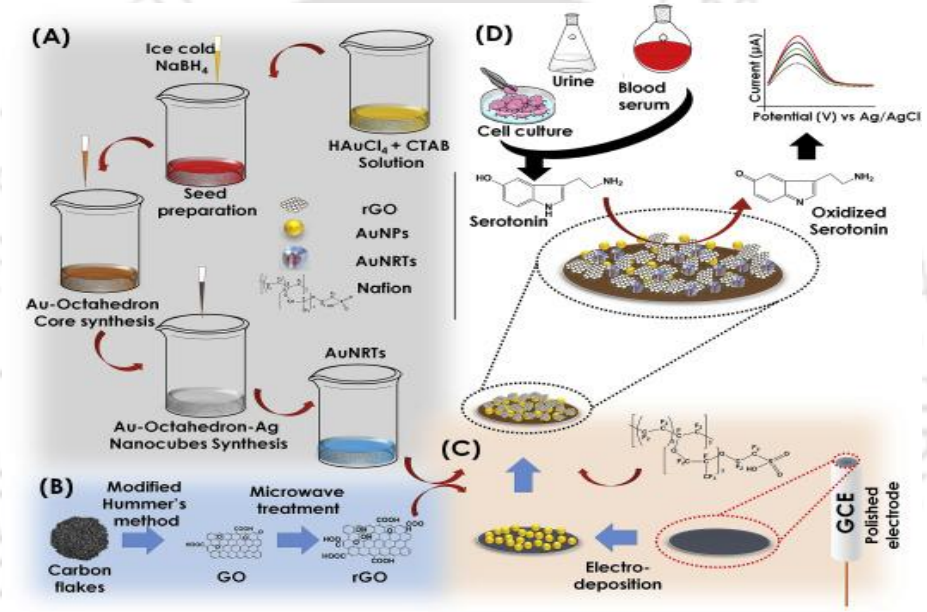

Abstract: Abnormal level of serotonin (ST) in body fluids is related to various clinical conditions including behavioral and psychotic disorders; hence its fast detection in clinically relevant ranges have tremendous importance in medical science. In view of this, we have developed a novel biosensor for ST detection using Au-nanorattles (AuNRTs)- reduced graphene oxide (rGO) nanocomposite coated on to the gold nanoparticles (AuNPs) deposited glassy carbon electrode (GCE). The nanocomposite/sensor probe was characterized using UV–Vis, TEM, SAED, EDX, AFM, and electrochemical techniques including LSV and EIS. Thereafter, the suitability of fabricated GCE/AuNPs/AuNRTs-rGO-Naf sensor probe was applied for ST determination which showed a linear dynamic range (LDR) of $3 \times 10{-}6$ - $1 \times 10{-}3$ M and the detection limit (DL) of 3.87 (±0.02) $\times 10{-}7$ (RSD < 4.2%) M, which falls in the ranges of normal as well as various abnormal pathophysiological conditions. The designed sensor is successfully applied to detect ST in various real matrices viz. urine, blood serum, and in vitro model to show its direct clinical/practical applicability. Interferences due to the coexisting molecules were assessed and the long-term stability of the designed sensor was also examined which was found to be 8 weeks.

Mahato, K., **Purohit, B.**, Bhardwaj, K., Jaiswal, A., & Chandra, P. (2019). Novel electrochemical biosensor for serotonin detection based on gold nanorattles decorated reduced graphene oxide in biological fluids and in vitro model. Biosensors and Bioelectronics, 142, 111502.

Full Paper Wiley Online Library ELECTROANALYSIS

DOI: 10.1002/elan.201900337

Gold-Iron Bimetallic Nanoparticles Impregnated Reduced Graphene Oxide Based Nanosensor for Label-Free Detection of Biomarker Related to Non-Alcoholic Fatty Liver Disease

Ashutosh Kumar,[a] Buddhadev Purohit,[a] Kuldeep Mahato,[a] Riddhipratim Mandal,[a] Ananya Srivastava,[b] and Pranjal Chandra*[a]

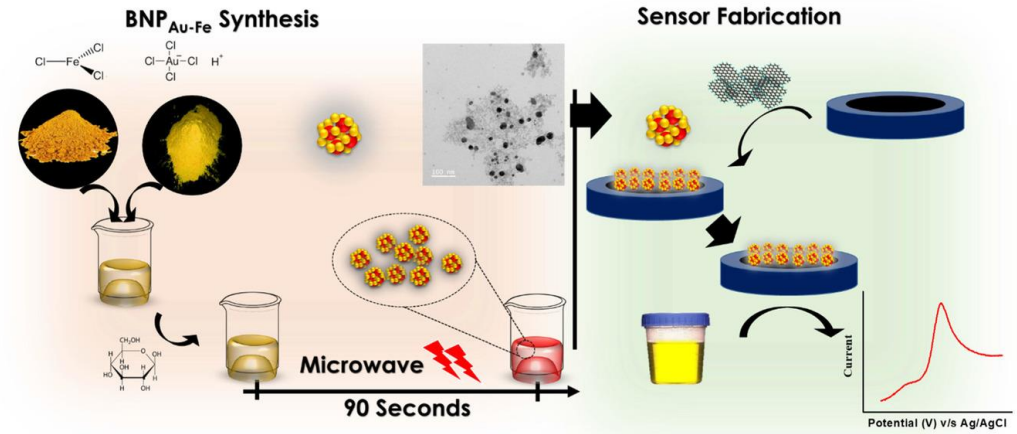

Abstract: We report for the first time a microwave assisted, one pot, direct, and facile synthesis of monodispersed iron-gold bimetallic nanoparticles (BNPAu-Fe) using glucose as a reducing agent in merely 90 s. The as such synthesized BNPAu-Fe were thoroughly characterized using UV-Vis, XRD, TEM, EDX, elemental mapping, and raman spectroscopy. These BNPAu-Fe were further impregnated with reduced graphene oxide (rGO) and coated onto glassy carbon electrode (GCE) to develop a sensor probe for label free electrochemical detection of acetaminophen, which is considered to be a most potent biomarker related to non-alcoholic fatty liver disease. The sensor probe was systematically characterized by cyclic voltammetry (CV) and electrochemical impedance spectroscopy (EIS). The BNPAu-Fe-rGO nanocomposite matrix showed the sensing of acetaminophen with a wide dynamic range between 50 and 800 nM with detection limit (DL) of 0.14 nM (±0.05) nM (RSD<4.12 %) that was lower compared to previously reported acetaminophen sensors. To show the practical application of the sensor probe, acetaminophen was detected in human urine samples, which showed the percentage recovery between 86.65% and 91.32%. To the best of our knowledge, this is the first report where BNPAu-Fe impregnated rGO was used to detect acetaminophen. Interferences due to various molecules such as glucose, serum albumin, glycine, glutamic acid, alanine, citric acid, and ascorbic acid were tested individually and in mixed sample. Longterm stability of sensor probe was examined which was found to be stable up to 12 weeks. The sensor fabricated using BNPAu-Fe-rGO nanocomposite has many attractive features such as; simplicity, rapidity, and label free detection, hence it could be a method of choice for acetaminophen detection in clinical setting.

Kumar, A., **Purohit, B.**, Mahato, K., Mandal, R., Srivastava, A., & Chandra, P. (2019). Gold-Iron Bimetallic Nanoparticles Impregnated Reduced Graphene Oxide Based Nanosensor for Label-free Detection of Biomarker Related to Non-alcoholic Fatty Liver Disease. Electroanalysis, 31(12), 2417-2428.

Full Paper Wiley Online Library ELECTROANALYSIS

DOI: 10.1002/elan.201900406

Design and Development of Ultrafast Sinapic Acid Sensor Based on Electrochemically Nanotuned Gold Nanoparticles and Solvothermally Reduced Graphene Oxide

Ashutosh Kumar,[a] Buddhadev Purohit,[a] Kuldeep Mahato,[a] Sharmili Roy,[a] Ananya Srivastava,[b] and Pranjal Chandra*[a]

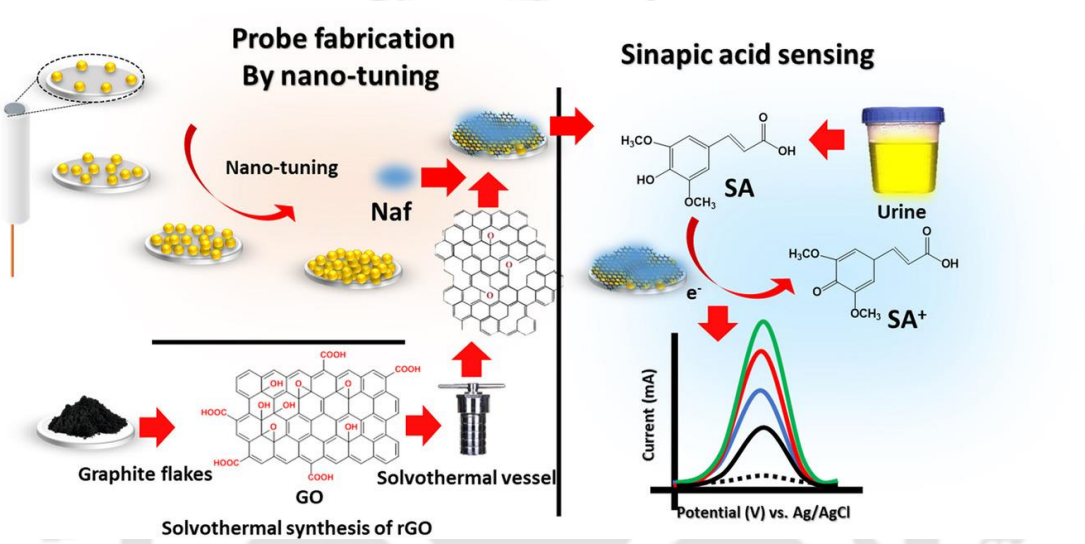

Abstract: We report for the first time sinapic acid (SA) sensing based on nanocomposite comprising electrochemically tuned gold nanoparticles (EAuNPs) and solvothermally reduced graphene oxide (rGO). The synthesized EAuNPs, rGO, and EAuNPs-rGO nanocomposite were characterized using X-ray diffraction (XRD), transmission electron microscopy (TEM), selected area electron diffraction (SAED), particle size analysis, and Raman spectroscopy. A proof-of-concept electrochemical sensor for SA was developed based on synthesized EAuNPs-rGO nanocomposite, which was characterized by electrochemical techniques such as cyclic voltammetry (CV) and electrochemical impedance spectroscopy (EIS). The developed sensor detected SA with a linear dynamic range (LDR) between 20 μM and 200 μM and detection limit (DL) of 33.43 (±0.21) nM (RSD< 3.32 %). To show the useful purpose of the sensor probe in clinical applications, SA was detected in human urine samples, which showed the percentage recovery between 82.6 % and 92.8%. Interferences due to various molecules such as L-cystine, glycine, alanine, serum albumin, uric acid, citric acid, ascorbic acid, and urea were tested. Longterm stability of the sensor probe was examined, which was found to be stable up to 6 weeks. The sensor fabricated using EAuNPs-rGO nanocomposite has many attractive features such as; simplicity, rapidity, and labelfree detection; hence, it could be a method of choice for SA detection in various matrices.

Kumar, A., **Purohit, B.,** Mahato, K., Roy, S., Srivastava, A., & Chandra, P. (2019). Design and Development of Ultrafast Sinapic Acid Sensor Based on Electrochemically Nanotuned Gold Nanoparticles and Solvothermally Reduced Graphene Oxide. Electroanalysis.

BIOGRAPHY

Buddhadev Purohit is currently a research scholar at the Laboratory of Bio-Physio sensors and Nano-bioengineering, Department of Biosciences and Bioengineering, Indian Institute of Technology Guwahati, INDIA. He hails from Jharabahali, Subarnapur, Odisha. He holds degrees of Bachelors of Science (B.Sc.) in Botany, and Masters of Science (M.Sc.) in Life Sciences from Sambalpur University, Sambalpur, Odisha. He has qualified in GATE 2016 with All India Rank 158 in Life Sciences. He has also qualified NET (Life Sciences) conducted by MHRD-GoI. After graduating, he worked as a guest faculty of Botany teaching undergraduate biochemistry classes at Gangadhar Meher University, Sambalpur. Thereafter, he joined Indian Institute of Technology Guwahati for his doctoral studies under the supervision of Dr. Pranjal Chandra, Professor (Assist.) and Ramanujan Fellow. His research work is centered at the development of electrochemical biosensors by incorporating metallic dendrites and its composite materials. He has published / communicated more than 15 high impact journals, which includes journals like Biosensors and Bioelectronics, Electroanalysis, Microchimica Acta, Current Opinion in Biomedical Engineering, etc. He is also an invited reviewer of peer-reviewed scientific journals such as Material science and energy technology, Elsevier and Sensor International, KeAi publishing and Elsevier.